



**Michigan
Technological
University**

Michigan Technological University

Digital Commons @ Michigan Tech

Dissertations, Master's Theses and Master's Reports

2021

Open-Source TIG-Based Metal 3D-Printing

Shane Oberloier

Michigan Technological University, swoberlo@mtu.edu

Copyright 2021 Shane Oberloier

Recommended Citation

Oberloier, Shane, "Open-Source TIG-Based Metal 3D-Printing", Open Access Dissertation, Michigan Technological University, 2021.

<https://doi.org/10.37099/mtu.dc.etdr/1301>

Follow this and additional works at: <https://digitalcommons.mtu.edu/etdr>

 Part of the [Electrical and Electronics Commons](#), and the [Robotics Commons](#)

OPEN-SOURCE TIG-BASED METAL 3D-PRINTING

By

Shane W. Oberloier

A DISSERTATION

Submitted in partial fulfillment of the requirements for the degree of

DOCTOR OF PHILOSOPHY

In Electrical Engineering

MICHIGAN TECHNOLOGICAL UNIVERSITY

2021

© 2021 Shane W. Oberloier

This dissertation has been approved in partial fulfillment of the requirements for the
Degree of DOCTOR OF PHILOSOPHY in Electrical Engineering.

Department of Electrical and Computer Engineering

Dissertation Co-Advisor: *Dr. Glen Archer*

Dissertation Co-Advisor: *Dr. Joshua Pearce*

Committee Member: *Dr. Michael Roggemann*

Committee Member: *Dr. Yu Zou*

Department Chair: *Dr. Glen Archer*

Table of Contents

Author Contribution Statement.....	vii
Acknowledgements.....	viii
Abstract	ix
1 Introduction.....	1
2 Finding Ideal Parameters for 3-D Printing Using Particle Swarm Optimization	2
2.1 Abstract	2
2.2 Introduction	2
2.3 Materials and Methods	4
2.3.1 Materials and 3-D Printer.....	4
2.3.2 Software	4
2.3.3 Parameter Acquisition.....	7
2.3.4 LDPE Optimization on Gigabot X Experiment Design.....	8
2.4 Results and Discussion.....	11
2.4.1 Parameter Acquisition.....	11
2.4.2 LDPE Optimization on Gigabot X Results	13
2.4.3 Impact and Applications	16
2.4.4 PSO vs Random Selection	16
2.4.5 Future Work	16
2.5 Conclusions	17
2.6 References	17
3 Open Source Framework for a Broadly Expandable and Reconfigurable Data Acquisition and Automation Device (BREAD)	23
3.1 Hardware in context	23
3.2 Hardware description	23
3.2.1 Schematic Design Procedures for Slices.....	24
3.2.1.1 Starting Out the Design.....	24
3.2.1.2 Design Standards & Conventions	24
3.2.2 Board Design Procedures for Slices	25
3.2.2.1 Starting out the Design.....	25
3.2.2.2 Considerations for Digital Manufacturing	25
3.2.2.3 Design Standards & Conventions	26
3.2.3 Documentation Procedures for Slices	27
3.2.3.1 Standard Datasheet.....	27
3.2.3.2 Repository	27
3.2.4 Mechanical Definitions for Slices.....	27
3.2.4.1 PCB Dimensions.....	27
3.2.4.2 Positioning & Sizing Constraints.....	28
3.2.5 Electrical Definitions for Slices	28

3.2.5.1	Loaf Interface Connector	29
3.2.5.2	External Connector	30
3.2.5.3	Default Circuitry & Connections	30
3.2.6	Software Definitions for Slices	31
3.2.6.1	Programming Standards.....	31
3.2.6.2	SLC_Functions.h	31
3.2.6.3	SLC_TEMP.h.....	31
3.2.7	Building Loafs	31
3.2.7.1	Single Slice Usage	32
3.2.7.2	Single Loaf Usage.....	32
3.2.7.3	Multi-Loaf Usage.....	32
3.2.8	Existing Slices.....	33
3.2.8.1	SLC_LVAI Amplified Analog Input Slice	33
3.2.8.2	SLC_IDIO Isolated Digital Input/Outputs	36
3.2.8.3	SLC_AAFM Audio Analysis / Fourier Transform	38
3.2.8.4	SLC_CR10 +/- 10A Current Sensor	42
3.2.8.5	SLC_RLAY 4 Channel Relay Controller	45
3.2.8.6	SLC_STEP 4 Channel Stepper Motor Controller.....	47
3.2.8.7	SLC_THRM 4 Channel Type-K Thermocouple Reader	50
3.2.8.8	SLC_USB2 2 Channel USB Port	52
3.2.9	Example System: TIG-Based Metal 3D Printer Monitor	54
3.2.9.1	Required Functions & Slices	55
3.2.9.2	Configuration	55
3.2.9.3	Firmware	56
3.3	Design files summary	56
3.4	Bill of materials summary	57
3.5	Build instructions	66
3.5.1	General Component Construction and Programming.....	66
3.5.2	Emergency Stop Wiring.....	70
3.5.3	Example System: TIG-based Metal 3D Printer Monitor	70
3.6	Operation instructions	72
3.6.1	Commands	72
3.6.2	Example System: TIG-based Metal 3D Printer Monitor	76
3.7	Validation and characterization.....	76
3.7.1	Slice Characterization	76
3.7.1.1	SLC_LVAI: Amplified Analog Input Slice Characterization	77
3.7.1.2	SLC_IDIO: Isolated Digital Input/Outputs Characterization	78
3.7.1.3	SLC_AAFM: Audio Analysis / Fourier Transform Characterization	80
3.7.1.4	SLC_CR10: +/- 10A Current Sensor Characterization...	81
3.7.1.5	SLC_RLAY: 4 Channel Relay Controller Characterization	83

3.7.1.6	SLC_STEP: 4 Channel Stepper Motor Controller Characterization	83
3.7.1.7	SLC_THRM: 4 Channel Type-K Thermocouple Reader Characterization	83
3.7.1.8	SLC_USB_P: 2 Channel USB Port Characterization	84
3.7.2	Example System: TIG-based Metal 3D Printer Monitor	84
3.7.3	Economic Analysis	85
3.7.4	Continued Development and Application.....	87
3.7.5	Future Work	88
3.8	References	88
4	Low-Cost Open Source TIG-Based Metal 3-D Printer.....	95
4.1	Hardware in context	95
4.2	Hardware description	96
4.3	Design files summary	97
4.4	Bill of materials summary	99
4.5	Build instructions	104
4.5.1	Printer Modifications	104
4.5.2	Extruder Build.....	106
4.5.3	Enclosure Build.....	109
4.5.4	Wiring	115
4.5.5	Initial setup.....	116
4.5.6	Using a Raspberry Pi as the Printer Host.....	116
4.6	Operation instructions	116
4.6.1	Safety Concerns	116
4.6.2	Lightning Operation.....	117
4.6.3	Jogging Axes.....	118
4.6.4	Running Commands.....	118
4.6.5	Running Scripts.....	118
4.6.6	Emergency Stop	118
4.6.7	Lightning Modification.....	118
4.6.8	Adding GUI Elements.....	118
4.6.9	Parametric G-Code.....	119
4.6.10	Initial Tuning	120
4.6.11	Constraints for Operation.....	120
4.7	Validation and characterization.....	120
4.7.1	Base Parameter Acquisition	120
4.7.2	Optimization	121
4.7.3	Characterization	122
4.7.4	Microstructure Characterization	123
4.8	Discussion	123
4.8.1	Capabilities	123
4.8.2	Deposition Repeatability.....	126
4.8.3	Constraints	126
4.8.4	Cost Analyses.....	127
4.8.5	Future Work	129

4.9	Conclusions	130
4.10	References	130
5	Particle Swarm Optimization of Printing Parameters for Open Source TIG-Based Metal 3-D Printing	136
5.1	Introduction	136
5.2	Materials and Methods	137
5.2.1	Open Source TIG-Bot	137
5.2.2	PSO Experimenter	139
5.2.3	Process Variables	140
5.2.4	Test structures	141
5.2.5	Line Optimization Test	142
5.2.6	Plane Optimization Test.....	143
5.2.7	Rectangular Prism Optimization Test.....	143
5.3	Theory/Calculation.....	143
5.3.1	Particle Swarm Optimization Summary	143
5.3.2	TIG Welding Theory and Variables	144
5.4	Results	146
5.4.1	Line Optimization	146
5.4.2	Plane Optimization.....	147
5.4.3	Prism Optimization	147
5.5	Discussion	148
5.5.1	Particle Swarm Optimization Effectiveness	148
5.5.2	Limitations and Future Work.....	148
5.5.3	Implications for Distributed Metal Additive Manufacturing.....	148
5.6	Conclusions	148
5.7	References	149
6	Conclusions.....	156
6.1	General Conclusions.....	156
6.2	Conclusions on Finding Ideal Parameters for 3-D Printing Using Particle Swarm Optimization	156
6.3	Conclusions on Open Source Framework for a Broadly Expandable and Reconfigurable Data Acquisition and Automation Device (BREAD)	156
6.4	Conclusions on Low-Cost Open Source TIG-Based Metal 3-D Printer	156
6.5	Conclusions Particle Swarm Optimization of Printing Parameters for Open Source TIG-Based Metal 3-D Printing	156

Author Contribution Statement

- Chapter 1 consists of completely original work by the author.
- Chapter 2 has been submitted to Additive Manufacturing. Contributions were made by the following individuals:
 - Shane Oberloier: Conceptualization, Methodology, Shane Oberloier, Nicholas G. Whisman : Software, Data curation, Visualization, Investigation, Validation, Joshua M. Pearce: Supervision. Shane Oberloier, Nicholas G. Whisman, Joshua M. Pearce: Writing- Original draft preparation, Writing- Reviewing and Editing
- Chapter 3 has been submitted to HardwareX. Contributions were made by the following individuals:
 - Shane Oberloier: Conceptualization, Methodology, Shane Oberloier, Nicholas G. Whisman : Software, Data curation, Visualization, Investigation, Validation, Joshua M. Pearce: Supervision. Shane Oberloier, Nicholas G. Whisman, Joshua M. Pearce: Writing- Original draft preparation, Writing- Reviewing and Editing
- Chapter 4 has been submitted to HardwareX. Contributions were made by the following individuals:
 - Conceptualization: Shane Oberloier and Joshua M. Pearce, Methodology, Software, Visualization, Validation, Data curation: Shane Oberloier Wilson J. Holmes, and Aliaksei Petsiuk, Writing- Original draft preparation: : Shane Oberloier and Joshua M. Pearce Investigation: Shane Oberloier Wilson J. Holmes, Supervision.: Joshua M. Pearce; Writing: Reviewing and Editing: Shane Oberloier Wilson J. Holmes, Aliaksei Petsiuk, and Joshua M. Pearce.
- Chapter 5 has been submitted to Additive Manufacturing. Contributions were made by the following individuals
 - Conceptualization: Shane Oberloier and Joshua M. Pearce, Methodology, Software, Visualization, Validation, Data curation: Shane Oberloier Wilson J. Holmes Writing- Original draft preparation: : Shane Oberloier and Joshua M. Pearce Investigation: Shane Oberloier Wilson J. Holmes, Supervision.: Joshua M. Pearce; Writing: Reviewing and Editing: Shane Oberloier Wilson J. Holmes and Joshua M. Pearce.
- Chapter 6 consists of completely original work by the author

Acknowledgements

Thank you to my daughter, Hazel, for being a constant source of joy over the busy and sometimes stressful period of writing this dissertation.

A special thanks to the Secret Pizza Society for going above and beyond with their support.

Abstract

Metal 3-D printing has been relegated to high-cost proprietary high-resolution systems and low-resolution low-cost metal inert gas (MIG) systems. In order to provide a path to high-resolution, low-cost, metal 3-D printing, this manuscript proposes a new open source metal 3-D printer design based around a low-cost tungsten inert gas (TIG) welder coupled to a commercial open source self replicating rapid protyper. Optimal printing parameters for the machine are acquired using a novel computational intelligence software. TIG has many advantages over MIG, such as having a low heat input, clean beads, and the potential for both high-resolution prints as well as insitu alloying of complex geometries. The design can be adapted to most RepRap-class systems and has a basic yet powerful free and open source software (FOSS) package for the characterization of the 3-D printer. This system can be used for fabricating custom metal scientific components and tools, near net-shape structural metal component rapid prototyping, adapting and depositing on existing metal structures, and is deployable for in-field prototyping for appropriate technology applications.

1 Introduction

The works presented in this dissertation embody key components to the development of the first TIG-Based Rep-Rap Metal 3D Printer. In the first chapter, a novel GUI implementation of the Partical Swarm Optimization computational intelligence algorithm is designed and characterized using a large scale printer and LDPE plastic. This algorithm will later be used to optimize the Metal 3D Printer's parameters in Chapter 5. The second chapter details a custom and highly flexible and scalable data acquisition and automation system that can be used to characterize the quality of the welding process. And finally in chapter 4, the design and additional characterization of the machine is carried out.

2 Finding Ideal Parameters for 3-D Printing Using Particle Swarm Optimization

2.1 Abstract

As additive manufacturing rapidly expands the number of materials including waste plastics and composites, there is an urgent need to reduce the experimental time needed to identify optimized printing parameters for novel materials. Computational intelligence (CI) in general and particle swarm optimization (PSO) algorithms in particular has been shown to accelerate finding optimal printing parameters. Unfortunately, the implementation of CI has been prohibitively complex for non-computer scientists, or they are not open-source. To overcome these limitations this article develops, tests and validates PSO Experimenter, an easy-to-use open-source platform based around the PSO algorithm. PSO Experimenter is used to find optimal printing parameters for a relatively unexplored potential distributed recycling and additive manufacturing (DRAM) material that is widely available: low-density polyethylene (LDPE). LDPE has been used to make filament, but this study for the first time it was used in the open source FPF/FGF system. PSO Experimenter successfully identified functional printing parameters for this challenging to print waste plastic. The results indicate that PSO Experimenter can provide 97% reduction in research time for 3-D printing parameter optimization. It is concluded that PSO Experimenter is a user-friendly and effective free software for finding ideal parameters for the burgeoning challenge of DRAM as well as a wide range of other fields and processes.

2.2 Introduction

The field of 3-D printing is constantly expanding into new materials, such as biofilms [1], elastomer resins [2], dental materials [3], pre-ceramic polymers [4], ceramics [5], silicone [6] and even edible inks [7]. Additionally, there are many conventional recycled thermoplastics [8], which are just now being embraced by the 3-D printing community. These include not only the two most popular fused filament materials: polylactic acid (PLA) [9-12] and acrylonitrile butadiene styrene (ABS) [13-17], but also common thermoplastics like high-density polyethylene (HDPE) [18-21], polypropylene (PP) and polystyrene (PS) [20], thermoplastic polyurethane (TPU) [22], polyethylene terephthalate (PET) [23-24] and polycarbonate (PC) [25].

The creation of recycled plastic filament extruders like the open source recyclebots [13,18,26], that upcycle post-consumer plastic waste into 3-D printing filament, also allow for the further democratization of distributed recycling and manufacturing (DRAM) [13,27,28]. Consumers have a direct economic incentive to recycle with DRAM [13,28] because they can use their waste to fabricate many consumer products for far less than they can be purchased from conventional manufacturing [29-32]. DRAM thus has the potential to radically impact global value chains [33]. In addition to reducing 3-D printing costs by several orders of magnitude, DRAM decreases embodied energy of 3-D printing filament by 90% thus radically improving the environmental impact [34-36].

Unfortunately, each melt and extrude cycle of a recyclebot impairs the mechanical properties of PLA [10], HDPE [21], and even of PET [23]. This limits the recycling cycles to approximately five [10] before reinforcement or blending with virgin materials becomes necessary. Polymer composites using carbon-reinforced plastic [37], fiber-filled composites [38-39], and various types of waste wood [40-41] have been used in recyclebot systems, and more complex DRAM systems can use 3D-printed PC as molds for intrusion molding [25] for windshield wiper composites [42] as well as acrylonitrile styrene acrylate (ASA) and stamp sand waste composites [43]. Zander et al. [44] has studied PET, PP, and PS blends with styrene ethylene butylene styrene (SEBS) and maleic anhydride compatibilizers that were able to increase tensile strength.

DRAM presents a significant challenge to 3-D printing operators. Post-consumer waste has a wide variety of contaminants, exact polymer specifications are unknown, the polymer history (e.g. number of cycles) may be unknown, etc.

Many novel materials require unique end effectors [45], or entirely new machines for 3-D printing [46] and there has been a rise of direct extrusion fused particle fabrication fused granule fabrication (FPF/FGF) based systems [25,47-49]. A conventional method for finding idealized printing parameters is to print a consistent model using a matrix of parameters, effectively sweeping through every possible permutation [47,50]. This is time consuming and inefficient and does not scale well across the myriad numbers of potentially recyclable waste plastic streams.

Computational intelligence (CI) can be leveraged to minimize the time it takes to optimize for process parameters experimentally [51]. CI methods such as hierarchical machine learning [6], symbiotic organism search algorithms and particle swarm optimization (PSO) [52], have been proven as effective methods to find optimal printing parameters. In this context – a particle refers to a “candidate solution” which must be tested and will evolve over each iteration. Typically, the implementation of the CI algorithm is prohibitively complex for non-computer scientists, or they are not open-source. In this paper, “PSO Experimenter” [53], an easy-to-use open-source platform based around the PSO algorithm, is introduced. Though PSO Experimenter is made for general implementations, the application of 3-D printing will be explored specifically.

PSO Experimenter will first be evaluated by applying it to known test functions which have similar responses to 3-D printing parameter-sweeps. Then, PSO Experimenter will be used to find optimal printing parameters for a relatively unexplored potential DRAM material that is widely available: low-density polyethylene (LDPE). LDPE has been used to make filament [54], but in this study for the first time it will be used in the open source FPF/FGF system of the Gigabot X [55]. The GigabotX is used because it exemplifies a complex 3-D printer by printing from pellets, shards, particles or granules (as opposed to filament), has multiple (3) heat zones in the extruder, and prints on a large scale (570 x 595 x 470 mm) [55].

The optimization will be carried out in 3 steps. First the particles (tests) will be defined as 200 mm long singular extrusion lines. Second, the particles will be defined as 100 x 100

mm single-layer planes. Third, the particles will be defined as 40 x 40 x 40 solid cubes. Each test will have pertinent parameters dictated by PSO experimenter for each particle. In order to optimize parameters, a fitness function and test set will also be proposed. This fitness method is generalizable to all other 3-D printing applications.

2.3 Materials and Methods

2.3.1 Materials and 3-D Printer

LDPE pellets (Figure 2.1a) were obtained from McDonough Plastics and were 3-D printed in a 3-heat-zone Gigabot X (re:3D, Texas) (Figure 2.1b). The Gigabot X is a direct pellet material extrusion based 3-D printer with the nozzle arranged vertically in which a compression screw and three hot zones (demonstrated in Figure 2.1c) enable a relatively constant flow of recycled material through the print nozzle.

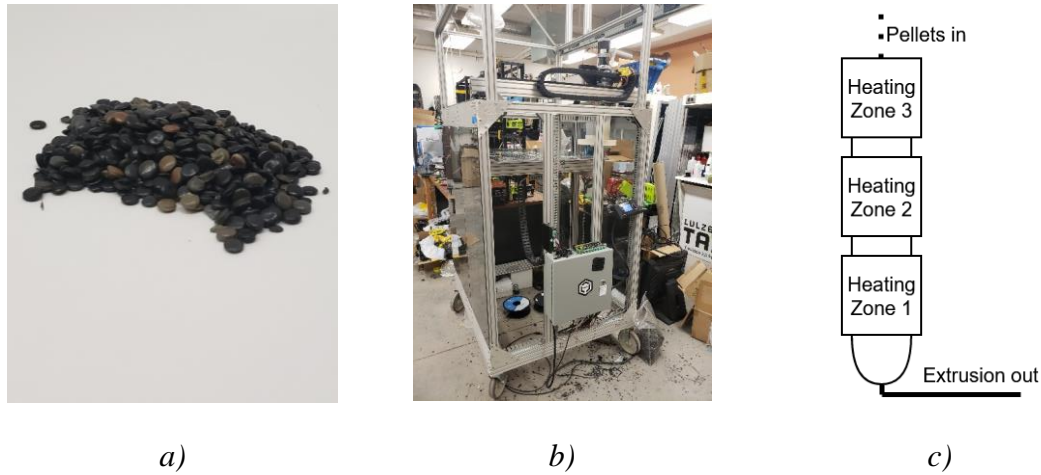


Figure 2.1: a. Raw LDPE pellets. b. The Gigabot X. c. The 3 heating zones of the extruder

2.3.2 Software

PSO Experimenter is an easy-to-use, minimalist optimization platform which utilizes the particle swarm optimization and is licensed under GPL3.0. PSO consists of a list of particles which have a personal optimum configuration, current position, and a velocity. In the context of PSO, position refers to a certain set of parameters to be experimentally tested. Additionally, the group optimum (best of all the personal optimums across all iterations) is known by each particle. PSO is an iterative method, after each iteration the algorithm works to minimize the fitness of each particle.

PSO Experimenter allows users to create an unlimited number of variables, allowing for exploration in n-dimensional space. Each variable must have a name, minimum value, maximum value, and an initial guess. Additionally, the variable can be constrained to integer values only (input 1 for integer only, 0 for floating point). PSO Experimenter does not allow for addition of new variables after the first iteration is generated, however

variables that may come in to play later in optimization can be constrained by entering a value to constrain at in the Constrain column.

Name	Min Val	Max Val	Initial Guess	Int Only	Constrain
1 T0	175	250	245	1	nan
2 T1	175	250	245	1	nan
3 T2	175	240	245	1	nan
4 Flow	100	300	222	0	nan
5 Bed_Temp	80	120	100	1	nan
6 Print_Speed	10	60	25	0	nan

Figure 2.2. Screen shot of PSO Experimenter during variable entry.

Before the first iteration, each particles position is initialized with a position being a uniformly distributed random vector. PSO Experimenter allows for the input of an initial guess for each variable, and a proximity to that guess. Specifically, the initial position for each particle is generated using Equation 2-1 [52].

$$x_i = \left[U\left(\max\left(x_{gi} - \frac{rp}{2}, x_{mini}\right), \min\left(x_{gi} + \frac{rp}{2}, x_{maxi}\right)\right) \right] \quad (2-1)$$

Where x_i is defined as the current position at variable i , U is the random uniform distribution between two given values, x_{gi} is the guess value for variable i , x_{mini} is the minimum allowable value for variable i , x_{maxi} is the maximum allowable value for variable i , r is the range between x_{mini} and x_{maxi} , and p defines the proximity to x_{gi} .

Additionally, the particle's velocity is initialized according to equation 2-2 [52,56].

$$v_i = U(-|x_{maxi} - x_{mini}|, |x_{maxi} - x_{mini}|) \quad (2-2)$$

Where v_i is the velocity for variable i .

For each iteration of the algorithm, the particle's position must be tested and then assigned a resultant fitness. When a new iteration is generated, the particle's velocity is updated by equation 2-3 [52,56] where x_{pbi} is the position in variable i for the particle's current personal best, and x_{gbi} is the position for the swarm's current group best. The weight parameters are defined in Table 2.1.

$$v_i \leftarrow k_v v_i + k_p U(0,1)(x_{pbi} - x_i) + k_g U(0,1)(x_{gbi} - x_i) \quad (2-3)$$

Table 2.1: Main parameters for tuning PSO behavior.

Variable	Description
k_v	The emphasis given to the velocity component
k_p	The emphasis given to a particle's personal best position
k_g	The emphasis given to the swarm's group best position

Finally, the particles new position at variable i is updated in Equation 2-4 [52, 56].

$$x_i \leftarrow x_i + v_i \quad (2-4)$$

The workflow in PSO experimenter starts with variable entry. The ranges and initial guesses for each variable can be acquired four different ways:

1. Literature review – Reviewing works in academia exploring a process similar to the optimization objective can yield information on commonly used parameter values.
2. Expert consultation – In cases when the process is completely novel, a subject-matter expert may have intuition on what ranges to search for each given variable.
3. Initial experimentation – Arbitrary, but guided, experimentation can show some parameters that work, and some which do not. These experiments can provide insight on what ranges to search in.
4. Previous optimization experiments – The output of a previous PSO experiment can be used as a starting point for further optimizations.

In this study, the first trial's variable parameters are found via literature review and initial experimentation. The two following tests use the values from the previous optimization experiment.

In addition to variable information, the optimization parameters must be entered. These weights can either be found in literature review, or via experimentation with a test function that has a similar response to the system being optimized. After all variables and parameters are entered, the first iteration can be generated.

The first iteration will have a fixed number of particles, each with a unique set of variable values that must be used in the process or experiment. Either during or after (or both) the experiment, measurements must be taken to quantify the success of that particular combination. A fitness function must be established which is a function of the measurements, and trends downwards as measurements become more desirable. The simplest fitness function can be a normalized sum of accuracy measurements. The resulting fitness for each particle can be entered into PSO Experimenter, and the next iteration is

generated. The optimization process can either be ran for a fixed number of iterations, or until the fitness is below a desirable threshold. The general workflow for PSO Experimenter can be seen in Figure 2.3.

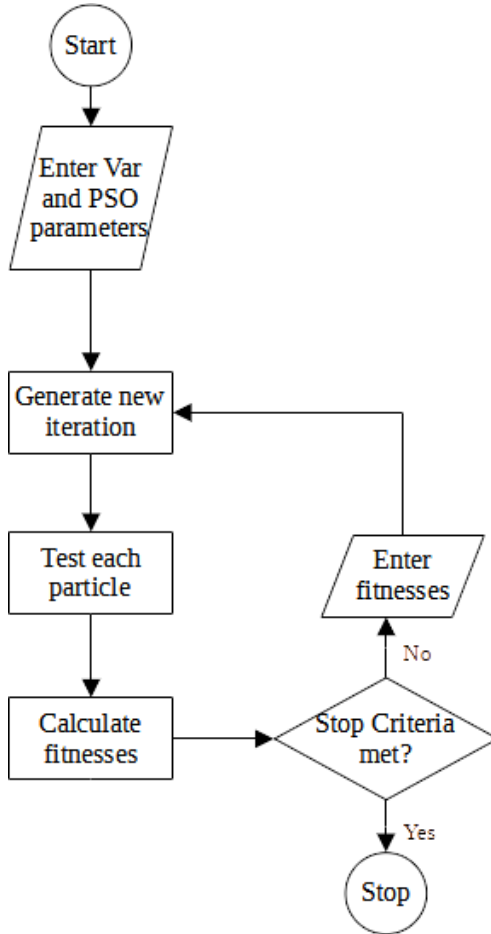


Figure 2.3. PSO Experimenter general workflow.

PSO Experimenter also allows for saving and loading particle and experiment data. The data is saved in clearly formatted CSVs so that historical data can be viewed for further analysis. Additionally, this open format allows the user to intervene and change parameters as needed (though this is not always recommended, since errors in alteration can render the file unusable, it can be useful for specialized corrections).

2.3.3 Parameter Acquisition

In this study, the process being optimized is printing recycled waste LDPE pellets using a Gigabot X 3-D printer. PSO typically uses thousands of particles in the swarm, but since this experiment requires physical processes and measurements [57], only 5 particles will be used. Since this number is low, the experimental parameters must be chosen such that the particles are more explorative (rather than exploitative) to prevent early convergence on

a local minimum. More explorative particles will spend more iterations exploring the sample space, and their velocity will slowly decay as they begin to converge [57].

In order to find the ideal experimental parameters, PSO Experimenter will be used to optimize test functions that have trends similar to the response of a 3-D printer. 3-D printing is assumed to be a hyper-valley – many minima that are very close in fitness to the global minima, stretched out across the sample space [58]. Functions like the Beale function (equation 5) and the Goldstein-Price function (equation 6) are valley-like and will be used as benchmarks to set expectations for the physical experiments [59].

$$f(x, y) = (1.5 - x + xy)^2 + (2.25 - x + xy^2)^2 + (2.625 - x + xy^3)^2 \quad (2-5)$$

$$f(x, y) = [30 + (2x - 3y)^2(18 - 32x + 12x^2 + 48y - 36xy + 27y^2)] \quad (2-6)$$

The Beale function has a minimum of 0 at $f(3, 0.5)$, and the Goldstein-Price has a minimum of 3 at $(0, -1)$. Their respective plots can be seen in Figure 2.4.

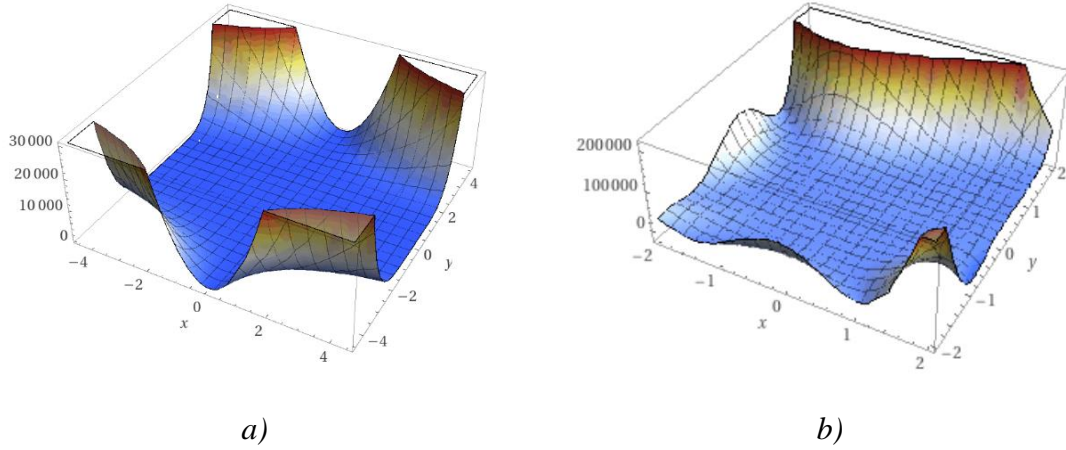


Figure 2.4. a. Plot of Beale function. b. Plot of Goldstein-Price function.

Each function is built into a spreadsheet such that the fitness is defined by the X and Y input values. First PSO Experimenter will be configured with a k_v of 0.1, k_p of 1 and k_g of 2. Each function will be tested for 20 iterations to generate a baseline, and then the velocity weight (which alters how explorative the particles are) will be set to 0.5. The responses will be compared, and the parameter set that yields the highest accuracy will be used in the physical experiments.

2.3.4 LDPE Optimization on Gigabot X Experiment Design

For the first optimization experiment single 200mm lines are extruded (Figure 2.5a). For this trial, physical dimensions including length (l) accuracy, width (w) accuracy, width constancy, and mass (m) accuracy. Accuracy is defined in Equation 2-7. Consistency is defined in Equation 2-8, where the measurements are evenly distributed along the length of the extrusion. The initial variable parameters are listed in Table 2.2.

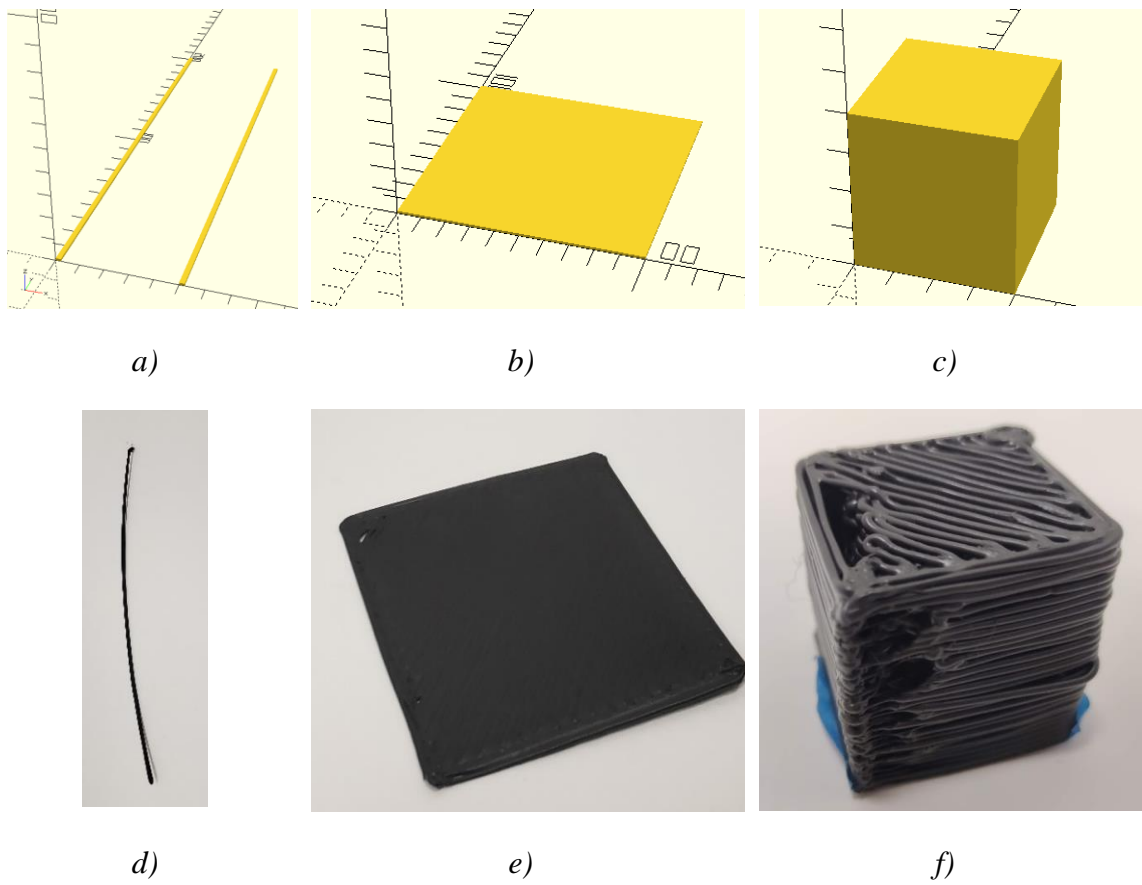


Figure 2.5: a. A rendering of the line test. b. A rendering of the plane test. c. A rendering of the cube test. d. An image of a resulting line test. e. An image of a resulting plane test. f. An image of a resulting cube test. It should be noted these test examples are before any optimization.

$$A(X_m, X_d) = \frac{|X_m - X_d|}{X_d} \quad (2-7)$$

Where X_m is the measured value (or in some cases the averaged measured value), and X_d is the desired value.

$$C(X_{m1}, X_{m2} \dots X_{mn}) = \text{avgdev}(X_{m1}, X_{m2}, \dots, X_{mn}) \quad (2-8)$$

Table 2.2: Experimental parameters for line optimization

Variable	Min	Max	Guess	Int?	Description
T_1	175°C	250°C	245°C	True	Temperature zone one on Gigabot X extruder
T_2	175°C	250°C	245°C	True	Temperature zone two on Gigabot X extruder
T_3	175°C	250°C	245°C	True	Temperature zone three on Gigabot X extruder
F	100%	300%	222%	False	Extrusion flow multiplier
T_B	80°C	120°C	100°C	True	Bed temperature
V_P	10 mm/s	60 mm/s	25 mm/s	False	Print speed (end effector movement rate)

The fitness function is defined by the weighted sum of the measurements (Equation 2-9). The weights are assigned according to expert knowledge. The experiment will use optimization parameters found from the test functions in the previous step, and will run for either 20 iterations, or until the fitness is less than 0.1.

$$f_{line} = 0.2C(w_{m1}, \dots, w_{m5}) + 0.2A(w_{avg}, 2.2mm) + 0.1A(l_m, 200mm) + 0.5A(m_m, 0.4g) \quad (2-9)$$

The second trial will be optimizing the length accuracy, width accuracy, height consistency, height accuracy, and mass accuracy of 100 by 100 mm planes (Figure 2.5b). The optimization parameters will remain the same with the addition of E , the edge overlap of the infill percentage (with a range of 10 to 20%, and initial guess of 15%). The initial guess values will be selected as the optimum parameters from the previous trial (with a proximity value of 0.25). For this trial, additional factors including layer height (h), and print time (t) will also be considered. The fitness function is defined in Equation 2-10.

$$f_{plane} = 0.1C(h_{m1}, \dots, h_{m5}) + 0.1A(h_{avg}, 1.01mm) + 0.1A(l_{avg}, 100mm) + 0.1A(w_{avg}, 100mm) + 0.1A(t_m, 6.5min) + 0.5A(m_m, 9.4g) \quad (2-10)$$

The final trial optimizes the height, width, length and mass accuracy of a 40 by 40 by 40mm cube (Figure 2.5c). The optimization parameters will once again remain the same with the inclusion of the layer height H_L ranging from 0.6mm to 1.5mm, and infill density D_I ranging from 100% to 250%. The initial guess will be selected as the optimum parameters from the plane trial (with a proximity of 0.25). The fitness function for this trial is shown in Equation 2-11.

$$f_{plane} = 0.1A(w_{avg}, 40mm) + 0.1A(l_{avg}, 40mm) + 0.1A(h_{avg}, 40mm) + 0.7A(m_m, 58.2g) \quad (2-11)$$

2.4 Results and Discussion

2.4.1 Parameter Acquisition

20 iterations of optimization on the Beale function were run on the waste LLDPE on the Gigabot X. The individual experiment fitnesses (particles) and group best fitness can be seen in Figure 2.6.

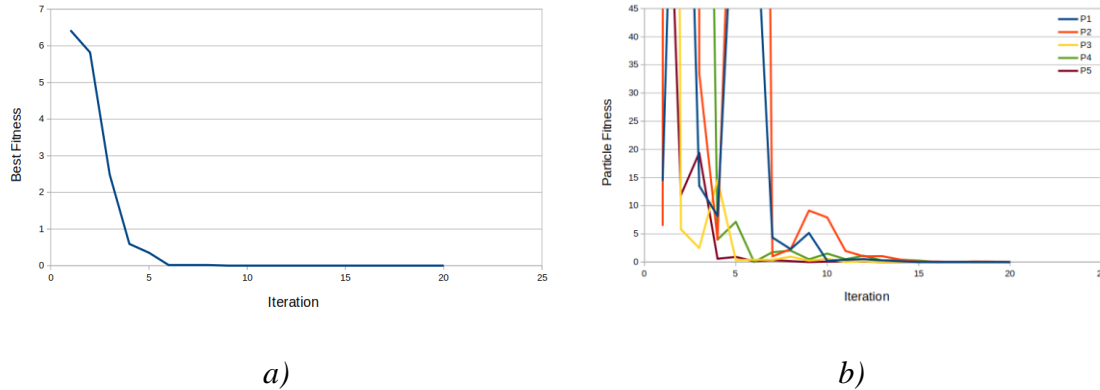


Figure 2.6: Performance of PSO on Beale function a. Total best fitness b. Particle fitness over time

Next, 20 iterations of optimization on the Golstein-Price function were run on the same material and process system. The individual particle fitnesses and group best fitness can be seen in Figure 2.7. Then optimization is run with a velocity weight of 0.5. The group fitnesses between both trials can be compared in Figure 2.8. The hypothesis that a higher velocity weight will cause more exploration has been confirmed, and in addition enabled particles to converge on a more desirable fitness value. This indicates that the parameters listed in Table 4 should be used for 3-D print optimization.

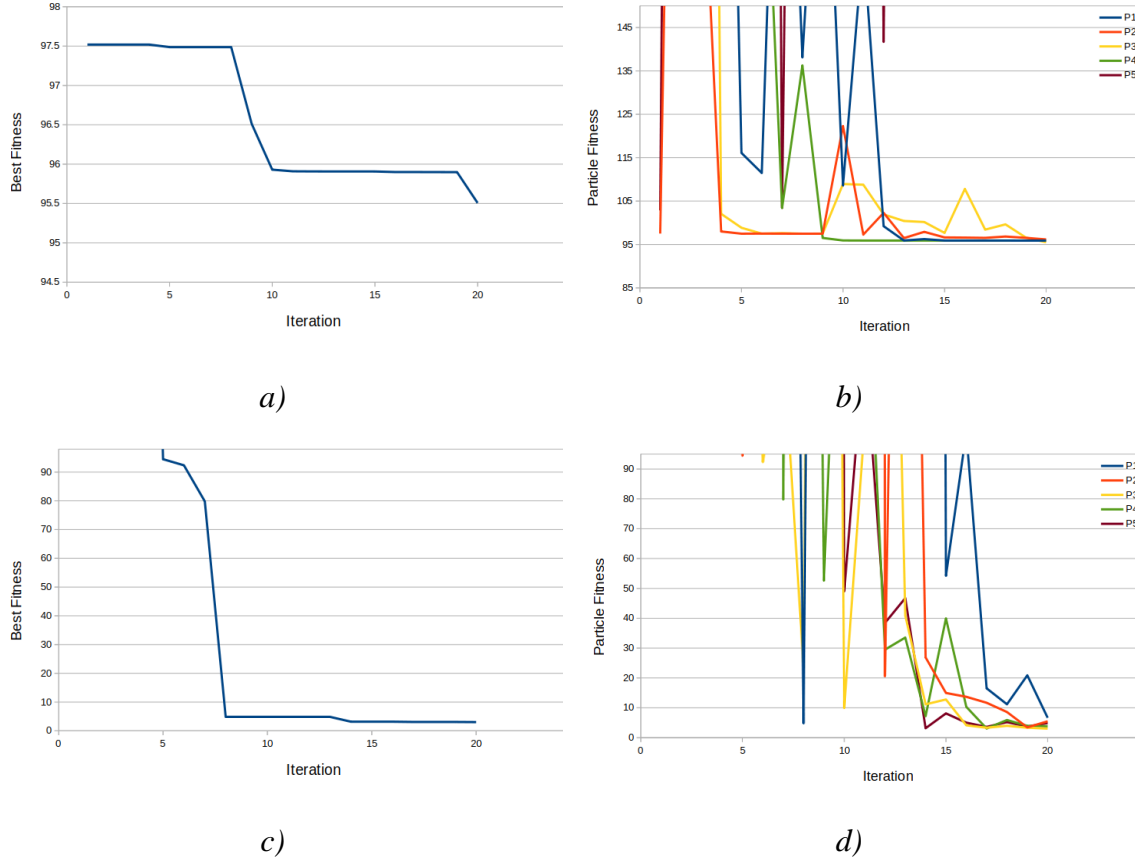


Figure 2.7: Performance of PSO on Goldstein-Price function a. Total best fitness with $k_v = 0.1$ b. Particle fitness over time $k_v = 0.1$ c. Total best fitness with $k_v = 0.5$ d. Particle fitness over time $k_v = 0.5$.

Table 2.4: Recommended parameters for PSO tuning of 3-D printing.

Variable	Value
k_v	0.5
k_p	1
k_g	2

In addition, from Figure 2.6a, the physical experiment should expect to see a convergence around 6 iterations. This experiment set successfully demonstrated that PSO Experimenter should be attempted for 3-D printer optimization.

2.4.2 LDPE Optimization on Gigabot X Results

The line trial was able to reach a fitness of less than 0.1 after 6 iterations. The optimization performance can be viewed in Figure 2.8. The ideal parameters for printing lines are listed in Table 2.5 column 3.

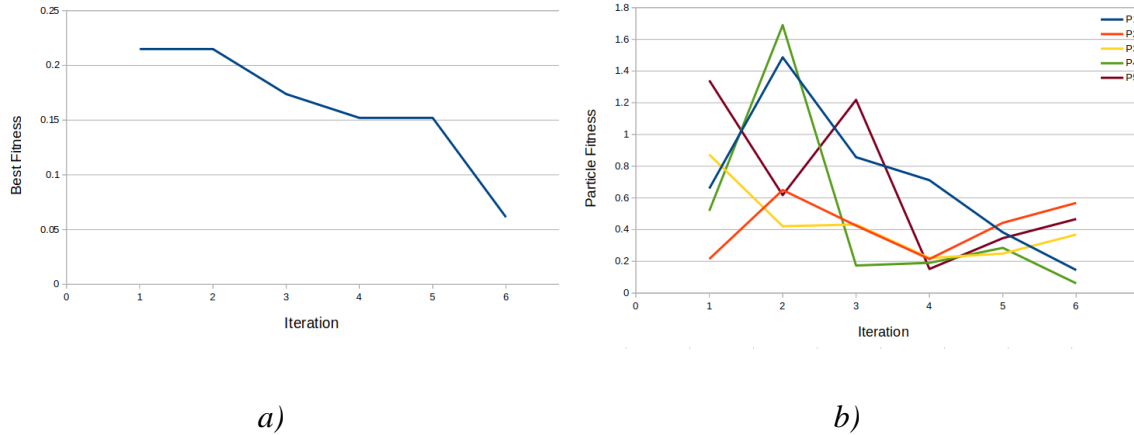


Figure 2.8: Performance of PSO on line tests a. Total best fitness b. Particle fitness over time

Table 2.5: Ideal printing parameters for FPF/FGF of waste LDPE on a three temperature zone extruder.

Var.	Description	Lines Value	Planes Value	Cube Value
T_1	Temperature zone one on Gigabot X extruder	225°C	220°C	225°C
T_2	Temperature zone two on Gigabot X extruder	200°C	200°C	205°C
T_3	Temperature zone three on Gigabot X extruder	175°C	172°C	166°C
F	Extrusion flow multiplier	150%	165%	156%
T_B	Bed temperature	90°C	95°C	94°C
V_P	Print speed (end effector movement rate)	10 mm/s	38 mm/s	35 mm/s
E	Edge Overlap of infill	NA	18%	18%
H_L	Layer Height	NA	NA	0.6mm
D_I	Infill Density	NA	NA	165%

The plane trial was able to reach a fitness of less than 0.1 after 1 iteration. The optimization performance can be viewed in Figure 2.9. The ideal parameters for printing planes are listed in Table 2.5 column 4.

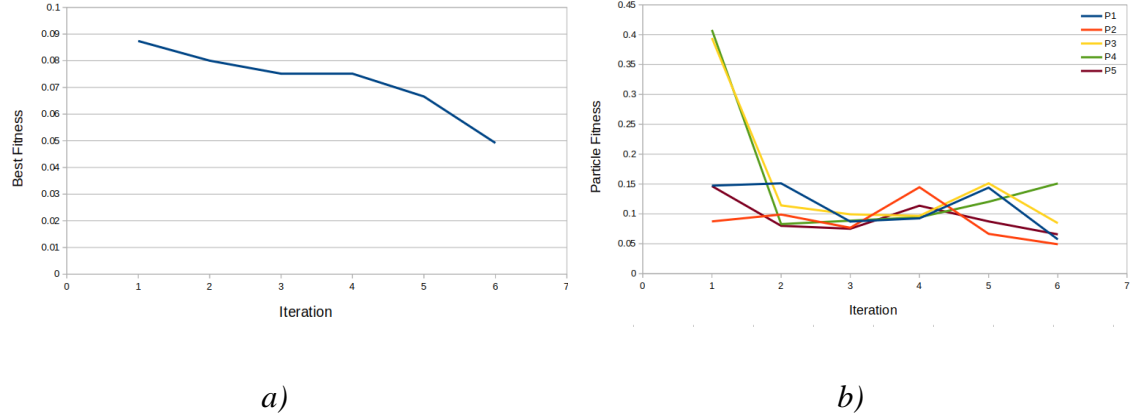


Figure 2.9: Performance of PSO on plane tests a. Total best fitness b. Particle fitness over time

The cube trial was able not able to reach a fitness of 0.1 after 6 iterations, but due to machine (inability to make perfectly square corners causes the volume estimate to be imprecise) limitations may not be achievable. The optimization performance can be viewed in Figure 2.10. The ideal parameters for printing lines are listed in Table 2.5 column 5, and these parameters are accepted as ideal parameters for general use in printing with LDPE. An additional result of this experimentation is the finding that the print surface should be covered in clear polypropylene packaging tape for optimum adhesion.

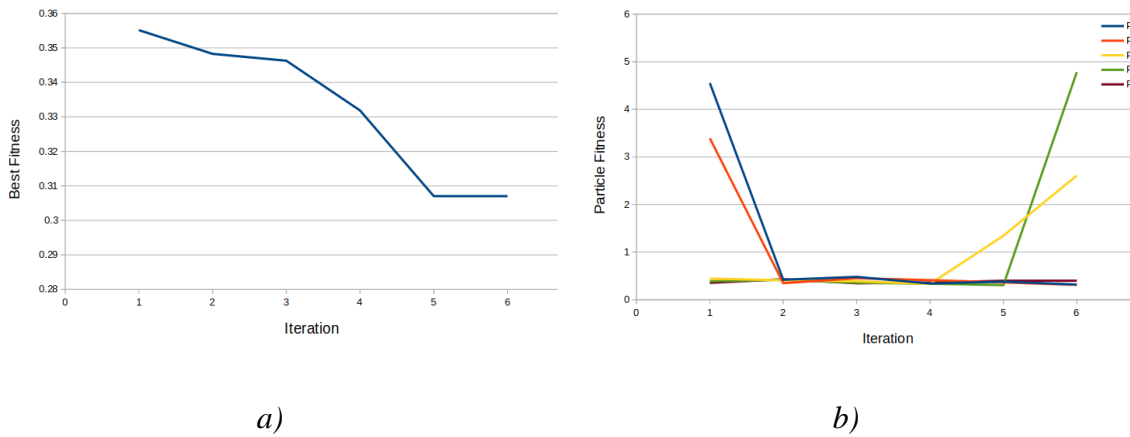


Figure 2.10: Performance of PSO on cube tests a. Total best fitness and b. Particle fitness over time.

The optimization improved the print quality as shown in Figure 2.11, an optimized test cube, which can be compared directly to Figure 2.5f. The print is not a complete digital replication of the design as there still is some deformation at the base and not quite perfect final layer print. This is somewhat expected because LLDPE is a known challenging 3-D printing material with only a few vendors offering it [60].



Figure 2.11. Optimized print setting results of LDPE waste printed into a test cube.

The printing quality, however, is high enough to be used for large (human)-scale functional objects as this stool as shown in Figure 2.12. The device has a mass of 0.56lb, which at a cost of \$1/lb and 0.28lb of PETG used for the legs at \$9.50 per pound [61] results in a cost for the stool of \$3.22. This is an 87 percent savings from commercial devices that can cost over \$24 [62], and could be further reduced using reclaimed materials for legs. These results agree with past work [63] that found substantial economic potential for DRAM [61] including specific investigations on the potential for large-scale 3-D printing of athletic equipment from plastic waste [49].



Figure 2.12. An LDPE 3-D Printed Stool base on PETG legs.

2.4.3 Impact and Applications

The time for preparation, printing, and measurement of a line sample takes approximately 10 minutes. With the first physical trial settling below a fitness of 0.1 after 6 iterations, the total time elapsed is 5 hours. If this same experiment were to be run as a conservative matrix test, where temperature zones are all kept at the same temperature and tested across 10 increments, bed temp is kept at a constant, and federate and print speed's range was cut into 10 increments it would require over 166 hours. This indicates that PSO Experiment can provide 97% reduction in research time for 3-D printing optimization. Because of this, PSO Experiment is recommended for all future material parameter acquisition, as it can explore the sample space with self-adjusting granularity and can substantially reduce time, money, and material usage. This is in line with past work that showed PSO utility for build orientation [64] support structures [65] and fused filament 3-D printing [66].

This accelerated testing for new materials is particularly useful in the DRAM context as the 3-D printing process parameter optimization may need to be completed for each new waste material source, even if the primary polymer is the same. This is because past results have shown that not only do additives and processing matter but so does color [30], number of cycles [9], water absorption and thus storage and thermal history as well as source [24] can impact 3-D printing parameter optimization and final properties of the manufactured part.

PSO Experimenter could be used to optimize not only waste materials but also various other materials such as polypropylene or high density polyethylene, which are not yet commonly used in commercial fused filament-based 3-D printing because of their challenging thermal expansion coefficients. In addition, the software could be used to take the guess work out of tuning and calibrating machines like circuit mills [67], metal 3-D printers [68] and bio-printers [1].

2.4.4 PSO vs Random Selection

Particle Swarm Optimization is not a random walk [52], it has a directed search which lowers optimization time. As a comparison, if the optimization process was defined such that there are 1000 combinations of variables, the probability of randomly selecting the optimum is 0.1%. Considering an equal number of trials to the PSO (30 per experiment) as Bernoulli trials with a success probability of 0.1%, the probability of successfully identifying a global optimum can be modeled as a Binomial Random Variable [69]. This model shows that arbitrary guessing of combinations yields a 2.91% chance of successfully arriving at the optimum. Clearly each optimization run performed in this manuscript has arrived at acceptable optimums, indicating that the PSO algorithm is aiding in the process and it is not pure randomness.

2.4.5 Future Work

PSO Experimenter can be further improved by being integrated directly into a printer control software, to directly control the machine for experiments. Additionally, PSO

experimenter can be applied to a myriad of diverse applications such as: custom filament extrusion, circuit board milling, recipes and farming.

2.5 Conclusions

PSO Experimenter was created to expedite the acquisition of ideal process parameters. As a case study, the free and open software was used to find ideal parameters for recycled waste LDPE direct extrusion 3D printing using an open source AM system. The algorithm was able to find ideal parameters in 6 iterations, taking a time of 5 hours. This time saving results in an 97% reduction from matrix-based process parameter testing. PSO Experimenter is a user-friendly and effective free software for finding ideal parameters for DRAM as well as a wide range of fields and processes.

2.6 References

1. Krige, Adolf, Jakub Haluška, Ulrika Rova, and Paul Christakopoulos. "Design and Implementation of a Low Cost Bio-Printer Modification, Allowing for Switching between Plastic and Gel Extrusion." *HardwareX* 9 (April 1, 2021): e00186. <https://doi.org/10.1016/j.ohx.2021.e00186>.
2. Abdollahi, Sara, Alexander Davis, John H. Miller, and Adam W. Feinberg. "Expert-Guided Optimization for 3D Printing of Soft and Liquid Materials." *PLOS ONE* 13, no. 4 (April 5, 2018): e0194890. <https://doi.org/10.1371/journal.pone.0194890>.
3. Lee, Jian-Yuan, Jia An, and Chee Kai Chua. "Fundamentals and Applications of 3D Printing for Novel Materials." *Applied Materials Today* 7 (June 1, 2017): 120–33. <https://doi.org/10.1016/j.apmt.2017.02.004>.
4. Kulkarni, Apoorv, Gian Domenico Sorarù, and Joshua M. Pearce. "Polymer-derived SiOC replica of material extrusion-based 3-D printed plastics." *Additive Manufacturing* 32 (2020): 100988. <https://doi.org/10.1016/j.addma.2019.100988>.
5. Veteška, Peter, Zora Hajdúchová, Jozef Feranc, Katarína Tomanová, Ján Milde, Michaela Kritikos, Ľuboš Bača, and Marián Janek. "Novel Composite Filament Usable in Low-Cost 3D Printers for Fabrication of Complex Ceramic Shapes." *Applied Materials Today* 22 (March 1, 2021): 100949. <https://doi.org/10.1016/j.apmt.2021.100949>.
6. Menon, Aditya, Barnabás Póczos, Adam W. Feinberg, and Newell R. Washburn. "Optimization of Silicone 3D Printing with Hierarchical Machine Learning." *3D Printing and Additive Manufacturing* 6, no. 4 (August 1, 2019): 181–89. <https://doi.org/10.1089/3dp.2018.0088>.
7. Feng, Chunyan, Min Zhang, and Bhesh Bhandari. "Materials Properties of Printable Edible Inks and Printing Parameters Optimization during 3D Printing: A Review." *Critical Reviews in Food Science and Nutrition* 59, no. 19 (October 28, 2019): 3074–81. <https://doi.org/10.1080/10408398.2018.1481823>.
8. Hunt, E.J.; Zhang, C.; Anzalone, N.; Pearce, J.M. Polymer recycling codes for distributed manufacturing with 3-D printers. *Resour. Conserv. Recycl.* 2015, 97, 24–30, doi:10.1016/j.resconrec.2015.02.004.

9. Sanchez, F.A.C.; Lanza, S.; Boudaoud, H.; Hoppe, S.; Camargo, M. Polymer Recycling and Additive Manufacturing in an Open Source context: Optimization of processes and methods.; 2015; p. 1591.
10. Cruz Sanchez, F.A.; Boudaoud, H.; Hoppe, S.; Camargo, M. Polymer recycling in an open-source additive manufacturing context: Mechanical issues. *Addit. Manuf.* 2017, 17, 87–105, doi:10.1016/j.addma.2017.05.013.
11. Anderson, I. Mechanical Properties of Specimens 3D Printed with Virgin and Recycled Polylactic Acid. *3D Print. Addit. Manuf.* 2017.
12. Pakkanen, J.; Manfredi, D.; Minetola, P.; Iuliano, L. About the Use of Recycled or Biodegradable Filaments for Sustainability of 3D Printing. In Proceedings of the Sustainable Design and Manufacturing 2017; Campana, G., Howlett, R.J., Setchi, R., Cimatti, B., Eds.; Springer International Publishing: Cham, 2017; pp. 776–785.
13. Zhong, S.; Pearce, J.M. Tightening the loop on the circular economy: Coupled distributed recycling and manufacturing with recyclebot and RepRap 3-D printing. *Resour. Conserv. Recycl.* 2018, 128, 48–58, doi:10.1016/j.resconrec.2017.09.023.
14. Mohammed, M.I.; Wilson, D.; Gomez-Kervin, E.; Tang, B.; Wang, J. Investigation of Closed-Loop Manufacturing with Acrylonitrile Butadiene Styrene over Multiple Generations Using Additive Manufacturing. *ACS Sustain. Chem. Eng.* 2019, 7, 13955–13969, doi:10.1021/acssuschemeng.9b02368.
15. Mohammed, M.I.; Wilson, D.; Gomez-Kervin, E.; Vidler, C.; Rosson, L.; Long, J. The Recycling of E-Waste ABS Plastics by Melt Extrusion and 3D Printing Using Solar Powered Devices as a Transformative Tool for Humanitarian Aid. 13.
16. Mohammed, M.I.; Wilson, D.; Gomez-Kervin, E.; Rosson, L.; Long, J. EcoPrinting: Investigation of Solar Powered Plastic Recycling and Additive Manufacturing for Enhanced Waste Management and Sustainable Manufacturing. In Proceedings of the 2018 IEEE Conference on Technologies for Sustainability (SusTech); 2018; pp. 1–6.
17. Boldizar, A.; Möller, K. Degradation of ABS during repeated processing and accelerated ageing. *Polym. Degrad. Stab.* 2003, 81, 359–366, doi:10.1016/S0141-3910(03)00107-1.
18. Baechler, C.; DeVuono, M.; Pearce, J.M. Distributed recycling of waste polymer into RepRap feedstock. *Rapid Prototyp. J.* 2013, 19, 118–125, doi:10.1108/13552541311302978.
19. Chong, S.; Pan, G.-T.; Khalid, M.; Yang, T.C.-K.; Hung, S.-T.; Huang, C.-M. Physical Characterization and Pre-assessment of Recycled High-Density Polyethylene as 3D Printing Material. *J. Polym. Environ.* 2017, 25, 136–145, doi:10.1007/s10924-016-0793-4.
20. Pepi, M.; Zander, N.; Gillan, M. Towards Expeditionary Battlefield Manufacturing Using Recycled, Reclaimed, and Scrap Materials. *JOM* 2018, 70, 2359–2364, doi:10.1007/s11837-018-3040-8.
21. Oblak, P.; Gonzalez-Gutierrez, J.; Zupančič, B.; Aulova, A.; Emri, I. Processability and mechanical properties of extensively recycled high density polyethylene. *Polym. Degrad. Stab.* 2015, 114, 133–145, doi:10.1016/j.polymdegradstab.2015.01.012.
22. Woern, A.L.; Pearce, J.M. Distributed Manufacturing of Flexible Products: Technical Feasibility and Economic Viability. *Technologies* 2017, 5, 71, doi:10.3390/technologies5040071.

23. Lee, J.H.; Lim, K.S.; Hahm, W.G.; Kim, S.H. Properties of recycled and virgin poly(ethylene terephthalate) blend fibers. *J. Appl. Polym. Sci.* 2013, 128, 1250–1256, doi:10.1002/app.38502.
24. Little, Helen A., Nagendra G. Tanikella, Matthew J Reich, Matthew J. Fiedler, Samantha L. Snabes, and Joshua M. Pearce. "Towards distributed recycling with additive manufacturing of PET flake feedstocks." *Materials* 13, no. 19 (2020): 4273.
25. Reich, M.J.; Woern, A.L.; Tanikella, N.G.; Pearce, J.M. Mechanical Properties and Applications of Recycled Polycarbonate Particle Material Extrusion-Based Additive Manufacturing. *Materials* 2019, 12, 1642, doi:10.3390/ma12101642.
26. Woern, Aubrey L., Joseph R. McCaslin, Adam M. Pringle, and Joshua M. Pearce. "RepRapable Recyclebot: Open Source 3-D Printable Extruder for Converting Plastic to 3-D Printing Filament." *HardwareX* 4 (October 1, 2018): e00026. <https://doi.org/10.1016/j.ohx.2018.e00026>.
27. Pavlo, S.; Fabio, C.; Hakim, B.; Mauricio, C. 3D-Printing Based Distributed Plastic Recycling: A Conceptual Model for Closed-Loop Supply Chain Design. In Proceedings of the 2018 IEEE International Conference on Engineering, Technology and Innovation (ICE/ITMC); 2018; pp. 1–8.
28. Cruz Sanchez, F.A.; Boudaoud, H.; Camargo, M.; Pearce, J.M. Plastic recycling in additive manufacturing: A systematic literature review and opportunities for the circular economy. *J. Clean. Prod.* 2020, 264, 121602, doi:10.1016/j.jclepro.2020.121602.
29. Gwamuri, J.; Wittbrodt, B.T.; Anzalone, N.C.; Pearce, J.M. Reversing the Trend of Large Scale and Centralization in Manufacturing: The Case of Distributed Manufacturing of Customizable 3-D-Printable Self-Adjustable Glasses; Social Science Research Network: Rochester, NY, 2014;
30. Wittbrodt, B.T.; Glover, A.G.; Laureto, J.; Anzalone, G.C.; Oppliger, D.; Irwin, J.L.; Pearce, J.M. Life-cycle economic analysis of distributed manufacturing with open-source 3-D printers. *Mechatronics* 2013, 23, 713–726, doi:10.1016/j.mechatronics.2013.06.002.
31. Petersen, E.E.; Pearce, J. Emergence of Home Manufacturing in the Developed World: Return on Investment for Open-Source 3-D Printers. *Technologies* 2017, 5, 7, doi:10.3390/technologies5010007.
32. Petersen, E.E.; Kidd, R.W.; Pearce, J.M. Impact of DIY Home Manufacturing with 3D Printing on the Toy and Game Market. *Technologies* 2017, 5, 45, doi:10.3390/technologies5030045.
33. Laplume, A.O.; Petersen, B.; Pearce, J.M. Global value chains from a 3D printing perspective. *J. Int. Bus. Stud.* 2016, 47, 595–609, doi:10.1057/jibs.2015.47.
34. Kreiger, M.; Anzalone, G.C.; Mulder, M.L.; Glover, A.; Pearce, J.M. Distributed Recycling of Post-Consumer Plastic Waste in Rural Areas. *MRS Online Proc. Libr. Arch.* 2013, 1492, 91–96, doi:10.1557/opl.2013.258.
35. Kreiger, M.A.; Mulder, M.L.; Glover, A.G.; Pearce, J.M. Life cycle analysis of distributed recycling of post-consumer high density polyethylene for 3-D printing filament. *J. Clean. Prod.* 2014, 70, 90–96, doi:10.1016/j.jclepro.2014.02.009.

36. Zhong, S.; Rakhe, P.; Pearce, J.M. Energy Payback Time of a Solar Photovoltaic Powered Waste Plastic Recyclebot System. *Recycling* 2017, 2, 10, doi:10.3390/recycling2020010.
37. Tian, X.; Liu, T.; Wang, Q.; Dilmurat, A.; Li, D.; Ziegmann, G. Recycling and remanufacturing of 3D printed continuous carbon fiber reinforced PLA composites. *J. Clean. Prod.* 2017, 142, 1609–1618, doi:10.1016/j.jclepro.2016.11.139.
38. Parandoush, P.; Lin, D. A review on additive manufacturing of polymer-fiber composites. 2017, doi:10.1016/j.compstruct.2017.08.088.
39. Heller, B.P.; Smith, D.E.; Jack, D.A. Planar deposition flow modeling of fiber filled composites in large area additive manufacturing. *Addit. Manuf.* 2019, 25, 227–238, doi:10.1016/j.addma.2018.10.031.
40. Pringle, A.M.; Rudnicki, M.; Pearce, J.M. Wood Furniture Waste-Based Recycled 3-D Printing Filament. *For. Prod. J.* 2017, 68, 86–95, doi:10.13073/FPJ-D-17-00042.
41. Zander, N.E. Recycled Polymer Feedstocks for Material Extrusion Additive Manufacturing. In *Polymer-Based Additive Manufacturing: Recent Developments*; ACS Symposium Series; American Chemical Society, 2019; Vol. 1315, pp. 37–51 ISBN 978-0-8412-3426-0.
42. Dertinger, S.C.; Gallup, N.; Tanikella, N.G.; Grasso, M.; Vahid, S.; Foot, P.J.S.; Pearce, J.M. Technical pathways for distributed recycling of polymer composites for distributed manufacturing: Windshield wiper blades. *Resour. Conserv. Recycl.* 2020, 157, 104810, doi:10.1016/j.resconrec.2020.104810.
43. Meyer, T.K.; Tanikella, N.G.; Reich, M.J.; Pearce, J.M. Potential of distributed recycling from hybrid manufacturing of 3-D printing and injection molding of stamp sand and acrylonitrile styrene acrylate waste composite. *Sustain. Mater. Technol.* 2020, 25, e00169, doi:10.1016/j.susmat.2020.e00169.
44. Zander, N.E.; Gillan, M.; Burckhard, Z.; Gardea, F. Recycled polypropylene blends as novel 3D printing materials. *Addit. Manuf.* 2019, 25, 122–130, doi:10.1016/j.addma.2018.11.009.
45. Shakor, P., Nejadi, S., Sutjipto, S., Paul, G., & Gowripalan, N. (2020). Effects of deposition velocity in the presence/absence of E6-glass fibre on extrusion-based 3D printed mortar. *Additive Manufacturing*, 32, 101069.
46. Kretzschmar, N., Lippinen, S., Klar, V., Pearce, J.M., Ranger, T.L., Seppälä, J. and Partanen, J., 2019. Mechanical properties of ultraviolet-assisted paste extrusion and postextrusion ultraviolet-curing of three-dimensional printed biocomposites. *3D Printing and Additive Manufacturing*, 6(3), pp.127-137.
47. Woern, Aubrey L., Dennis J. Byard, Robert B. Oakley, Matthew J. Fiedler, Samantha L. Snabes, and Joshua M. Pearce. "Fused Particle Fabrication 3-D Printing: Recycled Materials' Optimization and Mechanical Properties." *Materials* 11, no. 8 (August 2018): 1413. <https://doi.org/10.3390/ma11081413>.
48. Alexandre, Arthur, Fabio A. Cruz Sanchez, Hakim Boudaoud, Mauricio Camargo, and Joshua M. Pearce. "Mechanical properties of direct waste printing of polylactic acid with universal pellets extruder: comparison to fused filament fabrication on open-source desktop three-dimensional printers." *3D Printing and Additive Manufacturing* 7, no. 5 (2020): 237-247.

49. Byard, D. J., Woern, A. L., Oakley, R. B., Fiedler, M. J., Snabes, S. L., & Pearce, J. M. "Green fab lab applications of large-area waste polymer-based additive manufacturing". *Additive Manufacturing*, 27, (2019): 515-525.
50. Nilsiam, Yuenyong. "Low-Cost Open-Source Gmaw-Based Metal 3-D Printing: Monitoring, Slicer, Optimization, and Applications." ProQuest Dissertations and Theses. Ph.D., Michigan Technological University, 2017. <https://www.proquest.com/docview/1911305832/abstract/E27C5CA169F24F0FPQ/1>.
51. Keller, James M., Derong Liu, and David B. Fogel. *Fundamentals of Computational Intelligence: Neural Networks, Fuzzy Systems, and Evolutionary Computation*. John Wiley & Sons, 2016.
52. Saad, Mohd Sazli, Azuwir Mohd Nor, Mohamad Ezral Baharudin, Mohd Zakimi Zakaria, and A.F Aiman. "Optimization of Surface Roughness in FDM 3D Printer Using Response Surface Methodology, Particle Swarm Optimization, and Symbiotic Organism Search Algorithms." *The International Journal of Advanced Manufacturing Technology* 105, no. 12 (December 1, 2019): 5121–37. <https://doi.org/10.1007/s00170-019-04568-3>.
53. S. Oberloier, PSO Experimenter, (2021). <https://osf.io/muevs/> (accessed July 22, 2021).
54. Hart, K.R.; Frketic, J.B.; Brown, J.R. Recycling meal-ready-to-eat (MRE) pouches into polymer filament for material extrusion additive manufacturing. *Addit. Manuf.* 2018, 21, 536–543, doi:10.1016/j.addma.2018.04.011.
55. "Gigabot X Update – Re:3D | Life-Sized Affordable 3D Printing." Accessed July 7, 2021. <https://re3d.org/gigabotx-update/>.
56. A. Banks, J. Vincent, C. Anyakoha, A review of particle swarm optimization. Part I: background and development, *Nat Comput.* 6 (2007) 467–484. <https://doi.org/10.1007/s11047-007-9049-5>.
57. Wang, Dongshu, Dapei Tan, and Lei Liu. "Particle Swarm Optimization Algorithm: An Overview." *Soft Computing* 22, no. 2 (January 2018): 387–408. <https://doi.org/10.1007/s00500-016-2474-6>.
58. Tanikella, Nagendra G., Ben Wittbrodt, and Joshua M. Pearce. "Tensile Strength of Commercial Polymer Materials for Fused Filament Fabrication 3D Printing." *Additive Manufacturing* 15 (May 1, 2017): 40–47. <https://doi.org/10.1016/j.addma.2017.03.005>.
59. Bossek, Jakob. "Smoof: Single- and Multi-Objective Optimization Test Functions." *The R Journal* 9, no. 1 (2017): 103. <https://doi.org/10.32614/RJ-2017-004>
60. LLDPE Filament - Natural - 1.75mm - 1KG, Filaments.Ca. (2021). <https://filaments.ca/products/lldpe-filament-natural-1-75mm> (accessed October 26, 2021).
61. Amazon.com: Amazon Basics PETG 3D Printer Filament, 1.75mm, Black, 1 kg Spool : Industrial & Scientific, (2021). <https://www.amazon.com/dp/B07T4X4D2C/> (accessed November 13, 2021).
62. Amazon.com: DOI TOOL Plastic Stool Childrens Stool Household Stool Anti- Slip Seat Stool Chair for Living Room Study Room Bathroom : Home & Kitchen. <https://www.amazon.com/dp/B091GMYGTR/> (accessed October 25, 2021).

63. Santander, Pavlo, Fabio A. Cruz Sanchez, Hakim Boudaoud, and Mauricio Camargo. "Closed loop supply chain network for local and distributed plastic recycling for 3D printing: a MILP-based optimization approach." *Resources, Conservation and Recycling* 154 (2020): 104531.
64. H. Shen, X. Ye, G. Xu, L. Zhang, J. Qian, J. Fu, 3D printing build orientation optimization for flexible support platform, *Rapid Prototyping Journal*. 26 (2019) 59–72. <https://doi.org/10.1108/RPJ-09-2018-0252>.
65. Zhu, L., Feng, R., Li, X., Xi, J. and Wei, X., 2019. A Tree-Shaped Support Structure for Additive Manufacturing Generated by Using a Hybrid of Particle Swarm Optimization and Greedy Algorithm. *Journal of Computing and Information Science in Engineering*, 19(4).
66. Dey, A., Hoffman, D. and Yodo, N., 2020. Optimizing multiple process parameters in fused deposition modeling with particle swarm optimization. *International Journal on Interactive Design and Manufacturing (IJIDeM)*, 14(2), pp.393-405.
67. Oberloier, Shane, and Joshua M. Pearce. "Belt-Driven Open Source Circuit Mill Using Low-Cost 3-D Printer Components." *Inventions* 3, no. 3 (September 2018): 64. <https://doi.org/10.3390/inventions3030064>.
68. Nilsiam, Y., Sanders, P. and Pearce, J.M., 2017. Slicer and process improvements for open-source GMAW-based metal 3-D printing. *Additive Manufacturing*, 18, pp.110-120.
69. A. Leon-Garcia, *Probability, Statistics, and Random Processes for Electrical Engineering*, Prentice Hall, 2008.

3 Open Source Framework for a Broadly Expandable and Reconfigurable Data Acquisition and Automation Device (BREAD)

3.1 Hardware in context

The global library of open source electronic designs is constantly expanding and diversifying [1]. Examples include systems to accurately measure gas pressures [2] and properties [3]. There are devices used to aid in electrical engineering endeavours such as power monitoring [4] and phasor measurement [5] as well as complex fields such as neuroscience [6, 7], electrophoresis [8], and nuclear physics [9]. Platforms promoting and enabling citizen participation on environmental science have been prototyped [10, 11]. These devices are all made to carry out a hand full of functions well, but are often not capable of scaling up or easily being integrated with other designs. Just as other open source projects have found success by having modular frameworks and clearly documented specifications [1, 12-14], a framework to unify and enable interoperation of these open source electronics systems would be greatly beneficial to the scientific community.

Though open-source data acquisition (DAQ) systems have been published [15-17], National Instruments (closed source, proprietary) systems are used extensively in academia for diverse purposes ranging from analysis of agricultural tools [18] and snow analysis [19] to CNC systems [20] and battery research [21]. National Instruments cDAQ [22] systems are often chosen for their flexibility, modular design, and plug-and-play operation. The cost of such systems and those from their commercial competitors can be prohibitively expensive, ranging around \$1,000 USD for a chassis and anywhere between \$138 USD to \$2,846 USD per function card [22]. These costs limit access to high-quality DAQ in low resource settings [23], separating haves and have-nots [24]. In many cases the functions executed by the cDAQ cards could be carried out by an open source alternative, however as desired function count increases, the simplicity of integrating the designs decreases substantially.

To overcome these challenges and ensure greater accessibility to high-quality electronics sensing and DAQ systems, this manuscript proposes a framework where new open source electronics can be developed and have plug-and-play functionality with all other modules designed in this framework. The system, titled Broadly Reconfigurable and Expandable Automation Device (BREAD), consists of a basic set of guidelines and requirements to which others can contribute.

3.2 Hardware description

BREAD first and foremost is a set of specifications with intent to unify open source electronic designs as an open source DAQ and automation platform, and as such the focus of this manuscript will be on the generalized guidelines. Several daughter cards (referred to as slices), and a backplane (referred to as a loaf) have been developed and will also be

described. Finally, an example system for metal 3-D printing will be proposed, designed, built, tested and validated.

3.2.1 Schematic Design Procedures for Slices

First, the schematic standards will be laid out. Though many of the standards in this section do not effect the final design, proper and consistent documentation is crucial to the success of open source hardware projects [25-26].

3.2.1.1 Starting Out the Design

Every BREAD slice board design should be duplicated from the template slice, SLC-TEMP. This ensures that the mechanical dimensions of the board are correct, as well as the interface pin assignment. The design files can be modified using the most recent version the open source KiCAD [27].

3.2.1.2 Design Standards & Conventions

Standard Components & Connections

The standard components in the template design (included in SLC-TEMP) are essential for communication, computation, and measurement, and therefore should not be modified or moved in any way. Additionally, they should not be directly connected to, instead each connection should be made using net labels. The “bus” wiring functionality should only be used if 5 or more highly-coupled signals are present.

The standard components provided in the template include an Arduino Nano, interface connector, and power filtering capacitors. Together these components provide a robust system for commutation, measurement and control.

Component Selection

When possible, all discrete components should be of a 1206 (3.2mm x 1.6mm footprint) package or greater. Only commonly-available decade values should be used for discrete components such as resistors and capacitors. When selecting specialized components (i.e. Application Specific Integrated Circuits or ASICs), select the package that is easiest to be soldered (if possible, select through hole, socket-able chips).

Sub-Circuits

All designs should be split into sub-circuits. In most cases, each ASIC, filter, supply, conditioner, etc. should be their own sub-circuit. If a sub-circuit is repeated more than twice, it should be copied into a hierarchical sheet and replicated. All sub-circuits should interconnect using net labels.

Aesthetics, Labelling, and Comments

All net routing should be made such that there is minimal visual cross-over, and nets should be spread apart when possible. Though it is not required – any and all nets can be labelled. All sub-circuits should be surrounded by a graphical box with a title at the top. If enough space is available, a short description of the sub-circuit should be included. Labelling and terminology should be non-specific so sub-circuits can seamlessly be copied to new designs. All jumpers must be clearly labelled, as well as their default state. A jumper configuration table is recommended as shown in Table 3.1.

Table 3.1. An example jumper configuration table.

Jumper ID	Pin 0 & 1 Bridged	Pin 1 & 2 Bridged
J0	Utilize External Voltage Source	Utilize Internal Voltage Source
J1	AC Measurement Mode	DC Measurement Mode

Annotation & Net-List Generation

When annotating the schematics (generating component numbers and names) select the “First free after sheet number x100” option. This will help especially in designs which use hierarchical sheets. The standard components may be renamed. Generated net-lists should have the same name as the .pro file.

3.2.2 Board Design Procedures for Slices

3.2.2.1 Starting out the Design

The layout (kicad_pcb) file is included with the template design slice (included in SLC-TEMP). It is highly recommended that this layout be adapted for all designs for the sake of a consistent library of slices.

3.2.2.2 Considerations for Digital Manufacturing

As BREAD is an open-source system geared toward DIY engineers, scientists, and makers, it is highly desirable that the boards are manufacturable on commonly available circuit milling machines [28-29]. Designs that meet these criteria should:

- Have routing all done on a single layer (on the bottom layer)
- All surface-mount components should be flipped to the bottom layer
- All through-hole components should remain on the top layer
- Minimum trace size: 0.5mm, minimum feature spacing: 0.2mm, pad copper width > 0.5mm
- When trace cross-over is unavoidable use the second layer, but also use vias such that a fine-gauge wire can be substituted as a bridge.

- Do not use planes if possible – they can cause redundant milling for some CAM software packages.

It is also recognized that some boards cannot conform to these standards due to required parts, complexity, etc. In these cases, it is allowed. The goal of BREAD is to be an inclusive family of components, but the ability to digitally manufacture most boards is something that can be valuable to BREAD's overall success [25].

3.2.2.3 Design Standards & Conventions

Component placement

When placing components, take into consideration that the boards may be assembled by in-experienced solderers. Parts should be placed with clearance between one another to make accidental solder-bridging less likely. Additionally, components should be grouped with other components from their sub-circuit. All large components (likely through-hole) should stay on the top of the board. Devices that may generate heat should be given suitable clearance to dissipate the heat.

Routing

To reiterate a previously mention standard: If the board is a single layer - when trace cross-over is unavoidable use the second layer, but also use vias such that a fine-gauge wire can be substituted.

If the board is dual layer – the top layer's traces should be predominately vertical, and the bottom layer's traces should be predominately horizontal. If possible use large enough vias (1mm) with pads around them so that any users that can mill two-sided boards can use a thin wire to connect both sides of the via. If the board is more than 2 layers – it is outside of the range of the vast majority of DIYers, and thus the board will have to be manufactured professionally. In this case, considerations for PCB millers can be removed. Traces should be appropriately sized for their expected currents.

Planes

In most cases, planes are used for power distribution. For two-layer boards, the ground should be on the top layer, and the dominant supply voltage should be the bottom layer. Designers should sure to include proper thermal reliefs for any connections to the plane.

Labeling

All device designators should be in the same orientation and not covered by any devices. Jumpers should have indicators on what each one controls. All test points should have their corresponding net names labelling them. Each pin on the outgoing connector should have a clear label, as well as any indicator LEDs. The interface connector does not need labelled. The design should have a board designator with the following information:

- Card Name
- Part #

- Rev # and year

Finally, the OSH logo should be visible somewhere on the board (preferably near the board designator). An example of a board designator is shown below in Figure 3.1.



Figure 3.1: An example board designator and OSH logo

Gerber Generation

When generating gerbers, be sure that the grid origin and the drill and place offset are both at the bottom left corner of the board. Be sure to select “use auxiliary axis as origin” and generate the F.Cu, B.Cu, F.Paste, B.Paste, F.SilkS, B.SilkS, F.Mask, B.Mask, and Edge.Cuts layers. Additionally, generate all drill files and be sure to use the auxiliary axis as the drill origin. Having a properly placed auxiliary axis is helpful to those assembling with pick-and-place machines.

3.2.3 Documentation Procedures for Slices

3.2.3.1 Standard Datasheet

BREAD_SLC_TEMP_R0.odt is provided with the SLC_TEMP repository, and should be filled out according to the instructions embedded in the document. With each revision of the circuit, the document should be revisited (and the revision section should have notes on what was changed).

3.2.3.2 Repository

Though it is not required, it is highly recommended that the slice documentation and design files are hosted in an Open Science Framework (OSF) repository [30]. The repository should be organized by dividing it into 5 folders:

- Documentation
- Electrical Designator
- Firmware
- Gerbers
- Mechanical

3.2.4 Mechanical Definitions for Slices

3.2.4.1 PCB Dimensions

Slices are constructed on an 100mm by 70mm board with 4 mounting holes for am M3 bolt inset 5mm into the board at each corner (See Figure 3.2).

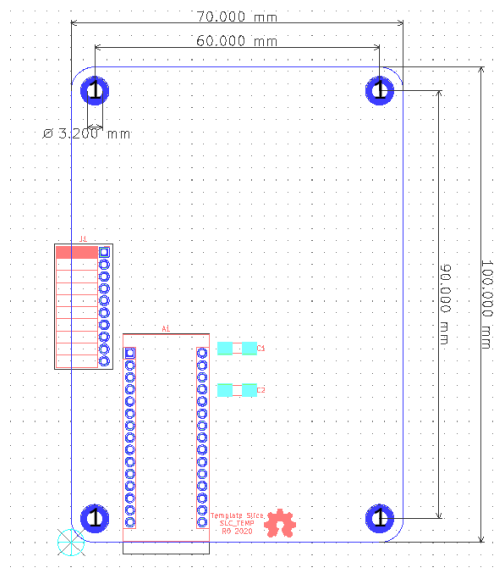


Figure 3.2: The Mechanical specifications of a slice PCB

3.2.4.2 Positioning & Sizing Constraints

For a standard slice, the Arduino Nano [13], interface connector, mounting holes, and board dimensions should remain consistent with SLC_TEMP. Doing so will ensure compatibility with the default enclosure.

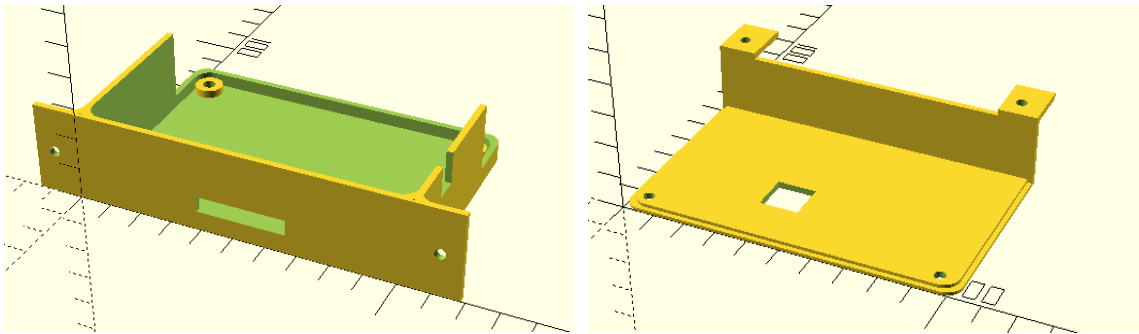


Figure 3.3: A rendering of the default enclosure for a slice.

3.2.5 Electrical Definitions for Slices

The electrical specifications for a slice assume the use of an Arduino Nano per SLC_TEMP. If resources permit, a Nano is recommended, however other controllers can be adapted to follow the BREAD protocols. The Arduino Nano is used as the default microcontroller platform due to low cost, high availability, and the use of an open source framework [13].

3.2.5.1 Loaf Interface Connector

Each slice should have a standard 10-pin female header centered on the left side (opposite to the external connector) of the PCB. The pin breakout is shown in Table 3.2 and a schematic is shown in Figure 3.4.

Table 3.2. Pin breakout names and descriptions.

Pin #	Name	Description
1	GND	System ground and reference
2	+12V	Voltage from loaf supply
3	I2C_CLK	Clock signal for communication between the slice and loaf
4	I2C_DAT	Data signal for communication between the slice and loaf
5	GND	System ground and reference
6	E_STOP	Signal (driven by loaf) which goes through physical interlocks acting as an E-Stop
7	INT	Interrupt pin (driven by slice) used to indicate to loaf that special attention is needed
8	SYNC	Digital signal (driven by loaf) used to synchronize actions across multiple slices
9	+12V	Voltage from loaf supply
10	GND	System ground and reference

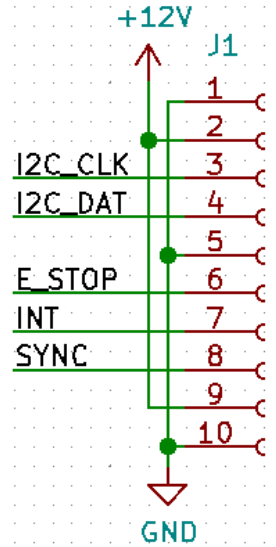


Figure 3.4: A schematic of the loaf interface connector.

3.2.5.2 External Connector

The most commonly used external connector (to devices and sensors) is the 2.54mm (0.1") pitch screw terminal. In some cases, however, specialized connectors may be needed. If possible, the connector should be a plug for a cable-end jack for ease of wiring.

3.2.5.3 Default Circuitry & Connections

Though substitutions are allowed, SLC_TEMP utilizes an Arduino Nano for processing, measurement, computation and communication. Additionally, the Arduino should have 10uF capacitors on both the 5V and 12V line. Every slice must have the loaf interface connector. The default components used on every standard slice are shown in Figure 3.5.

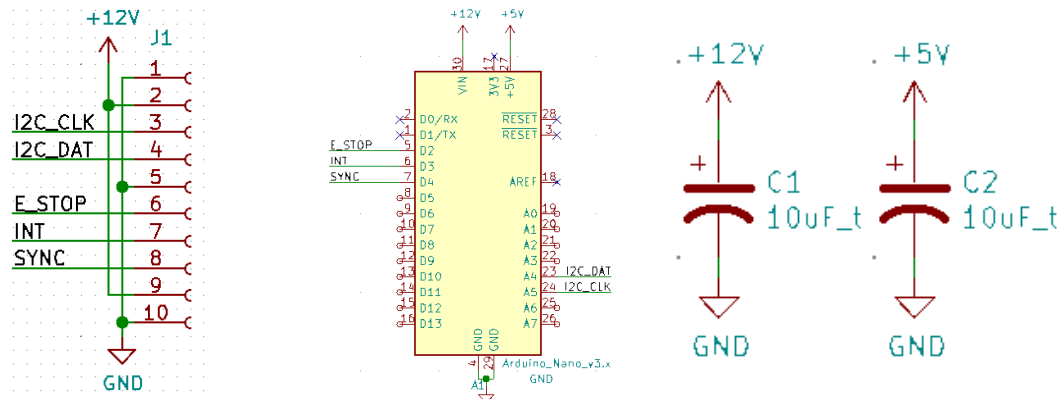


Figure 3.5: The default components used on every standard slice

3.2.6 Software Definitions for Slices

In order for BREAD to be a cohesive system, documentation, including code must also follow a set of guidelines.

3.2.6.1 Programming Standards

All firmware for the Arduino-based slices and loafs should be programmed in the IDE and follow the style guide as laid out by Arduino [31]. All pin names should be consistent with their names as represented on schematics. Every slice's firmware should instantiate “SLC_Functions.h” for all default functions such as initialization and loaf communication.

3.2.6.2 SLC_Functions.h

SLC_Functions.h is an Arduino library file which should be included with every slice firmware it contains the following functions:

- initialize: Responsible for attaining the I2C address (if slice is part of a loaf) as well as setting up communication
- bufferWrite: Allows for the writing of a variable sized buffer, which may be requested by the slice
- receiveDataSerial: Receives data from connected computer via USB into buffer
- receiveDataI2C: Receives data from connected loaf via I2C into buffer
- sendDataSerial: Transmits the send buffer via Serial
- sendDataI2C: Transmits the send buffer via I2C
- pollESTop: Internal function which check if ESTOP is high. If not – all functions will cease
- pollSync: Internal function that waits for the sync line to be brought high before executing the received command

3.2.6.3 SLC_TEMP.h

SLC_TEMP.h is an Arduino library, which must be made unique to each slice that compartmentalizes all of the functions that the loaf can call for the given slice. Since slices can be very diverse, there are no specific guidelines or required functions for this library.

3.2.7 Building Loafs

BREAD can be used in three different configurations: 1) in single slice mode, 2) single loaf mode, or 3) multi-loaf mode.

3.2.7.1 Single Slice Usage

In single slice mode, the slice is used as its own master, receiving and sending data to the connected computer as shown in Figure 3.6. In some (depending on the requirements of the card), an external power supply may be required.

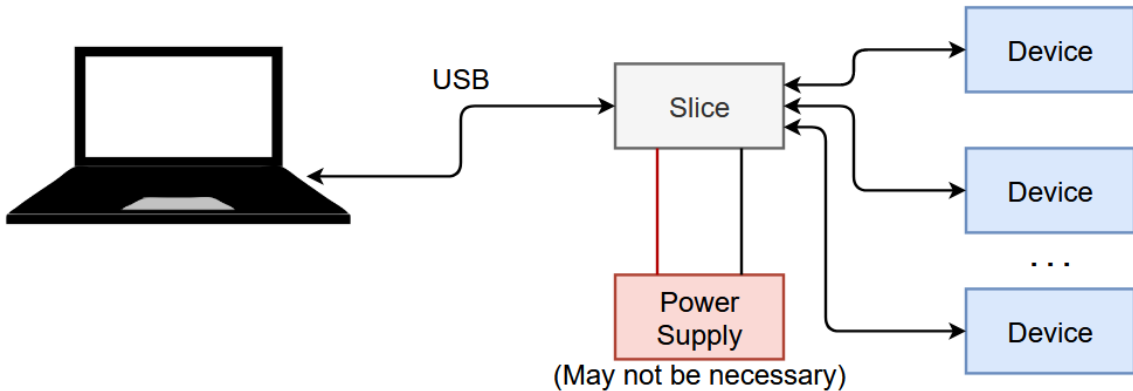


Figure 3.6. Schematic of single slice mode operation.

3.2.7.2 Single Loaf Usage

In single loaf mode the loaf acts as master to multiple slices as shown in Figure 3.7. Power to each slice is distributed via the loaf, as well as critical signals such as e-stop and sync. In this mode slices may still be controlled via serial or I2C, which is useful for diagnostics. On start-up each slice receives it's address from the loaf.

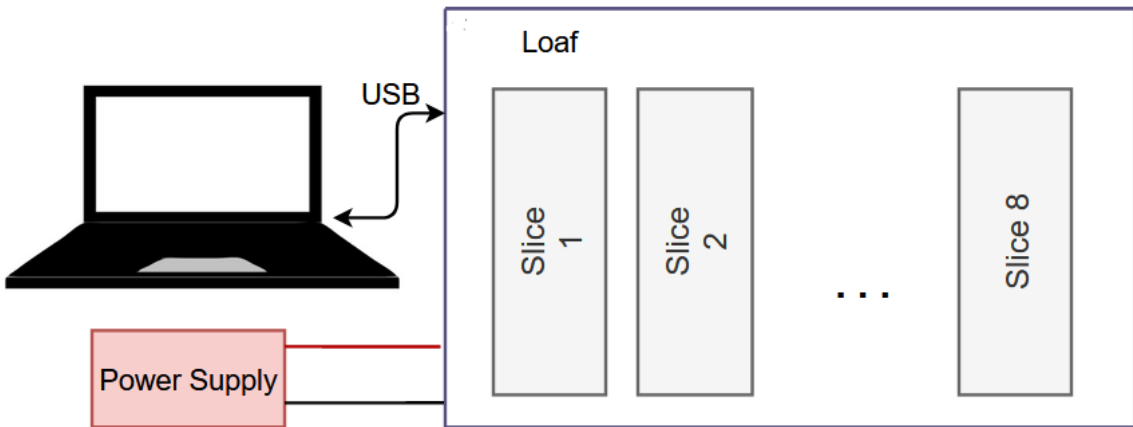


Figure 3.7. Schematic of single loaf mode operation.

3.2.7.3 Multi-Loaf Usage

Loafs are designed with an amplified up-stream and downstream connection point by way of an Ethernet connector. Using these connectors, multiple loafs (up to 8 loafs, totalling 64 possible slices) can be daisy-chained as shown in Figure 3.8. Each loaf will assign

addresses to its daughter slices. The loaf with address 0x00 will establish itself as the master. Depending on power requirements each loaf may need a separate power supply.

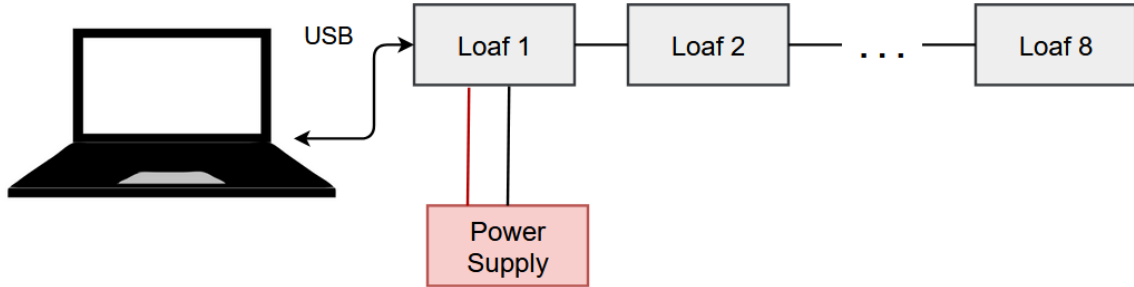


Figure 3.8. Schematic of multi-loaf mode operation.

3.2.8 Existing Slices

At the time of publishing there are 8 available slices. Their titles are:

1. SLC_LVAI: Amplified Analog Input Slice [32]
2. SLC_IDIO: Isolated Digital Input/Outputs [33]
3. SLC_AAFT: Audio Analysis / Fourier Transform [34]
4. SLC_CR10: +/- 10A Current Sensor [35]
5. SLC_RLAY: 4 Channel Relay Controller [36]
6. SLC_STEP: 4 Channel Stepper Motor Controller [37]
7. SLC_THRM: 4 Channel Type-K Thermocouple Reader [38]
8. SLC_USBP: 2 Channel USB Port [39]

The slice functions and characterization procedures are listed in the following sections, with additional information available in each slice's respective repository.

3.2.8.1 SLC_LVAI Amplified Analog Input Slice

SLC_LVAI has 6 adjustable analog measurement channels based around the MCP6004 [40] 4-channel operational amplifier. Two potentiometers are available to adjust offset and gain, theoretically allowing for a signal offset of 5V and a gain of 11. Additionally, a first-order low pass filter is implemented with a corner frequency of 160Hz (component can be replaced to alter cut off frequency).

SLC_LVAI can be used to interface with a multitude of small-signal voltage sensors such as light sensors [41], sound sensors [42], and pressure sensors [43]. This slice could be

used for applications such as solar tracking [44], automated chemical processing [45], and power measurement [4].

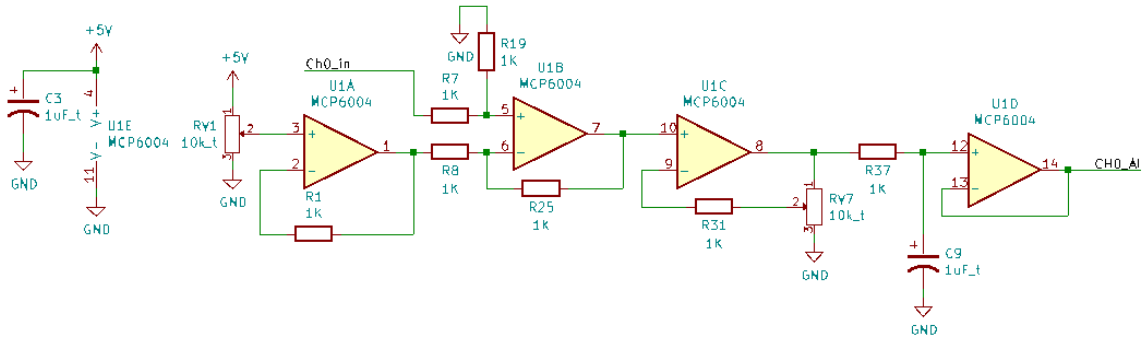


Figure 3.9: The offset, amplify, and filter circuit for channel 0 (typical for all channels)

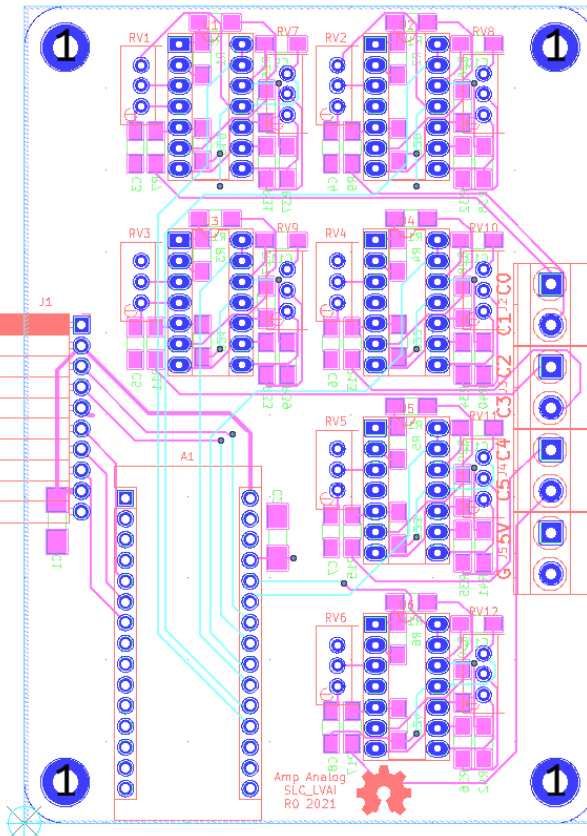


Figure 3.10: The routed circuit board for SLC_LVAI

The following functionality must be validated for the SLC_LVAI:

- Accurate reading of input analog signals.
- Ability to read in external commands and adjust accordingly.
- Ability to quickly and accurately export data.
- Ability to operate indefinitely and predictably.

Accurate Analog Readings

1. Input a known, measured signal into a channel of SLC_LVAI.
2. View this signal on both an oscilloscope and the serial monitor of the Arduino IDE.
3. Tweak Potentiometers until signal appears to be correct shape
4. Repeat process for every channel of SLC_LVAI.

Reading Commands

For slice-only use:

1. Connect Slice to personal computer and open the Arduino IDE.
2. Open the Serial Monitor and attempt to transmit a command in proper form.
3. Verify the system responds properly to any and all commands that are sent to it.
(Peripheral devices may need to be connected to see effects).

For system use:

1. Insert Slice into back plane.
2. Command the back plane to send a command to the slice.
3. Verify the system responds properly to any and all commands that are sent to it.
(Peripheral devices may need to be connected to see effects).

3.2.8.2 SLC_IDIO Isolated Digital Input/Outputs

SLC_IDIO consists of 8 optically isolated digital channels with selectable modes (input or output). The ILD207T opto-isolator provides 4000V of isolation and an output current of 30mA. This card can be used for interfacing with limit switches [46], buttons [47], and other binary input devices, as well as lighting indicators [48] and controlling external solid-state relays [49]. This functionality can be used for on-off control of devices, as well as measuring properties of digital waves such as frequency, modulation, and pulse lengths.

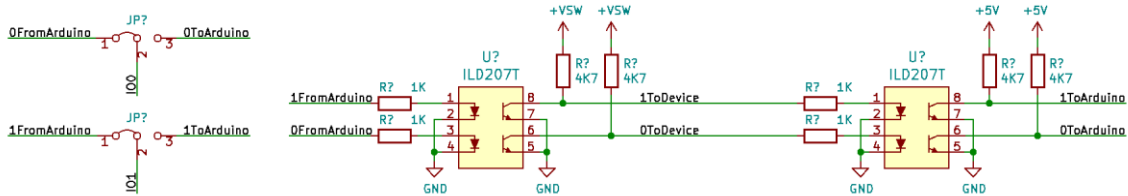


Figure 3.11: Jumpers for mode selection, and optical-isolation circuits for 2 channels in SLC_IDIO (typical for all 8 channels)

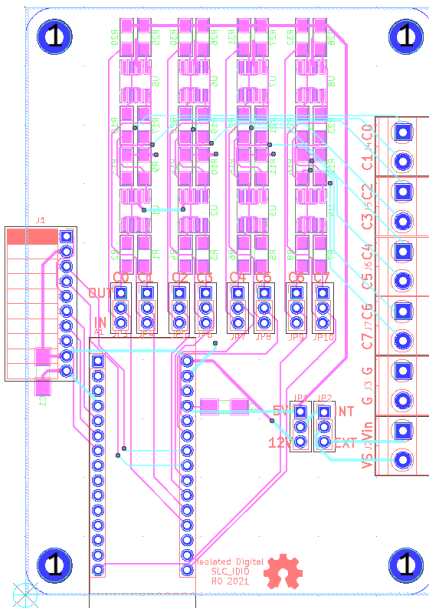


Figure 3.12: The routed circuit board for SLC_IDIO

The following functionality must be validated for the SLC_IDIO:

- Ability to operate each channel individually as either an input or an output.

- Ability to read in external commands and adjust accordingly.
- Ability to quickly and accurately export data.
- Ability to operate indefinitely and predictably.

I/O Operation

1. Connect the probes of an oscilloscope between a channel's output terminal and ground.
2. Set each channel to be an output and be set to high.
3. Ensure every channel reads as a logic high.
4. Apply a voltage across a channel's terminal and ground.
5. Set each channel to be an input.
6. Read every channel in the Serial Monitor, and ensure every channel can read a logic high and a logic low correctly.

Reading Commands

For slice-only use:

1. Connect Slice to personal computer and open the Arduino IDE.
2. Open the Serial Monitor and attempt to transmit a command in proper form.
3. Verify the system responds properly to any and all commands that are sent to it.
(Peripheral

devices may need to be connected to see effects).

For system use:

1. Insert Slice into back plane.
2. Command the back plane to send a command to the slice.
3. Verify the system responds properly to any and all commands that are sent to it.
Peripheral devices may need to be connected to see effects).

Exporting Data

1. Command SLC_IDIO to retrieve and send the signal status on every channel.
2. Observe this same dataset on the Serial Monitor.
3. Cross compare. Ensure no discrepancies.

Indefinite / Predictability Test

1. Command SLC_IDIO to read a simple, predictable digital signal such as a square wave.
2. Allow this process to continue for an arbitrarily large amount of time.
3. After such time has passed, ensure the system is still reliably and accurately reading said test signal.

3.2.8.3 SLC_AAFT Audio Analysis / Fourier Transform

SLC_AAFT consists of two separate audio channels – a quarter inch jack input and a standard aux input. The input analog signal is broken down into low, low-mid, mid, high-mid, and high ranges, bounded between ~0-5000 Hz. The signal can be offset and amplified using a circuit based around the MCP6004 [MCP6004] 4-channel operational amplifier. Potential applications include: analysis of system acoustics [50], musical audio analysis [51], and peak finder [52]. This slice is designed specifically to be connected with microphones (either for scientific measurement [53] or entertainment [54]) and musical instruments [55].

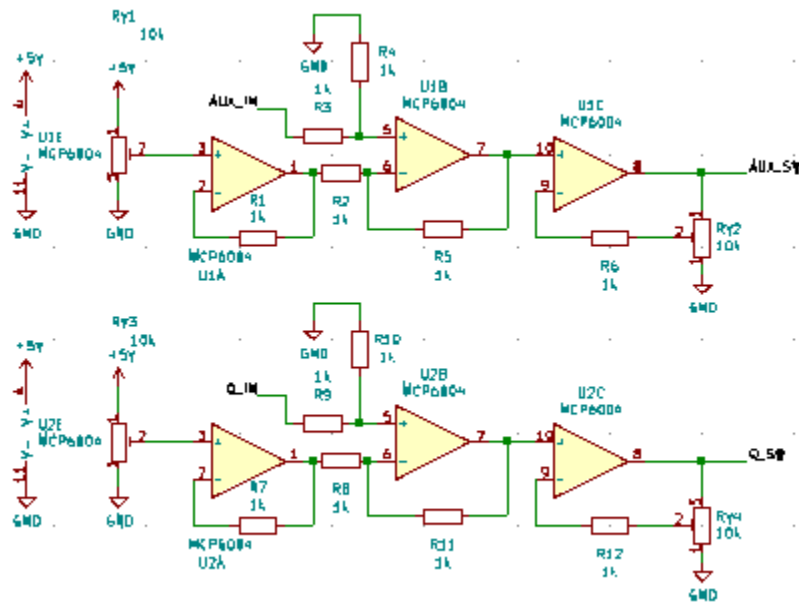


Figure 3.13: 4 Stage Amplifier for Each Channel

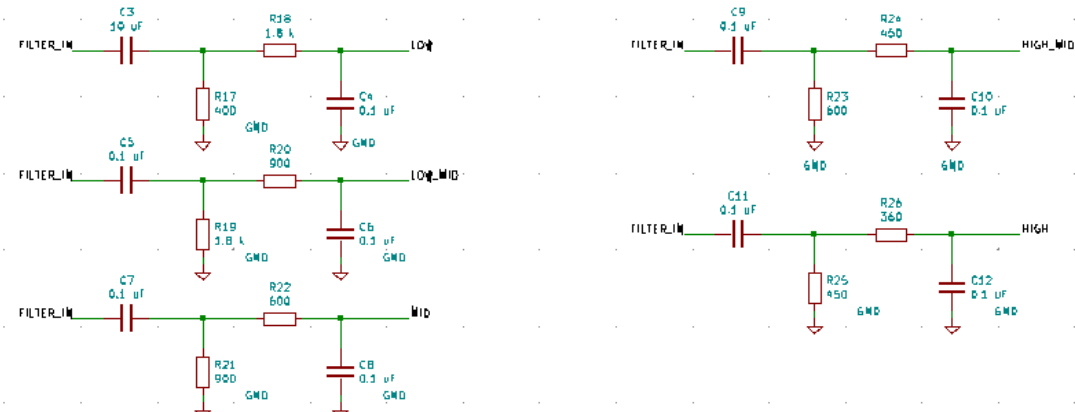


Figure 3.14: Frequency Breakdown Filters

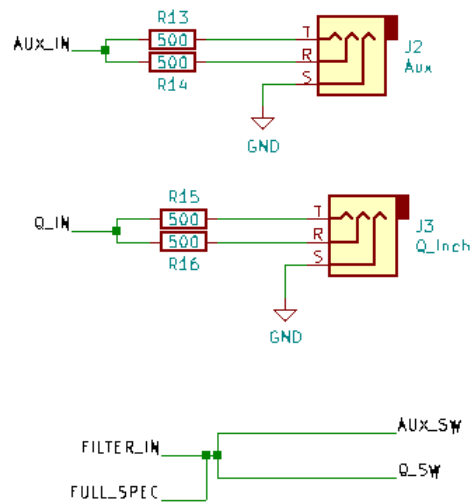


Figure 3.15: Channel Inputs and Signal Bridge

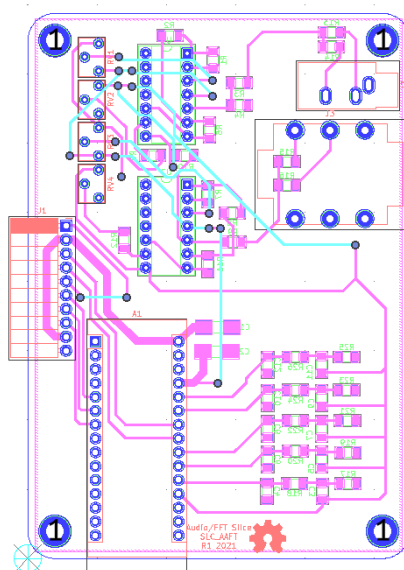


Figure 3.16: The routed circuit board for SLC_AAFT

The following functionality must be validated for the SLC_AAFT:

- Accuracy of board's Fast Fourier Transform (FFT).
- Ability to send FFT data quickly and accurately to separate module.
- Ability to take in external signal data and run an FFT on it.
- Ability to operate indefinitely and predictably.

FFT Accuracy

1. Feed a signal of known frequency composition into SLC_AAFT via one of the two channels.
2. View this signal on an oscilloscope concurrently.
3. Set the oscilloscope to output a real-time FFT of the input signal.
4. View SLC_AAFT's generated FFT in the serial plotter window of the Arduino IDE.
5. Cross compare. Ensure no major discrepancies.
6. Repeat for the additional channel.

FFT Data Transfer

1. Have SLC_AAFT run an FFT on a signal of known frequency composition.
2. Observe FFT results in Serial Monitor. Record.
3. Command separate device to read in entirety of FFT data. Observe and record.
4. Ensure no discrepancies.

External Signal FFT

1. Use another module (such as SLC_LVAI) to read and send a known signal to SLC_AAFT via I2C.
2. View the signal being read by said separate module on an oscilloscope.
3. Configure the oscilloscope to output a real-time FFT of this test signal.

4. Command SLC_AAF to run an FFT on this data.
5. Cross compare the two FFTs and ensure no discrepancies.

Indefinite / Predictability Test

1. Input a known signal into SLC_AAF via either input channel.
2. Have SLC_AAF continuously run an FFT on the data.
3. Allow to run for an arbitrarily long amount of time.
4. Ensure that the system is still producing results as expected at the end of said time period.

3.2.8.4 SLC_CR10 +/- 10A Current Sensor

SLC_CR10 consists of four individual current sensing channels based around the ACS723 Hall effect current sensor [56]. Current is routed through a hall effect current sensing chip, which then generates an analog signal to the Arduino to. Potential applications include: power analysis of known system [4] signal detector [57], and automatic surge [58] alert system.

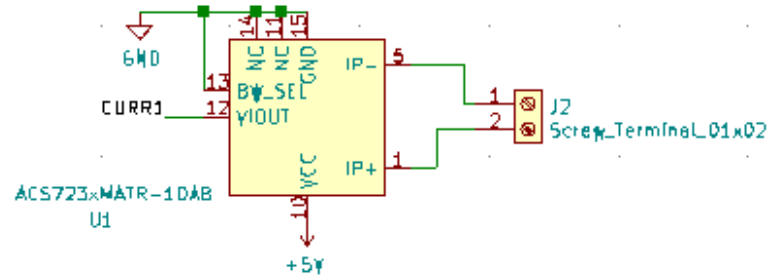


Figure 3.17: Typical sensor chip implementation for all channels

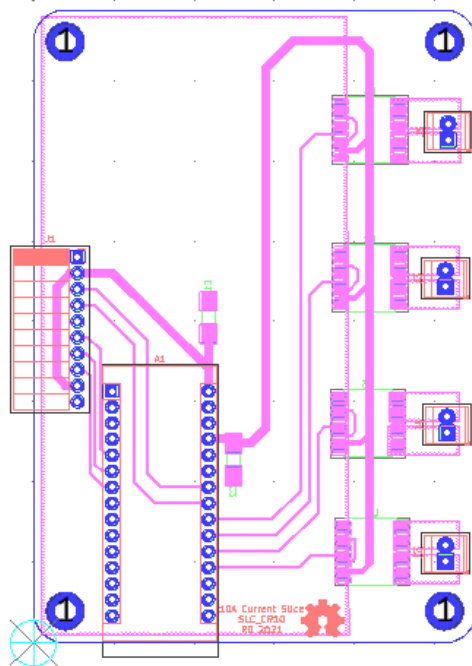


Figure 3.18: The routed circuit board for SLC_CR10

The following functionality must be validated for the SLC_CR10:

- Ability to read in external commands and adjust accordingly.
- Accuracy of input current signal on all channels.
- Ability to quickly and accurately export data.
- Ability to operate indefinitely and predictably.

Procedure

Current Signal Read

1. Set up a simple DC circuit with a known current, and hook SLC_CR(10/20/40) in series with it.
2. Verify the current read by the Slice is accurate.
3. Repeat with a different known current. Be sure to test range extremities.
4. Set up an AC circuit where the current signal is known / easily calculable.

5. Take current readings with SLC_CR(10/20/40). Plot the output data and ensure that the signal is being correctly read.
6. Repeat with a different known current signal. Be sure to test range extremities.
7. Repeat the above experiments on each channel.

Reading Commands

For slice-only use:

1. Connect Slice to personal computer and open the Arduino IDE.
2. Open the Serial Monitor and attempt to transmit a command in proper form.
3. Verify the system responds properly to any and all commands that are sent to it. (Peripheral devices may need to be connected to see effects).

For system use:

1. Insert Slice into back plane.
2. Command the back plane to send a command to the slice.
3. Verify the system responds properly to any and all commands that are sent to it. (Peripheral devices may need to be connected to see effects).

Signal Data Transfer

1. Issue a command to SLC_CR(10/20/40) to send current data for any given channel or mix of channels.
2. Record the sent data from the Slice.
3. Cross-compare with the received data. Ensure no discrepancies.

Indefinite / Predictability Test

1. Command the Slice to read current on one (or many) channel(s).
2. Read the current signals on the Serial Monitor.
3. Allow the readings to persist for an arbitrarily long amount of time.
4. Ensure, after the proper amount of time has passed, the system is still operating as expected.

3.2.8.5 SLC_RLAY 4 Channel Relay Controller

SLC_RLAY consists of 4 different relay control channels. Each channel is digitally controlled and opto-electrically isolated to allow for backwards voltage protection. Four analog input channels are provided as a potential feedback/sensing path. The potentiometer on each of these paths serves as a way to manually scale the input to a desired amplitude. Potential applications include: automatic signal switching and timing of power supplies.

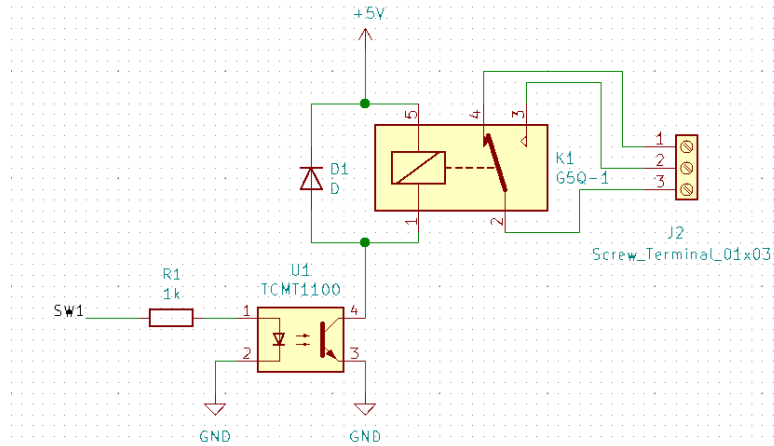


Figure 3.19: Common implementation of relay control channels

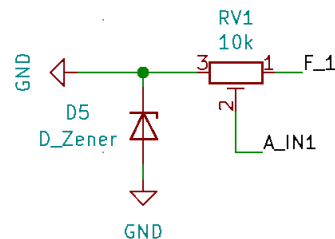


Figure 3.20: Analog feedback path

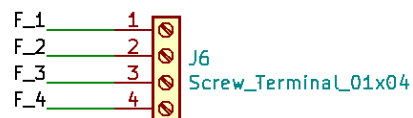


Figure 3.21: Feedback inputs

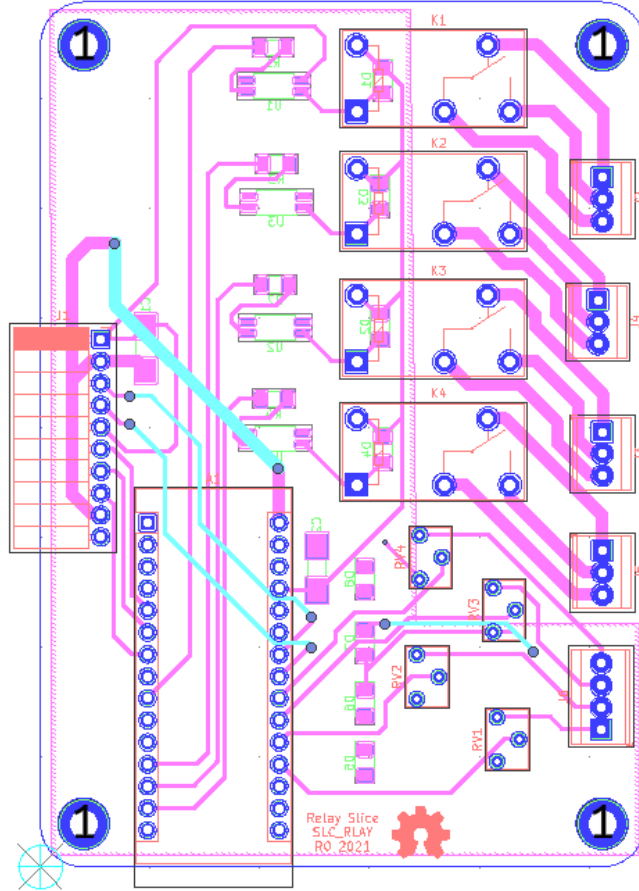


Figure 3.22: The routed circuit board for SLC_RLAY

The following functionality must be validated for the SLC_RLAY:

- Accuracy
- Ability to read in external commands and adjust accordingly.
- Ability to quickly and accurately export data.
- Ability to operate indefinitely and predictably.

Procedure

Reading Commands

For slice-only use:

1. Connect Slice to personal computer and open the Arduino IDE.
2. Open the Serial Monitor and attempt to transmit a command in proper form.
3. Verify the system responds properly to any and all commands that are sent to it.
(Peripheral devices may need to be connected to see effects).

For system use:

1. Insert Slice into back plane.
2. Command the back plane to send a command to the slice.
3. Verify the system responds properly to any and all commands that are sent to it.
(Peripheral devices may need to be connected to see effects).

Exporting Data

Indefinite / Predictability Test

3.2.8.6 SLC_STEP 4 Channel Stepper Motor Controller

SLC_STEP consists of four separately controllable stepper motor control channels driven by Pololu A4988 drivers [59], common in 3-D printing applications and easily replaceable. There is a port for custom power input. The step size, direction, speed, acceleration, and much more can be electronically controlled. Analog feedback paths are included. Potential applications include: 3-D printer control (and other CNC machines) [28, 60] and electro-mechanical system control [61].

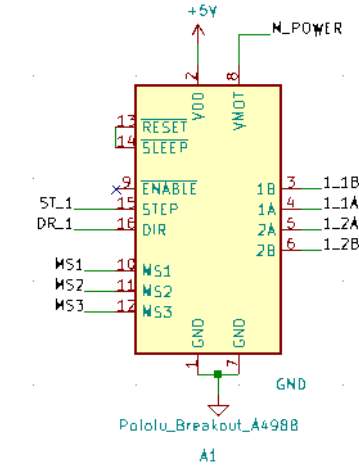


Figure 3.23: Stepper driver configuration for each channel

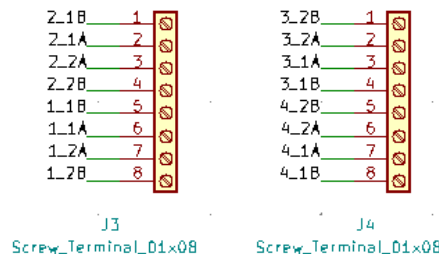


Figure 3.24: Motor output paths

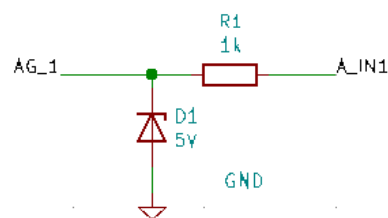
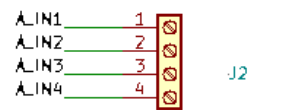


Figure 3.25: Analog feedback path for each channel



Screw_Terminal_01x04

Figure 3.26: Analog input terminal

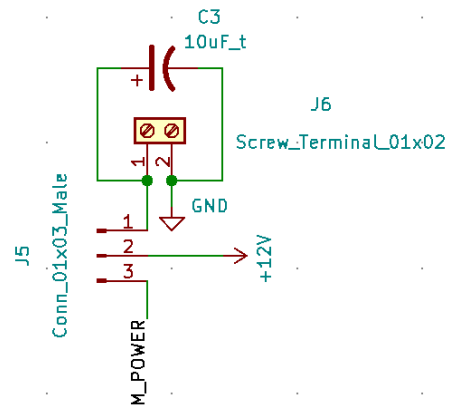


Figure 3.27: Custom Power Supply Input + Select

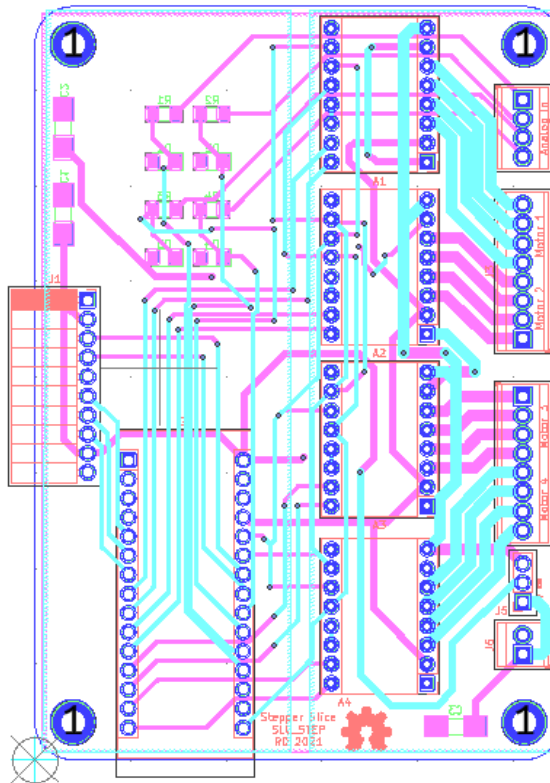


Figure 3.28: The routed circuit board for SLC_STEP

The following functionality must be validated for the SLC_STEP:

- Accuracy
- Ability to read in external commands and adjust accordingly.
- Ability to quickly and accurately export data.
- Ability to operate indefinitely and predictably.

Procedure

Reading Commands

For slice-only use:

1. Connect Slice to personal computer and open the Arduino IDE.
2. Open the Serial Monitor and attempt to transmit a command in proper form.

- Verify the system responds properly to any and all commands that are sent to it.
(Peripheral devices may need to be connected to see effects).

For system use:

- Insert Slice into back plane.
- Command the back plane to send a command to the slice.
- Verify the system responds properly to any and all commands that are sent to it.
(Peripheral devices may need to be connected to see effects).

Exporting Data

Indefinite / Predictability Test

3.2.8.7 SLC_THRM 4 Channel Type-K Thermocouple Reader

SLC_THRM consists of four MAX31855 [62] type-K thermocouple reading chips connected to a thermocouple port, with filtering circuitry in between for smooth reading. These chips are read by the Arduino via SPI. Potential applications include: closed loop heater control [63] and automatic heat-based alarm system [64].

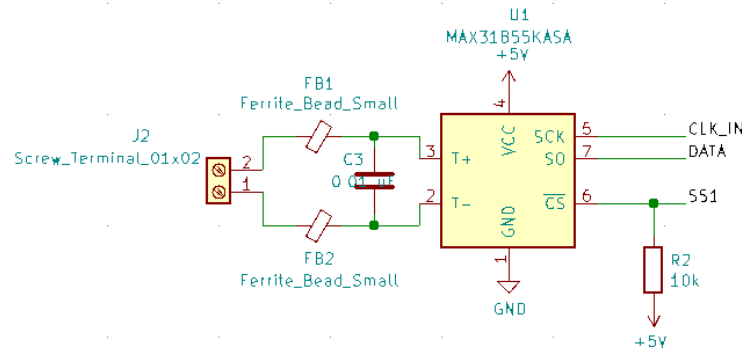


Figure 3.29: Common thermocouple channel circuitry

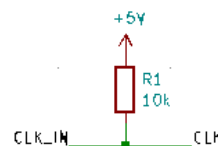


Figure 3.30: Common SPI Clock Pull-Up

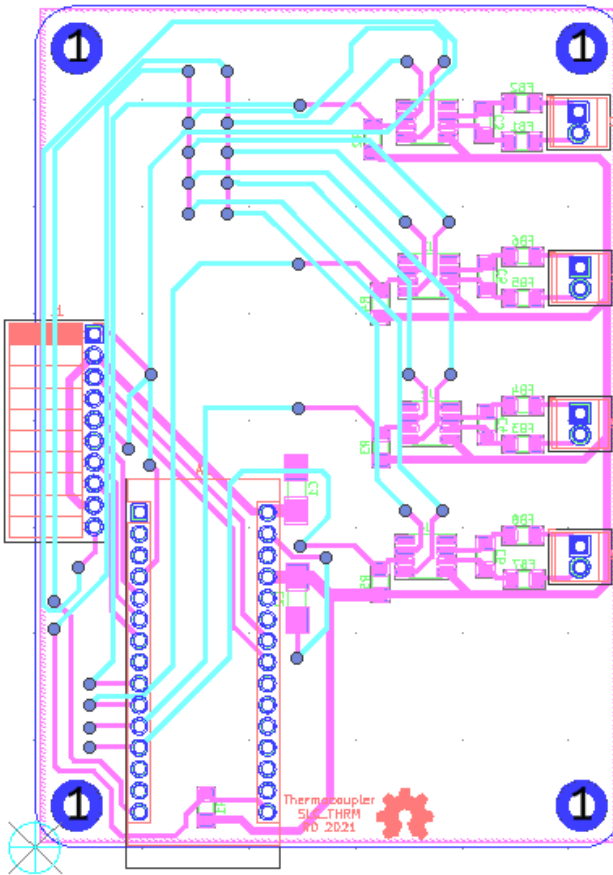


Figure 3.31: The routed circuit board for SLC_THRM

The following functionality must be validated for the SLC_THRM:

- Accuracy
- Ability to read in external commands and adjust accordingly.
- Ability to quickly and accurately export data.
- Ability to operate indefinitely and predictably.

Procedure

Reading Commands

For slice-only use:

1. Connect Slice to personal computer and open the Arduino IDE.

2. Open the Serial Monitor and attempt to transmit a command in proper form.
3. Verify the system responds properly to any and all commands that are sent to it.
(Peripheral devices may need to be connected to see effects).

For system use:

1. Insert Slice into back plane.
2. Command the back plane to send a command to the slice.
3. Verify the system responds properly to any and all commands that are sent to it.
(Peripheral devices may need to be connected to see effects).

Exporting Data

Indefinite / Predictability Test

3.2.8.8 SLC_USBP 2 Channel USB Port

SLC_USBP Consists of 2 generic USB A input slots connected to an electrically controlled switch designed for USB port signal switching. This then connects to an FT232 [65] chip to convert the USB signals to Arduino-readable SPI format. Potential applications include: External device communication and data collection.

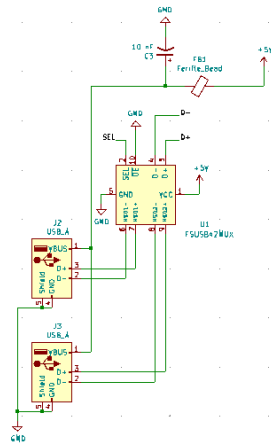


Figure 3.32: USB ports connected to multiplexer.

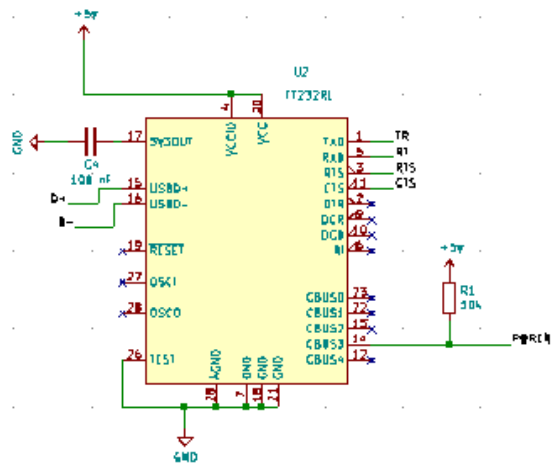


Figure 3.33: FT232 USB Signal Reader

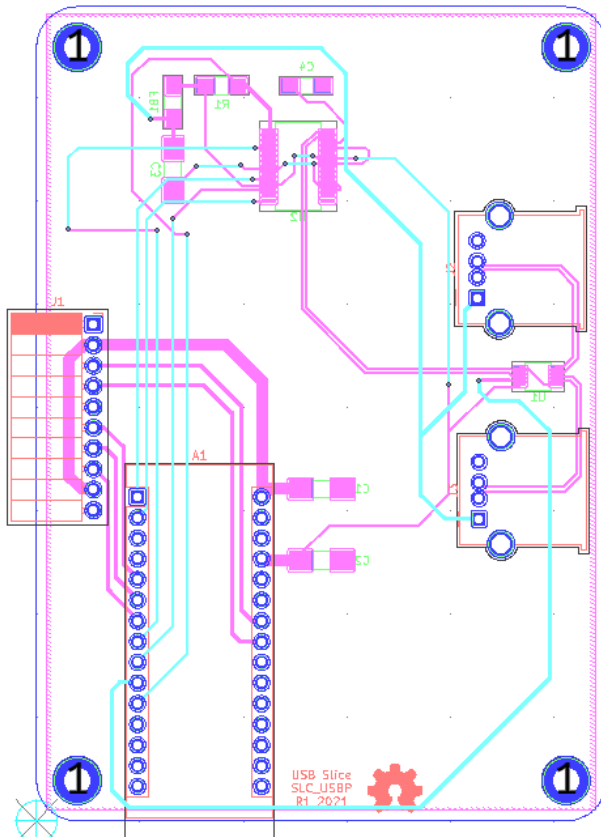


Figure 3.34: The routed circuit board for SLC_USBP

The following functionality must be validated for the SLC_USB_P:

Reading Commands

For slice-only use:

4. Connect Slice to personal computer and open the Arduino IDE.
5. Open the Serial Monitor and attempt to transmit a command in proper form.
6. Verify the system responds properly to any and all commands that are sent to it.
(Peripheral devices may need to be connected to see effects).

For system use:

4. Insert Slice into back plane.
5. Command the back plane to send a command to the slice.

Verify the system responds properly to any and all commands that are sent to it.
(Peripheral devices may need to be connected to see effects).

3.2.9 Example System: TIG-Based Metal 3D Printer Monitor

As with many processes, data acquisition can be an important component of characterizing novel rapid prototyping equipment [Pringle]. In this manuscript, a DAQ system utilizing BREAD componentry will be proposed and constructed for a novel, low-cost TIG-based metal 3-D printer. Metal 3-D printing has not become as ubiquitous as polymer 3-D printing, partially because there are no low-cost commercial options available [66]. Lowering the barrier to entry for digital metal manufacturing may allow engineers and hobbyists alike to create and share metal components in their designs.

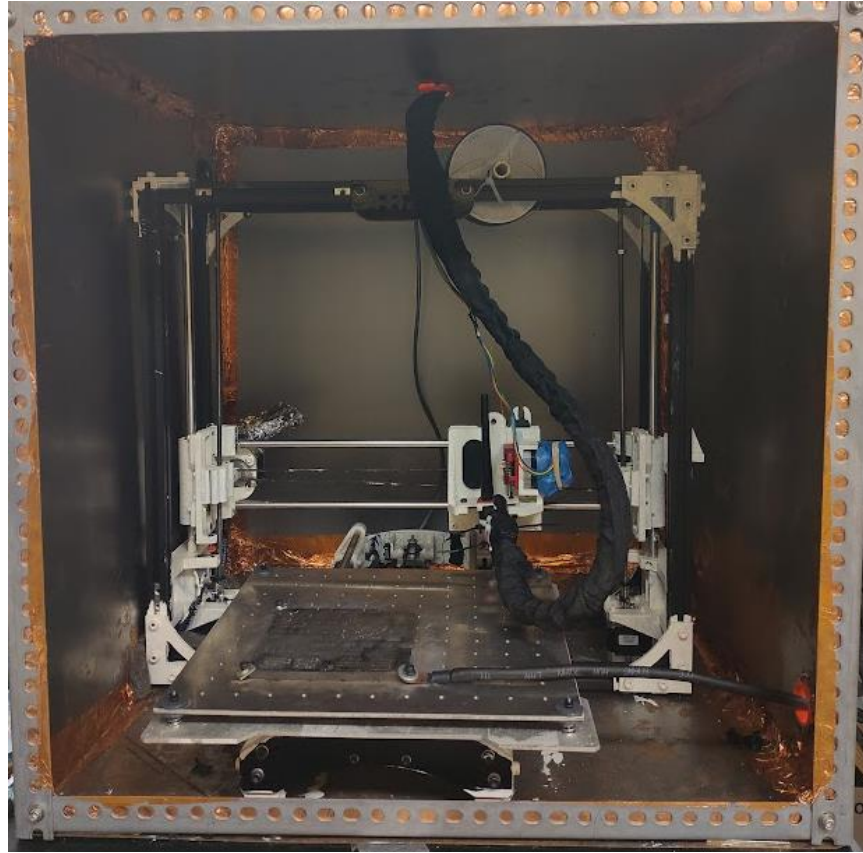


Figure 3.35: An open source TAZ 3-D printer converted to a TIG-based open source metal 3-D printer

3.2.9.1 Required Functions & Slices

Taking inspiration from traditional welding, the most important feedback to consider is light (intensity and modulation) and sound [67]. These signals generated by the arc can be used to indicate variables like improper currents, gas flow, feed rate, and stand-off distances [16]. Light can be measured using a photoresistor paired with the SLC_LVAI slice. Sound can additionally be measured via the SLC_LVAI slice.

In addition, the BREAD system will be used to take power measurements using a non-invasive current transformer placed on the return line. The sensor can also be measured using the SLC_LVAI slice. Finally, a SLC_THRM can be used to measure the temperature of 4 corners of the print substrate.

3.2.9.2 Configuration

The system is built using a LOAF_X08 8 slice backplane. The connection diagram is shown in Figure 3.36. The microphone and photoresistor are placed on the end-effector carriage to keep a consistent reference frame for measurement. The current sensor is placed around the ground wire of the welder. A type K thermocouple is mounted at each corner of the printing substrate.

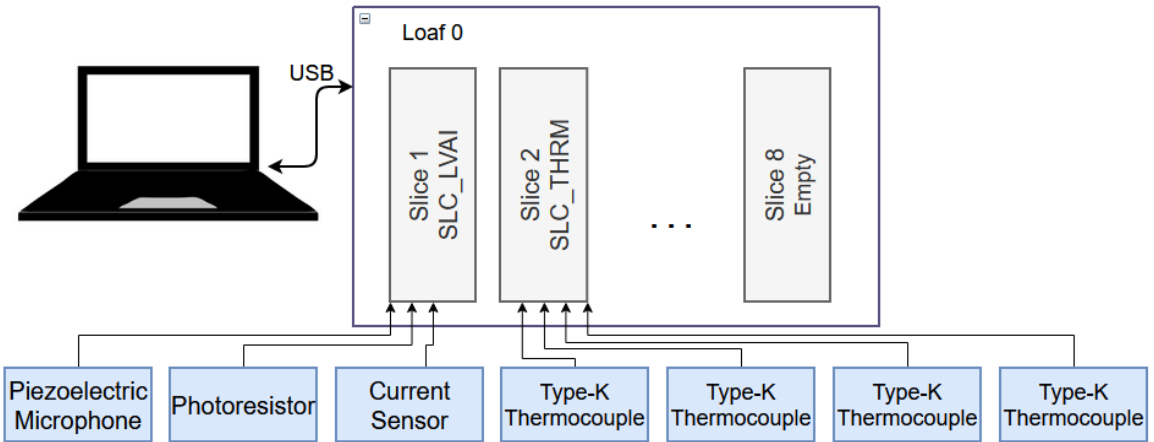


Figure 3.36: An example BREAD configuration for monitoring the quality of a welding process

3.2.9.3 Firmware

The firmware for this example system consists of a sample-record-repeat structure. The routine is set to sample at a frequency of 5Hz, with each sample being timestamped by the Arduino's system clock. The SLC_LVAI slice is set to capture an FFT on each sensor.

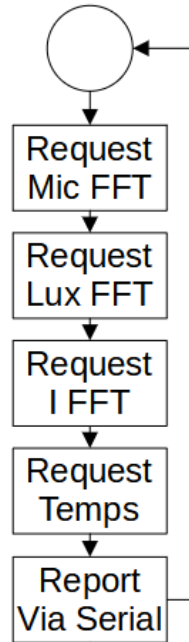


Figure 3.37: The weld monitoring sample loop

3.3 Design files summary

Each slice and loaf has the following primary design files:

Design file name	File type	Open source license	Location of the file
Firmware/firmware.ino	.ino Arduino Code	GPL 3.0	https://osf.io/742ez/
Gerbers	Gerber board files	GPL 3.0	https://osf.io/742ez/
Hardware/Bread_Slice.pro	KiCAD Project	GPL 3.0	https://osf.io/742ez/
Hardware/Bread_Slice.sch	KiCAD Schematic	GPL 3.0	https://osf.io/742ez/
Hardware/Bread_Slice.kicad_pcb	KiCAD PCB	GPL 3.0	https://osf.io/742ez/
Mecahnical/top.stl & top.scad	STL	GPL 3.0	https://osf.io/742ez/
Mecahnical/bottom.stl & bottom.scad	STL	GPL 3.0	https://osf.io/742ez/

- Firmware/firmware.ino: the default firmware to be programmed onto the slice / loaf
- Gerbers: a folder which contains all gerber files necessary for construction of the circuit board
- Hardware/Bread_Slice.pro: The main project file for the electrical design
- Hardware/Bread_Slice.sch: The schematic of the electrical design
- Hardware/Bread_Slice.kicad_pcb: The board routing for the slice
- Mecahnical/top.stl & top.scad: The Lid of the enclosure
- Mecahnical/bottom.stl & bottom.scad: The base of the enclosure

3.4 Bill of materials summary

SLC_LVAI: Amplified Analog Input Slice [SLC_LVAI]

Designator	Component	Number	Cost per unit - currency	Total cost - currency	Source of materials
A1	Arduino Nano	1	4.30	4.30	https://www.amazon.com/dp/B08Z7HQ2B6/
C1 – C2	CAP TANT 10UF 10% 25V 2312	2	0.72	1.44	https://www.digikey.com/short/7vz343n9
C3 – C14	CAP TANT 1UF 10% 25V 1206	12	0.51	6.12	https://www.digikey.com/short/fzn5wb0d
J1	01x10 Female Header Pins	1	0.79	0.79	https://www.digikey.com/short/23bfwwjh
J2 – J5	TERM BLK 2POS SIDE ENTRY 5MM PCB	4	0.47	1.88	https://www.digikey.com/short/3nv7nt34
R1 – R42	RES 1K OHM 1% 1/4W 1206	42	0.07	2.94	https://www.digikey.com/short/mbw4gq78
RV1 – RV12	TRIMMER 10K OHM 0.5W PC PIN TOP	12	1.79	21.48	https://www.digikey.com/short/w8rr4gdm
U1 – U6	IC OPAMP GP 4 CIRCUIT 14DIP	6	0.063	0.378	https://www.digikey.com/short/5mzc8t8t
PCB	Circuit Board	1	1.29	1.29	https://pcbshopper.com/

SLC_IDIO: Isolated Digital Input/Outputs [SLC_IDIO]

Designator	Component	Number	Cost per unit - currency	Total cost - currency	Source of materials
A1	Arduino Nano	1	4.30	4.30	https://www.amazon.com/dp/B08Z7HQ2B6/
C1 – C2	CAP TANT 10UF 10% 25V 2312	2	0.72	1.44	https://www.digikey.com/short/7vz343n9
J1	01x10 Female Header Pins	1	0.79	0.79	https://www.digikey.com/short/23bfwwjh
J3 – J6	TERM BLK 2POS SIDE ENTRY 5MM PCB	6	0.47	2.82	https://www.digikey.com/short/3nv7nt34
JP1 – JP10	3 Pin Header	10	0.04	0.4	https://www.amazon.com/dp/B07PKKY8BX/

R1 – R24	RES 1K OHM 1% 1/4W 1206	16	0.07	1.12	https://www.digikey.com/short/mbw4qq78
R9 – R32	RES 4.7K OHM 1% 1/4W 1206	16	0.1	1.6	https://www.digikey.com/short/93rfw21v
U1 – U8	OPTOISO 4KV 2CH TRANS 8SOIC	8	1.18	9.44	https://www.digikey.com/short/b80mfzb1
PCB	Circuit Board	1	1.29	1.29	https://pcbshopper.com/

SLC_AAF: Audio Analysis / Fourier Transform [SLC_AAF]

Designator	Component	Number	Cost per unit - currency	Total cost - currency	Source of materials
U1-2	4 Stage Amplifier Chip	2	0.44	0.88	https://www.digkey.com/en/products/detail/microchip-technology/MCP6004T-I-ST/523078
J2	Aux Cord Jack	1	1.18	1.18	https://www.digkey.com/en/products/detail/cui-devices/SJ1-3533NG/738701
RV1-4	10k 12 Turn Trim Pot	4	4.16	16.64	https://www.digkey.com/en/products/detail/bourns-inc/3266W-1-103LF/1087907
R26	1206 Packaging 360Ω Resistor	1	0.10	0.10	https://www.digkey.com/en/products/detail/yageo/AC1206FR-07360RL/5897483
R24-25	1206 Packaging 450Ω Resistor	2	0.10	0.20	https://www.digkey.com/en/products/detail/yageo/RC1206FR-

					<u>07453RL/7289 24</u>
R22-23	1206 Packaging 600Ω Resistor	2	0.10	0.20	https://www.digikey.com/en/products/detail/yageo/RC1206FR-07604RL/729038
R20-21	1206 Packaging 900Ω Resistor	2	0.10	0.20	https://www.digikey.com/en/products/detail/yageo/RC1206FR-07909RL/729166
R18-19	1206 Packaging 1.8 kΩ Resistor	2	0.10	0.20	https://www.digikey.com/en/products/detail/yageo/RC1206JR-071K8L/729204
R17	1206 Packaging 400Ω Resistor	1	0.10	0.10	https://www.digikey.com/en/products/detail/yageo/RT1206BR-D07400RL/5936956
R13-16	1206 Packaging 500Ω Resistor	4	0.10	0.40	https://www.digikey.com/en/products/detail/yageo/RC1206FR-07499RL/728944
R1-12	1206 Packaging 1 kΩ Resistor	12	0.10	1.20	https://www.digikey.com/en/products/detail/yageo/RC1206FR-071KL/728387
J3	Quarter Inch Jack	1	1.58	1.58	https://www.mouser.com/ProductDetail/Neutrik/NMJ6HCD2?qs=ZNZTMDotSRIKYI2qFVJbOA%3D%3D

C4-12	1206 Packaging 0.1 µF Capacitor	9	0.16	1.44	https://www.digikey.com/en/products/detail/yageo/CC1206KR-X7R8BB104/5884627
C3	1206 Packaging 10 µF Capacitor	1	0.66	0.66	https://www.digikey.com/en/products/detail/yageo/CC1206KK-X5R6BB106/5195344
C1-2	1206 Packaging 10 µF Capacitor	2	0.64	1.28	https://www.digikey.com/short/qfrbqfhd
A1	Arduino Nano	1	4.30	4.30	https://www.amazon.com/dp/B08Z7HQ2B6/
J1	01x10 Female Header Pins	1	0.79	0.79	https://www.digikey.com/short/23bfwwjh
PCB	Circuit Board	1	1.29	1.29	https://pcbsupplier.com/

SLC_CR10: +/- 10A Current Sensor [SLC_CR10]

Designator	Component	Number	Cost per unit - currency	Total cost - currency	Source of materials
U1-4	10A Current Sensor Chip	4	5.68	22.72	https://www.digikey.com/en/products/detail/allegro-microsystems/ACS723KMAT-R-10AB-T/5225374
J2-J5	1/10" Pitch 01x02 Screw Terminals	4	1.27	5.08	https://www.digikey.com/en/products/detail/te-connectivity-amp-connectors/282834-2/1150135

C1-2	1206 Packaging 10 µF Capacitor	2	0.64	1.28	https://www.digikey.com/short/qfrbqfh
A1	Arduino Nano	1	4.30	4.30	https://www.amazon.com/dp/B08Z7HQ2B6/
J1	01x10 Female Header Pins	1	0.79	0.79	https://www.digikey.com/short/23bfwwjh
PCB	Circuit Board	1	1.29	1.29	https://pcbshopper.com/

SLC_RLAY: 4 Channel Relay Controller [SLC_RLAY]

Designator	Component	Number	Cost per unit - currency	Total cost - currency	Source of materials
U1-4	Optocouplers	4	0.51	2.04	https://www.digikey.com/short/5fmc702d
RV1-4	10k Trimmer Potentiometer	4	4.16	16.64	https://www.digikey.com/short/ftm98v7t
R1-4	1k 1206 Packaging Resistor	4	0.10	0.40	https://www.digikey.com/short/d1dmzmbb
K1-4	G5Q1 SPDT Relay	4	1.52	6.08	https://www.digikey.com/short/vj4ir0vg
J6	01x04 1/10" Pitch Terminal Block	1	2.75	2.75	https://www.digikey.com/short/rnm0hhhn
J2-5	01x03 1/10" Pitch Terminal Block	4	2.06	8.24	https://www.digikey.com/short/71d77cj2
D5-8	5.1V Zener Diode	4	0.22	0.88	https://www.digikey.com/short/tvbtwpmt
D1-4	Standard THT Diode	4	0.21	0.84	https://www.digikey.com/short/tp4mrn5q
C1-2	10 µF 1206 Packaging Ceramic Capacitor	4	0.64	2.56	https://www.digikey.com/short/2ffb0248

A1	Arduino Nano	1	4.30	4.30	https://www.amazon.com/dp/B08Z7HQ2B6/
J1	01x10 Female Header Pins	1	0.79	0.79	https://www.digikey.com/short/23bfwwjh
PCB	Circuit Board	1	1.29	1.29	https://pcbshopper.com/

SLC_STEP: 4 Channel Stepper Motor Controller [SLC_STEP]

Designator	Component	Number	Cost per unit - currency	Total cost - currency	Source of materials
J5	01x03 1/10" Pitch Male Connector Pins	1	0.27	0.27	https://www.digikey.com/short/jv0b95z0
C1-3	1206 Packaging 10 µF Capacitor	3	0.64	1.92	https://www.digikey.com/short/qfrbqfhd
J6	01x02 1/10" Pitch Terminal Block	1	1.27	1.27	https://www.digikey.com/short/Ov8hf4h8
R1-4	1k 1206 Packaging Resistor	4	0.10	0.40	https://www.digikey.com/short/wp8502p7
J3-4	01x08 1/10" Pitch Terminal Block	2	6.45	12.90	https://www.digikey.com/short/mgn9fd88
J2	01x04 1/10" Pitch Terminal Block	1	2.75	2.75	https://www.digikey.com/short/tv7tzq1r
D1-4	5.1V Zener Diode	4	0.22	0.88	https://www.digikey.com/short/z0f0ztp2
A1-4	Pololu A4988 Stepper Driver	4	5.95	23.8	https://www.pololu.com/category/156/a4988-stepper-motor-driver-carriers
G1	Arduino Nano	1	4.30	4.30	https://www.amazon.com/dp/B08Z7HQ2B6/
J1	01x10 Female Header Pins	1	0.79	0.79	https://www.digikey.com/short/23bfwwjh

SLC_THRM: 4 Channel Type-K Thermocouple Reader [SLC_THRM]

Designator	Component	Number	Cost per unit - currency	Total cost - currency	Source of materials
R1-R5	RES 10K OHM 1% 1/2W 1206	4	0.10	0.40	https://www.digikey.com/short/p82bnb9p
U1-U4	MAX31855KASA+T	4	7.04	28.16	https://www.digikey.com/short/rbbt74n5
J2-J5	TERM BLK 2POS SIDE ENTRY 5MM PCB	4	0.47	1.88	https://www.digikey.com/short/3nv7nt34
FB1-FB8	FERRITE BEAD 1206 1LN	8	0.17	1.36	https://www.digikey.com/short/709wpzrb
C3-C6	CAP CER 10000PF 50V X7R 1206	4	0.29	1.16	https://www.digikey.com/short/9d02ztwz
C1-C2	CAP TANT 10UF 10% 25V 2312	2	0.72	1.44	https://www.digikey.com/short/7vz343n9
A1	Arduino Nano	1	4.30	4.30	https://www.amazon.com/dp/B08Z7HQ2B6/
J1	01x10 Female Header Pins	1	0.79	0.79	https://www.digikey.com/short/23bfwwjh
PCB	Circuit Board	1	1.29	1.29	https://pcbsupplier.com/

SLC_USBP: 2 Channel USB Port [SLC_USBP]

Designator	Component	Number	Cost per unit - currency	Total cost - currency	Source of materials
J2 -J3	CONN RCPT TYPEA 4POS R/A	2	1.81	3.62	https://www.digikey.com/short/wvqm7zfm
C1 – C2	CAP TANT 10UF 10% 25V 2312	2	0.72	1.44	https://www.digikey.com/short/7vz343n9
A1	Arduino Nano	1	4.30	4.30	https://www.amazon.com/dp/B08Z7HQ2B6/
J1	01x10 Female Header Pins	1	0.79	0.79	https://www.digikey.com/short/23bfwwjh

U1	IC USB SWITCH DPDT 10MSOP	1	0.79	0.79	https://www.digike.y.com/short/zhv31z2b
U2	IC USB FS SERIAL UART 28-SSOP	1	4.70	4.70	https://www.digike.y.com/short/r9nm9f5r
PCB	Circuit Board	1	1.29	1.29	https://pcbshopper.com/

LOAF_X08: 8 Channel Loaf Backplane [LOAF_X08]

Designator	Component	Number	Cost per unit - currency	Total cost - currency	Source of materials
A1	Arduino Nano	1	4.30	4.30	https://www.amazon.com/dp/B08Z7HQ2B6/
BAT1	BATT HLDR COIN 20MM 1 CEL PC PIN	1	1.72	1.72	https://www.digike.y.com/en/products/detail/mpd-memory-protection-devices/BH32T-C-G/2079906
C1 C2	CAP TANT 10UF 10% 25V 2312	2	0.72	1.44	https://www.digike.y.com/short/7vz343n9
C3 C4 C5	CAP CER 10000PF 50V X7R 1206	3	0.29	0.87	https://www.digike.y.com/short/9d02ztwz
D1 D2 D3 D4 D5 D6 D7 D8	LED RED CLEAR 5MM OVAL T/H	8	0.13	1.04	https://www.digike.y.com/en/products/detail/creeled-inc/C5SMF-RJF-CT0W0BB2/6138570
J2 J1	TERM BLK 2POS SIDE ENTRY 5MM PCB	2	0.47	0.94	https://www.digike.y.com/short/3nv7nt34
J3	CONN MICRO SD CARD PUSH-PUSH R/A	1	3.48	3.48	https://www.digike.y.com/en/products/detail/3m/2908-05WB-MG/1242497
J4 J5	MODULAR JACK RJ45 8P8C	2	0.62	1.24	https://www.digike.y.com/en/products/detail/adam-tech/MTJ-883X1/9832289
JP2 JP3 JP1 JP4 JP5	2 Pin Header	5	0.04	0.2	https://www.amazon.com/dp/B07PKKY8BX/

P1 P2 P3 P4 P5 P6 P7 P8	CONN HEADER VERT 10POS 2.54MM	8	1.64	13.12	https://www.digikey.com/en/products/detail/samtec-inc/TSW-110-09-G-S/7871365
R1	RES 10K OHM 1% 1/2W 1206	1	0.10	0.10	https://www.digikey.com/en/short/p82bnb9p
R3 R2 R5 R4	RES 4.7K OHM 1% 1/4W 1206	4	0.10	0.40	https://www.digikey.com/en/short/93rfw21v
U1	IC TRNSLTR BIDIRECTIONAL 14TSSOP	1	1.44	1.44	https://www.digikey.com/en/products/detail/onsemi/NLSX5014DTR2G/2512573
U2	IC RTC CLK/CALENDAR I2C 8-DIP	1	4.07	4.07	https://www.digikey.com/en/products/detail/maxim-integrated/DS1307/956883
U3	IC BUFFER 5.5V 20DIP	1	1.60	1.60	https://www.digikey.com/en/products/detail/texas-instruments/SN74AHC8541N/13502430
U4	IC REDRIVER I2C 2CH 400KHZ 8SO	1	3.62	3.62	https://www.digikey.com/en/products/detail/nxp-usa-inc/P82B96TD-112/739478
Y1	CRYSTAL 32.7680KHZ 12.5PF TH	1	0.32	0.32	https://www.digikey.com/en/products/detail/abracon-llc/AB38T-32-768KHZ/675229
PCB	Circuit Board	1	2.20	2.20	https://pcbsupplier.com/

3.5 Build instructions

3.5.1 General Component Construction and Programming

When building a component from the BREAD system, first download the entire folder structure from the relevant repository. Order all of the components listed in the BOM.csv file. In cases where the routing is performed on a single layer, the board can either be milled [28] or etched [68]. For more advanced boards (2 layers, or fine-pitched components), the board can be ordered from a commercial manufacturer. Either of the two aforementioned steps require reference to the files stored in the gerbers directory.

Most of the components are through hole and thus can easily be soldered using a standard fine-tipped soldering iron.

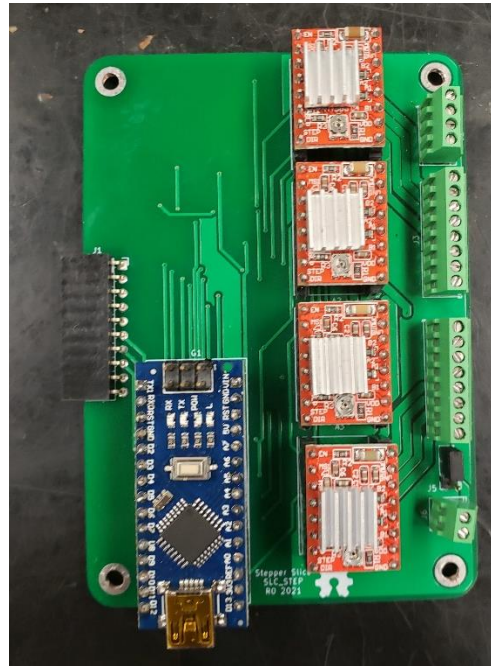


Figure 3.38: An example assembled slice, the SLC_STEP

The slice or loaf casing can be 3-D printed out of any available rigid material, with solid infill, and a layer height under 0.5mm.



Figure 3.39: 3-D Printing the Case

The enclosures are designed to facilitate embedded brass threads which are used for board mounting and attaching the opposite end of the enclosure. Use a fine-tipped soldering iron to heat up the threaded insert to 300°C and firmly press it into the appropriate cavity (Figure 3.40).



Figure 3.40: Heating up and installing the threaded inserts

If necessary, adjust jumpers to the desired position on the board, then install the board and the top cover, using the appropriate (usually M3) bolts (Figure 3.41).

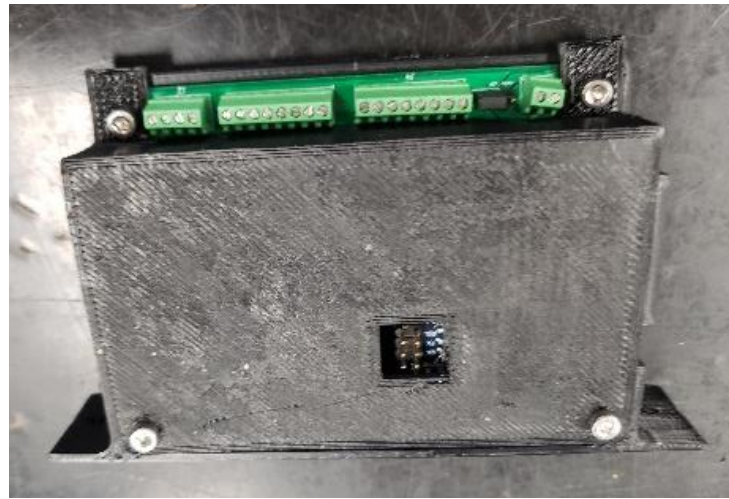


Figure 3.41: A fully assembled slice

In the case where slices are being placed in a loaf, it can be advantageous to wire all peripherals before placing the slice into the loaf as shown with the stepper motor in Figure 3.42.

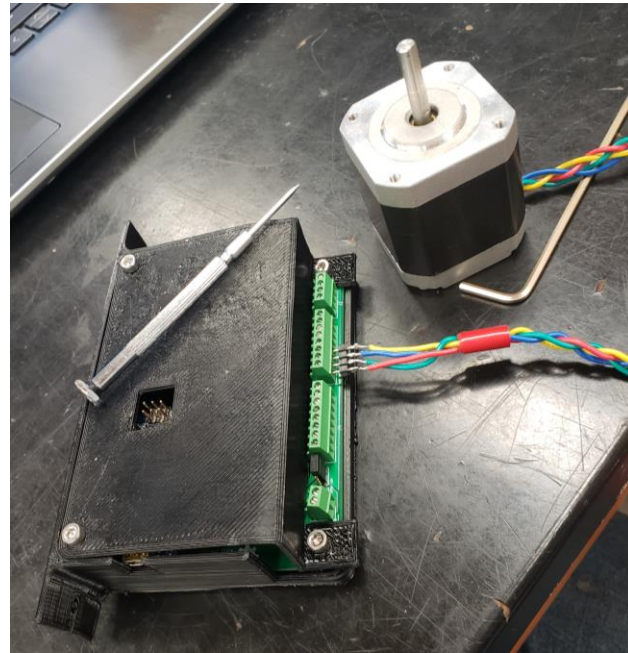


Figure 3.42: A slice with its relevant peripheral (stepper motor) installed.

After the slice has been assembled, the Arduino Nano can be programmed with the default firmware in the firmware folder. Open the firmware .ino file in the Arduino IDE [13] and connect the device to the programming computer via a USB cable. Customization of the firmware is supported and encouraged, but it is recommended that the command parsing and communication functions remain unaltered.

3.5.2 Emergency Stop Wiring

Each loaf has a set of contacts broken out for an emergency stop interlock chain. Specifically, on the LOAF_X08, the contacts are broken out on J1. The interlock chain can contain any contact-based device such as push buttons, limit switches, proximity switches, and relay contacts. The devices must be wired such that the “open state” indicates the device should be in an E-Stop State. If the E-Stop feature is not being used, these contacts should be shorted together.

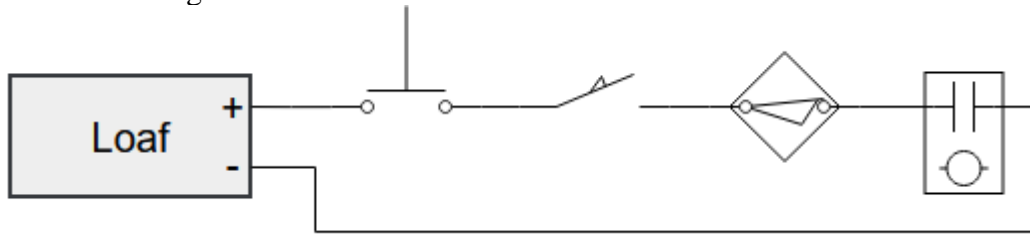


Figure 3.43: An example safety interlock chain consisting of a push button, limit switch, proximity switch, and a relay contact.

3.5.3 Example System: TIG-based Metal 3D Printer Monitor

The example configuration for monitoring the welding process for a TIG-based metal 3-D printer utilizes 1 loaf (LOAF_X08), an analog measurement slice (SLC_LVAI), and a thermocouple measurement slice (SLC_THRM). The slices should be programmed with the default firmware, and the loaf should be configured with the custom firmware available on [TIG Repo]. SLC_LVAI should be placed in the Slice 1 slot, and SLC_THRM should be placed in the Slice 2 slot.

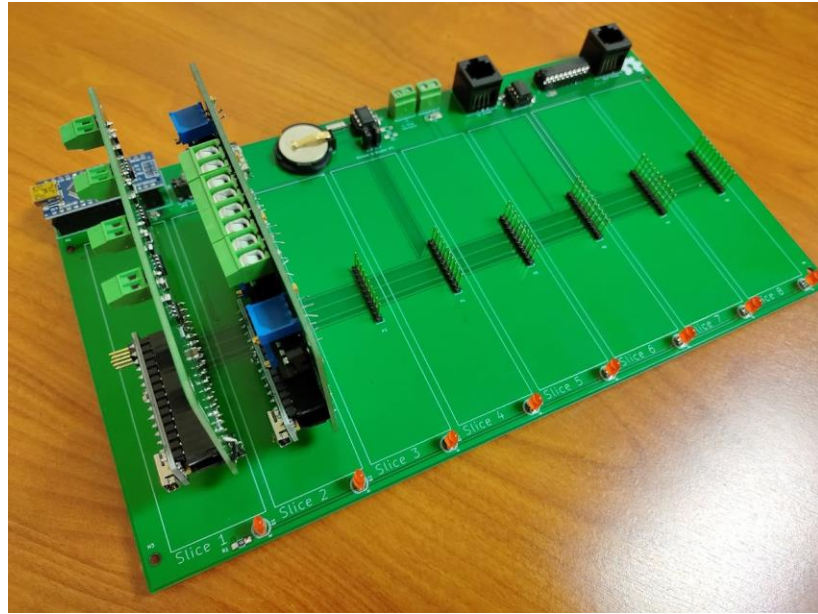


Figure 3.44: A skeletonized breakout of the metal 3-D printing monitor BREAD configuration.

The piezoelectric microphone and photoresistor should be linked to suitably long twisted shielded pair wires to shield the signals from any potential interference due to the welding process [68]. The sensors are placed in a 3-D printed carrier (Figure 3.45) and mounted to the end effector of the 3-D printer. The sensors are then linked into input channels on the SLC_LVAI. Additionally, a custom current transformer (Figure 3.46), which can be manufactured using an open source winder is placed around the ground wire of the welder (note that any current transformer can be substituted for this sensor). The transformer is also wired to SLC_LVAI. Finally, 4 type-k thermocouple probes are attached underneath the build substrate, electrically insulated by a thin piece of Kapton tape.

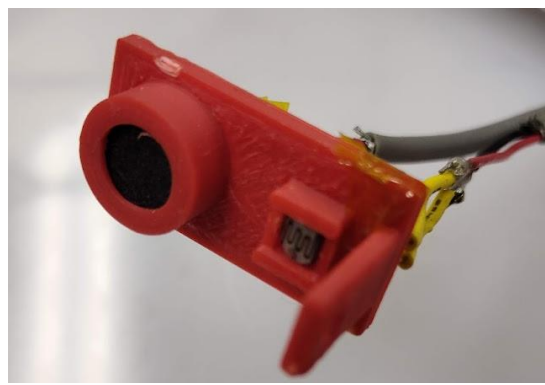


Figure 3.45: The Light and Sound measurement fixture

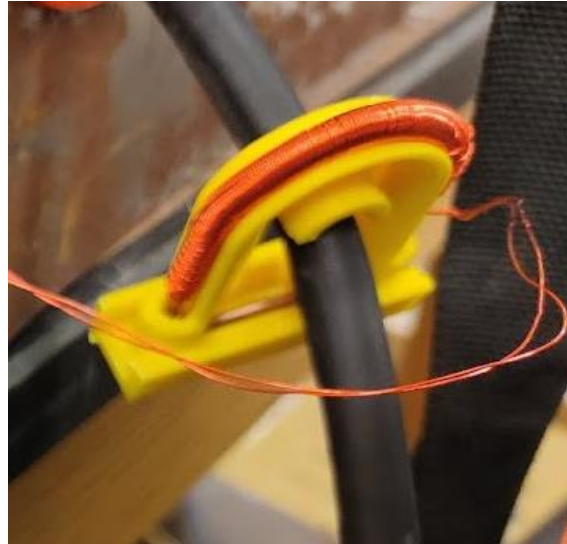


Figure 3.46: A custom current transformer placed around the ground wire of the welder

A worse-case scenario weld should be initialized (Turn off the gas and raise the tungsten electrode to ~3mm), and then the offset and gain of each analog channel should be adjusted to fully utilize the resolution of the ADC.

The loaf output can be monitored via the Arduino Serial Monitor (or equivalent) at 250000 baud.

3.6 Operation instructions

3.6.1 Commands

Commands can be executed 3 separate ways: Via USB to loaf which houses the slice, via a call of “executeCommand” in the slice firmware, or by direct USB connection to the slice.

When commanding a slice via USB that is housed on a loaf, a command can be sent through the terminal that follows the syntax given below:

```
Address, Command #, !R/W, Parameter1, Parameter2
```

Where address is the 7-bit address of the slice, command is an 8-bit unsigned integer, R/W is a Boolean which indicates a read command when 0, and a write command when 1. Parameters 1 and 2 can either be of the float data type or 32-bit binary sequences (must be entered as their decimal equivalent).

When commanding a slice via a call of the “executeCommand” function, the command syntax is as follows:

```
executeCommand(Address, Command#, !R/W, Parameter1, Parameter2)
```

Where all of the parameters are the same as previously defined, but Parameter1 and 2 must be of the float data type.

Finally, when directly commanding a slice via USB, the syntax is:

```
Address, Command #, !R/W, Parameter1, Parameter2
```

Each of the 8 slices explored in this paper have a unique set of commands summarized below in Tables 3.3 – 3.10.

Table 3.3: SLC_LVAI: Amplified Analog Input Slice Commands

Setup (no significant returns)			
Command: 0x01	!R/W Bit: 1	Parameter 1: Channels to Read	Parameter 2: Channels to FFT
Read Channel (Returns instantaneous value on given channel)			
Command: 0x02	!R/W Bit: 0	Parameter 1: Channel	Parameter 2: X
Mass Read Channel (returns instantaneous value of multiple channels)			
Command: 0x03	!R/W Bit: 0	Parameter 1: Channels to Read	Parameter 2: X
FFT Channel (returns FFT array of given channel)			
Command: 0x04	!R/W Bit: 0	Parameter 1: Channel	Parameter 2: X

Table 3.4: SLC_IDIO: Isolated Digital Input/Outputs Commands

Setup (no significant returns)			
Command: 0x01	!R/W Bit: 1	Parameter 1: Channels to Read	Parameter 2: Channel Direction
Read Channel (Returns instantaneous value on given channel)			
Command: 0x02	!R/W Bit: 0	Parameter 1: Channel	Parameter 2: X
Mass Read Channel (returns instantaneous value of multiple channels)			
Command: 0x03	!R/W Bit: 0	Parameter 1: Channels to Read	Parameter 2: X

Write Channel (Returns instantaneous value on given channel)			
Command: 0x04	!R/W Bit: 1	Parameter 1: Channel	Parameter 2: Value
Mass Write Channel (returns instantaneous value of multiple channels)			
Command: 0x05	!R/W Bit: 1	Parameter 1: Channels to Write	Parameter 2: Values to Write
PulseIn Channel (returns the pulse length on a channel)			
Command: 0x06	!R/W Bit: 0	Parameter 1: Channel	Parameter 2: High or Low Select
PulseOut Channel (returns the pulse length on a channel)			
Command: 0x07	!R/W Bit: 0	Parameter 1: Channel	Parameter 2: Freq

Table 3.5: SLC_AAFT: Audio Analysis / Fourier Transform Commands

Setup (no significant returns)			
Command: 0x01	!R/W Bit: 1	Parameter 1: Channels to Read	Parameter 2: Channels to FFT
Read Channel (Returns instantaneous value on given channel)			
Command: 0x02	!R/W Bit: 0	Parameter 1: Channel	Parameter 2: X
Mass Read Channel (returns instantaneous value of multiple channels)			
Command: 0x03	!R/W Bit: 0	Parameter 1: Channels to Read	Parameter 2: X

FFT Channel (returns FFT array of given channel)			
Command: 0x04	!R/W Bit: 0	Parameter 1: Channel	Parameter 2: X

Table 3.6: SLC_CR10: +/- 10A Current Sensor Commands

Setup (no significant returns)			
Command: 0x01	!R/W Bit: 1	Parameter 1: Channels to Read	Parameter 2: Channels to FFT
Write Channel (Returns instantaneous value on given channel)			
Command: 0x02	!R/W Bit: 0	Parameter 1: Channel	Parameter 2: X
Mass Write Channel (returns instantaneous value of multiple channels)			
Command: 0x03	!R/W Bit: 0	Parameter 1: Channels to Read	Parameter 2: X

Table 3.7: SLC_RLAY: 4 Channel Relay Controller Commands

Setup (no significant returns)			
Command: 0x01	!R/W Bit: 1	Parameter 1: Channels to Enable	Parameter 2: X
Write Channel (Returns instantaneous value on given channel)			
Command: 0x04	!R/W Bit: 1	Parameter 1: Channel	Parameter 2: X
Mass Write Channel (returns instantaneous value of multiple channels)			
Command: 0x05	!R/W Bit: 1	Parameter 1: Channels to Write	Parameter 2: Values to write

Table 3.8: SLC_STEP: 4 Channel Stepper Motor Controller Commands

Set Mode (no significant returns)			
Command: 0x01	!R/W Bit: 1	Parameter 1: Channels to Effect	Parameter 2: Mode of Channels
Set Value (no significant returns)			
Command: 0x04	!R/W Bit: 1	Parameter 1: Channels	Parameter 2: Values
Read Value (returns position of channel)			

Command: 0x05	!R/W Bit: 0	Parameter 1: Channels to Write	Parameter 2: Values to write
------------------	-------------	-----------------------------------	------------------------------

Table 3.9: SLC_THRM: 4 Channel Type-K Thermocouple Reader Commands

Setup (no significant returns)			
Command: 0x01	!R/W Bit: 1	Parameter 1: Channels to Read	Parameter 2: X
Write Channel (Returns instantaneous value on given channel)			
Command: 0x02	!R/W Bit: 0	Parameter 1: Channel	Parameter 2: X
Mass Write Channel (returns instantaneous value of multiple channels)			
Command: 0x03	!R/W Bit: 0	Parameter 1: Channels to Read	Parameter 2: X

Table 3.10: SLC_USBP: 2 Channel USB Port Commands

Setup (no significant returns)			
Command: 0x01	!R/W Bit: 1	Parameter 1: Channels to Enable	Parameter 2: X
Read Channel (Returns instantaneous value on given channel)			
Command: 0x02	!R/W Bit: 0	Parameter 1: Channel	Parameter 2: X
Write Channel (Writes value to specified channel)			
Command: 0x03	!R/W Bit: 1	Parameter 1: Channel	Parameter 2: Values

3.6.2 Example System: TIG-based Metal 3D Printer Monitor

Once the system is installed, operation is straight-forward. Connect the loaf to a computer via USB, open a serial monitor, and copy the data as needed. The firmware is configured to continually sample. Record timestamps during the start and finish of experiments to better correlate samples with their relevant moments during the experiment.

3.7 Validation and characterization

3.7.1 Slice Characterization

Each of the eight slices has undergone a basic characterization, and the results are listed below in their respective sections. All slices have had basic communication functionality validated (both via the Backplane and via USB).

3.7.1.1 SLC_LVAI: Amplified Analog Input Slice Characterization

The SLC_LVAI is a flexible analog input card, bolstered by its hardware gain and offset. When linked to USB, the slice can act as an effective method for low frequency signal visualization (Figure 3.47). The channels act linearly (Figure 3.48), and exhibit a low deviation from channel to channel (Figure 3.49).

Table 3.11: A Table summarizing the key features of the Analog Slice

Parameter	Value (or Range)
Allowable Voltage Range	0V – 5V
Maximum Frequency	120Hz
Maximum Gain	20.82 dB
Maximum Offset	5V

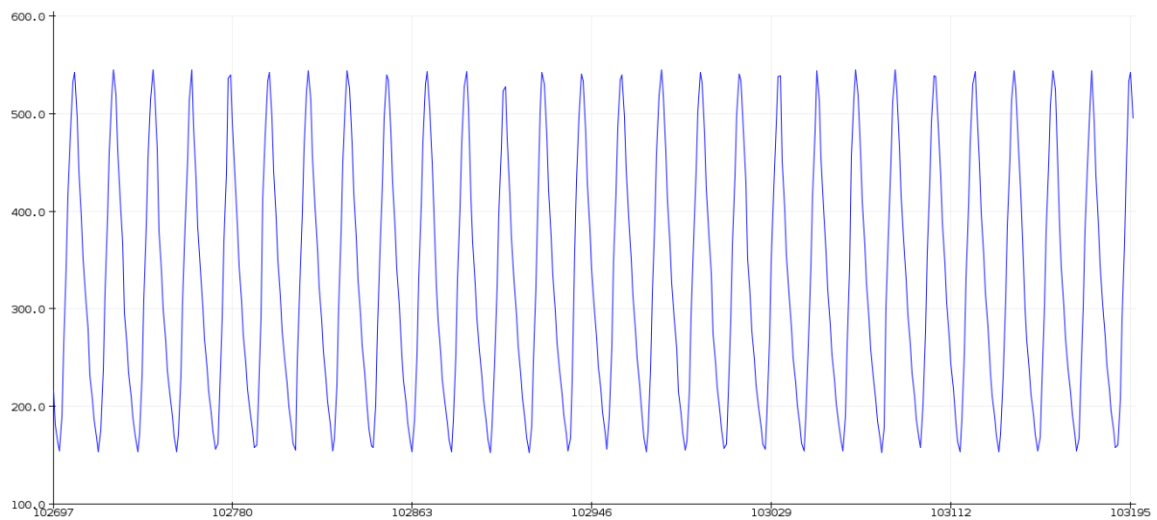


Figure 3.47: An example Analog reading generated from a signal supply linked to Channel 1 rendered in the Arduino IDE from serial data

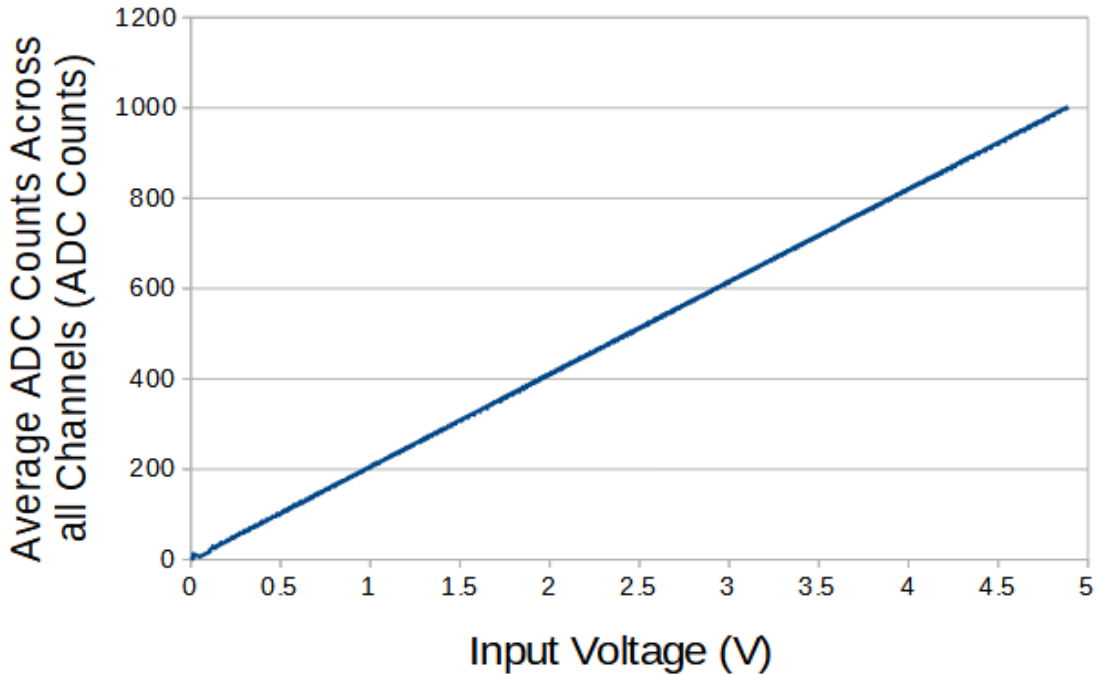


Figure 3.48: The average response of the channel per input voltage

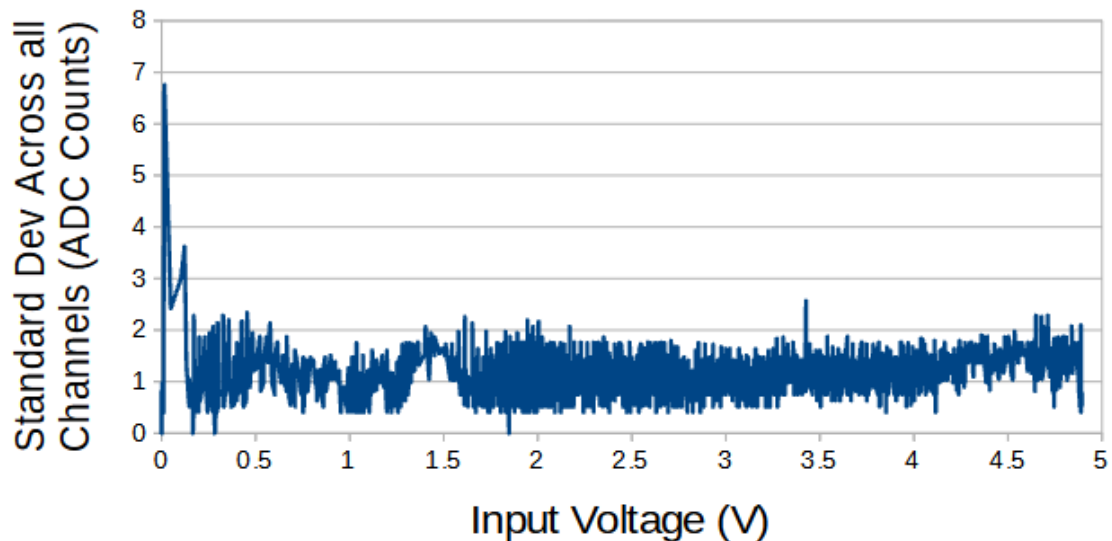


Figure 3.49: The standard deviation across all channels per voltage input

3.7.1.2 SLC_IDIO: Isolated Digital Input/Outputs Characterization

The slice is able to effectively act as a source for digital inputs and outputs. It can output pulses at a frequency of 2.5 kHz before significant distortion begins to occur (Figure 3.50).

Table 3.12: A Table summarizing the key features of the Digital Slice

Parameter	Value (or Range)
Input Voltage Range	1.2V – 70V
Max Input Current	30 mA
Max Input Frequency	10 kHz
Max Output Voltage	70V
Max Output Current	30 mA
Max Output Frequency	2.5 kHz

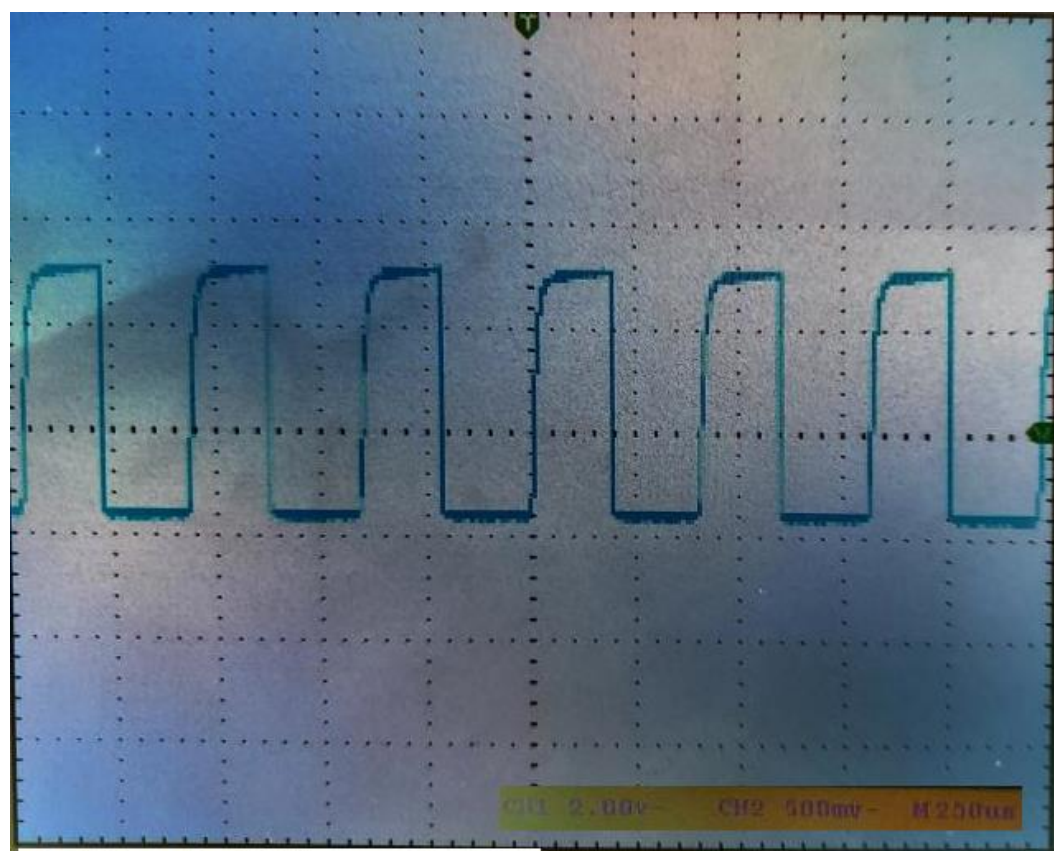


Figure 3.50: A channel of SLC_IDIO outputting a frequency of 2.5kHz

3.7.1.3 SLC_AAFT: Audio Analysis / Fourier Transform Characterization

When connected directly to USB, the SLC_AAFT acts an effective tool for visualizing signal spectra (Figure X). When exposed to a frequency, the uncalibrated SLC_AAFT shows linearity up until roughly 3.8 kHz, at which case the measurement becomes aliased (Figure X). This experimentally determines the usable range of the ADC to be 0 to 3.5 kHz.

Table 3.13: A Table summarizing the key features of the Audio Slice

Parameter	Value (or Range)
Allowable Voltage Range	0V – 5V
Maximum Frequency	3.5 kHz
Maximum Gain	20.82 dB
Maximum Offset	5V

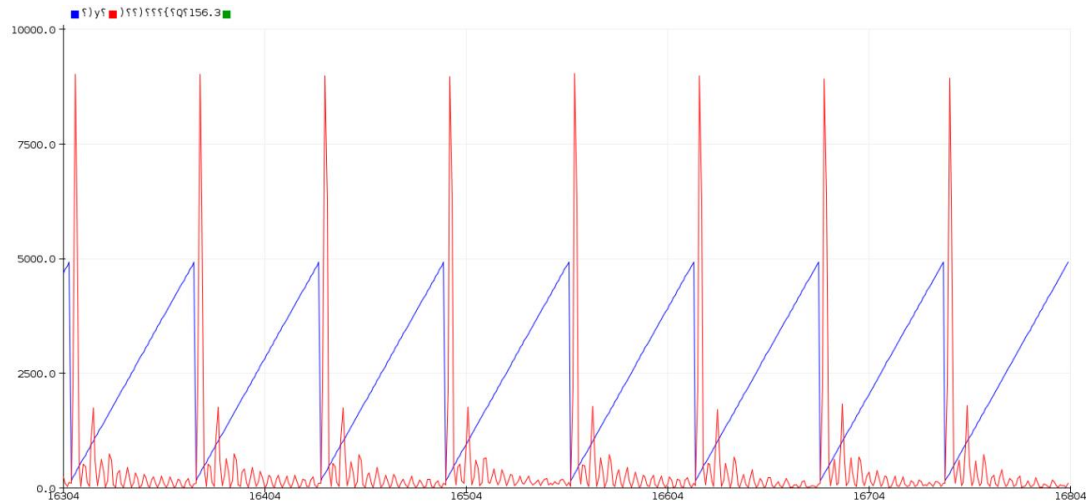


Figure 3.51: An example FFT reading generated from an electric guitar linked to Channel 1. The chord being played is Middle Cmaj. Red is the FFT Output, and blue is tracking the relevant frequency bin rendered in the Arduino IDE from serial data

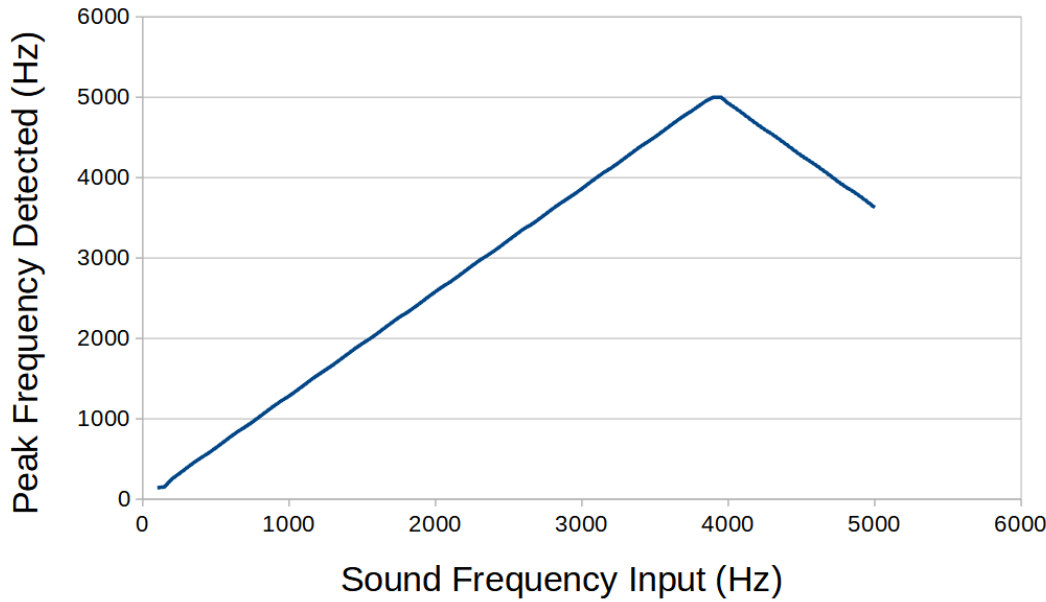


Figure 3.52: A varying frequency is input into a channel of the AAFT and the peak frequency is detected.

3.7.1.4 SLC_CR10: +/- 10A Current Sensor Characterization

When connected directly to USB, the SLC_CR10 is able to visually display up to four current measurements simultaneously (Figure 3.53). All four channels respond linearly (Figure X) with a standard deviation across all channels of 0.02A.

Table 3.14: A Table summarizing the key features of the Current Slice

Parameter	Value (or Range)
Maximum Measurable Current	-10A to 10A
Minimum Measurable	20mA
Maximum Frequency	100Hz

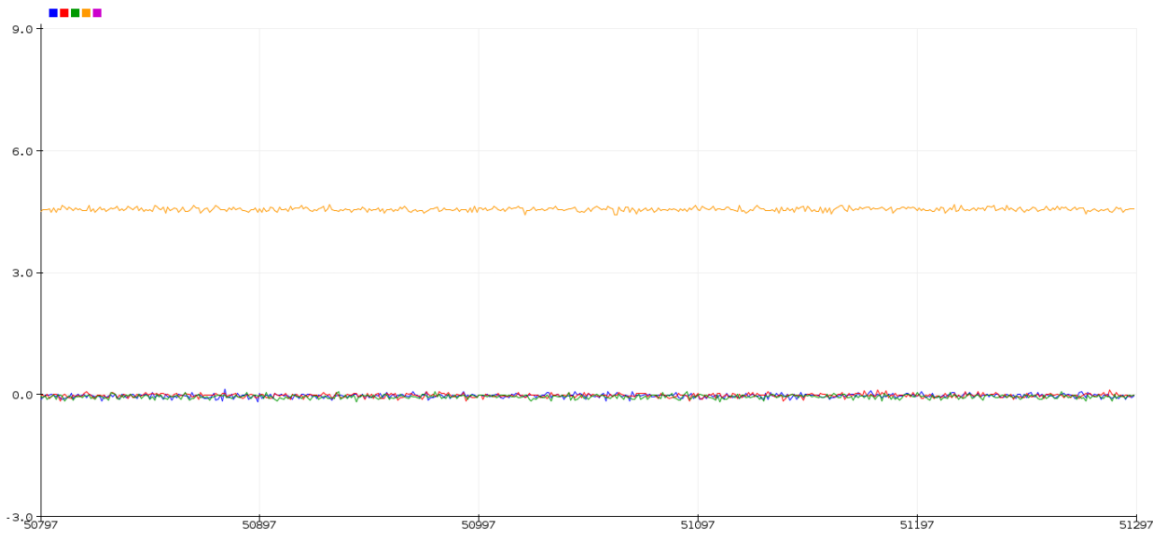


Figure 3.53: A DC current of 4A is passed through CH1, while the others are left at 0A.
Rendered in the Arduino IDE from serial data.

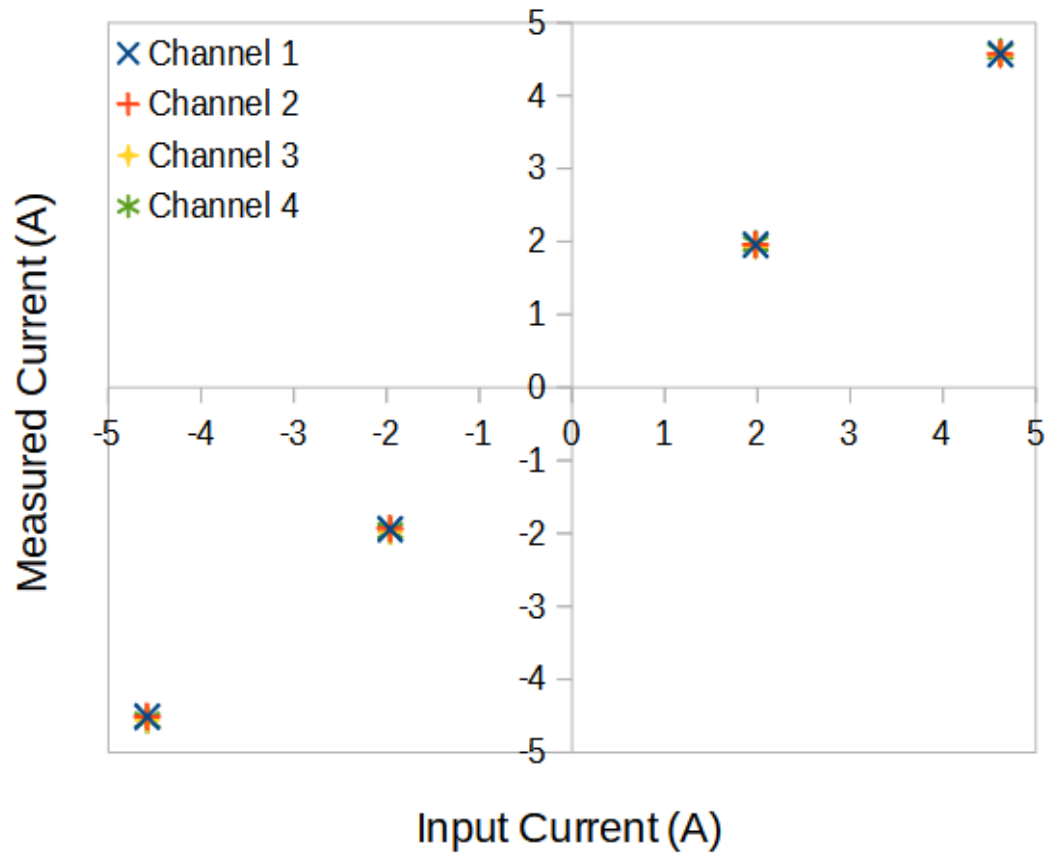


Figure 3.54: The current across all channels given 4 test loads.

3.7.1.5 SLC_RLAY: 4 Channel Relay Controller Characterization

SLC_RLAY can be used for switching high current devices.

Table 3.15: A Table summarizing the key features of the Relay Slice.

Parameter	Value (or Range)
Max Current	10A AC / 5A DC
Max Voltage	125V AC / 30VDC
Switch Time	5 ms

3.7.1.6 SLC_STEP: 4 Channel Stepper Motor Controller Characterization

SLC_STEP provides a flexible platform which can control a wide range of bi-polar stepper motors. As long as the stepper can operate under 2A per coil, and at speeds less than 10,000 steps per second, the SLC_STEP can drive them. This has been validated by running commercial NEMA 17 motors with no errors.

Table 3.16: A Table summarizing the key features of the Stepper Slice

Parameter	Value (or Range)
Max Motor Current	2A per coil
Max Output Rate (Used to determine speed)	10,000 Pulses / second

3.7.1.7 SLC_THRM: 4 Channel Type-K Thermocouple Reader Characterization

SLC_THRM is able to read from Type-K thermocouples with little noise (Figure 3.55).

Table 3.17: A Table summarizing the key features of the Thermocouple Slice

Parameter	Value (or Range)
Temperature Range	-200C to 1260°C
Minimum Measurable	0.25°C

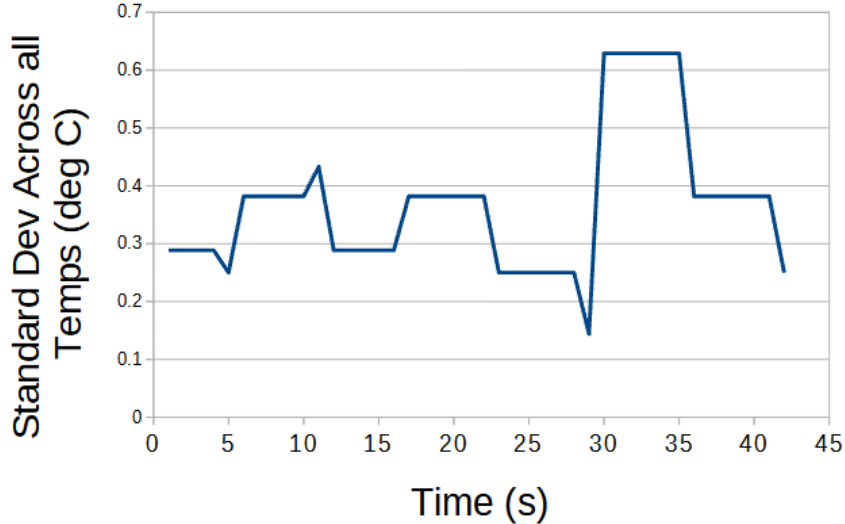


Figure 3.55: The standard deviation across all channels given a stable room temperature

3.7.1.8 SLC_USBP: 2 Channel USB Port Characterization

SLC_USBP is capable of connecting and communicating with up to two USB devices at a speed compatible with USB 2.0 (or slower).

Table 3.18: A Table summarizing the key features of the USB Slice

Parameter	Value (or Range)
Max Speed	USB 2.0

3.7.2 Example System: TIG-based Metal 3D Printer Monitor

The TIG-bot, an open source TIG-base metal 3-D printer [hardware paper], was set to run 2 tests, where a 16mm long line is extruded, with only the stand-off distance varying (which will directly impact weld quality). As the welding process is DC, there is no significant signal aside from the start up. This binary signal, however, can be used to determine if a start up was successful. This basic experiment has shown that the target signals are affected by the experimental variable and can now be correlated. This information can be used for a multitude of purposes such as close looped control to maintain an ideal weld, or instantaneous weld characterization.

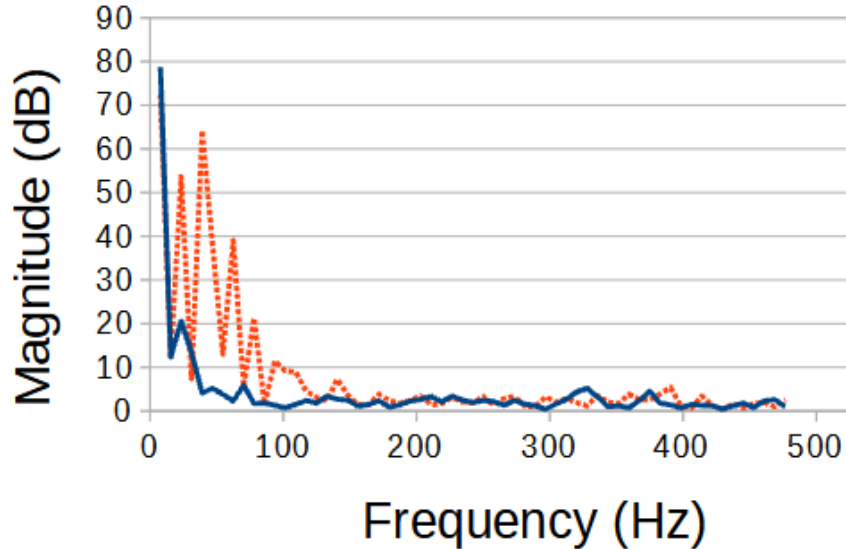


Figure 3.56: The light frequency spectrum of an ideal weld (blue solid) compared to the frequency spectrum of a flawed weld (red dotted)

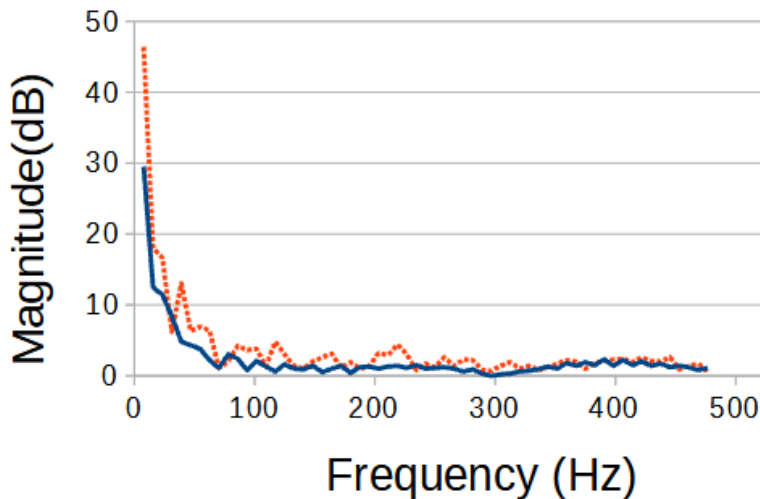


Figure 3.57: The sound frequency spectrum of an ideal weld (blue solid) compared to the frequency spectrum of a flawed weld (red dotted)

3.7.3 Economic Analysis

The closest commercial alternative to the BREAD system is National Instruments CRIo system. Like BREAD, it offers a backplane with several interchangeable cards. The focus of the CRIo system is to work with other industrial automation devices, where the aim of BREAD is to be completely inclusive. As an example, the CRIo system would need a digital output card AND an external motor driver, whereas BREAD features an all-in-one solution.

Six of the slices explored in this paper have near-equivalent counterparts (in base functionality) in the Crio system, and have been compared in the tables below:

Table 3.19: A comparison of key features for analog measurement devices

Description	# Channels	Max voltage	Resolution	Sample Rate	Gain Range	Offset Range	Cost (USD)
SLC_LVAI	6 Single Ended	5V	10 Bit	10 kS/S	11	5V	40.61
NI-9281 [70]	2 Differential	12V	24 Bit	513 S/S	1	0V	1369.00

Table 3.20: A comparison of key features for digital input / output devices

Description	Number of Channels	Max voltage	Switching frequency	Bidirectional	Isolation	Drive Current	Cost (USD)
SLC_IDIO	8	100V	2.5 kHz	Yes	4000VDC	30 mA	23.20
NI-9401 [71]	8	5V	10 MHz	Yes	60VDC	2 mA	604.00

Table 3.21: A comparison of key features for audio measurement

Description	# Channels	Max voltage	Resolution	Max Freq	Gain Range	Offset Range	Cost (USD)
SLC_AAFT	2	5V	10 Bit	3.5 kHz	11	5V	32.64
NI-9230 [72]	3	30V	24 Bit	6.4 kHz	1	0V	755.00

Table 3.22: A comparison of key features for current measurement

Description	# Channels	Current Range	Resolution	Sample Rate	Cost (USD)
SLC_CR10	4	+/-10A	10 bit	10 kS/S	35.46
NI-9227 [73]	4	+/-10A	24 Bit	1 kS/S	1599.00

Table 3.23: A comparison of key features for mechanical relay switching

Description	# Channels	Max Voltage	Max Current	Switch Time	Type	Cost (USD)
SLC_RLAY	4	125VAC / 30VDC	10 AAC / 5 ADC	5 mS	Electromechanical	46.81
NI-9482 [74]	4	250VAC / 60VDC	1.5 AAC / 1.5 ADC	15 mS	Electromechanical	249.00

Table 3.24: A comparison of key features for temperature measurement

Description	# Channels	Type Compatibility	Resolution	Cost (USD)
SLC_THRM	4	All Standard Types	0.25°C	40.87
NI-9210 [75]	4	All Standard Types	0.8°C	465.00

The average cost savings of a BREAD slice compared to an equivalent national instruments CRI0 card is 93%. The highest advantage NI systems can provide is high measurement resolution due to their 24-bit ADCs. However, BREAD's open design philosophy allows designs such as the SLC_LVAI to have on-board tuneable gain, effectively increasing resolution for lower voltage ranges. Additionally, if high resolution is required, a new slice can be easily evolved from SLC_LVAI using external ADCs (at an added cost).

3.7.4 Continued Development and Application

There are countless open-source circuits that are well executed, yet only serve one set of purposes. On HardwareX alone, there are systems for irrigation management [76], colorimetry [77], spectral acquisition [78, 79], and specialized environmental sensing circuits [80, 81]. The aforementioned electronics are a very small fraction of existing and documented designs that could be highly compatible with BREAD. The BREAD system can sustain rapid growth by adapting these existing and open designs into new slices.

Since the BREAD system currently has a significant overlap with the National Instruments Crio system, there are several applications that could easily be adapted for cost reductions. Specifically, BREAD could be employed as a general-purpose data acquisition system for experiments and measurements [82, 83]. BREAD can be employed for measuring and recording power usage & analysis [84, 85, 86]. BREAD can also be used for industrial automation, including robotics [87] and process control [88]. As BREAD's slice library grows, the capabilities and permutations create an endlessly flexible and capable choice for an electronics platform.

3.7.5 Future Work

There are countless open-source circuits that are well executed, yet only serve one set of purposes. On HardwareX alone, there are systems for irrigation management [76], colorimetry [77], spectral acquisition [78, 79], and specialized environmental sensing circuits [80, 81]. The aforementioned electronics are a very small fraction of existing and documented designs that could be highly compatible with BREAD. The BREAD system can sustain rapid growth by adapting these existing and open designs into new slices.

Since the BREAD system currently has a significant overlap with the National Instruments Crio system, there are several applications that could easily be adapted for cost reductions. Specifically, BREAD could be employed as a general-purpose data acquisition system for experiments and measurements [82, 83]. BREAD can be employed for measuring and recording power usage & analysis [84, 85, 86]. BREAD can also be used for industrial automation, including robotics [87] and process control [88]. As BREAD's slice library grows, the capabilities and permutations create an endlessly flexible and capable choice for an electronics platform.

3.8 References

1. J.M. Pearce, Economic savings for scientific free and open source technology: A review, *HardwareX*. 8 (2020) e00139. <https://doi.org/10.1016/j.ohx.2020.e00139>.
2. L. Goertzen, N. Mehr, M. Lopez, C. Udell, J.S. Selker, Low-cost and precise inline pressure sensor housing and DAQ for use in laboratory experiments, *HardwareX*. 8 (2020) e00112. <https://doi.org/10.1016/j.ohx.2020.e00112>.
3. D. Suriano, A portable air quality monitoring unit and a modular, flexible tool for on-field evaluation and calibration of low-cost gas sensors, *HardwareX*. 9 (2021) e00198. <https://doi.org/10.1016/j.ohx.2021.e00198>.
4. S. Oberloier, J.M. Pearce, Open source low-cost power monitoring system, *HardwareX*. 4 (2018) e00044. <https://doi.org/10.1016/j.ohx.2018.e00044>.
5. D.M. Laverty, R.J. Best, P. Brogan, I. Al Khatib, L. Vanfretti, D.J. Morrow, The OpenPMU Platform for Open-Source Phasor Measurements, *IEEE Transactions on Instrumentation and Measurement*. 62 (2013) 701–709. <https://doi.org/10.1109/TIM.2013.2240920>.
6. M.J.Y. Zimmermann, A. Maia Chagas, P. Bartel, S. Pop, L.L. Prieto-Godino, T. Baden, LED Zappelin': An open source LED controller for arbitrary spectrum visual

- stimulation and optogenetics during 2-photon imaging, *HardwareX*. 8 (2020) e00127. <https://doi.org/10.1016/j.ohx.2020.e00127>.
7. E.Y. Kimchi, B.F. Coughlin, B.E. Shanahan, G. Piantoni, J. Pezaros, S.S. Cash, OpBox: Open Source Tools for Simultaneous EEG and EMG Acquisition from Multiple Subjects, *ENeuro*. 7 (2020) ENEURO.0212-20.2020. <https://doi.org/10.1523/ENEURO.0212-20.2020>.
 8. D. Lagos-Susaeta, O. Salazar, J.A. Asenjo, openPFGE: An open source and low cost pulsed-field gel electrophoresis equipment, *HardwareX*. 8 (2020) e00128. <https://doi.org/10.1016/j.ohx.2020.e00128>.
 9. F. Carena, W. Carena, S. Chapelard, V. Chibante Barroso, F. Costa, E. Dénes, R. Divià, U. Fuchs, A. Grigore, T. Kiss, G. Simonetti, C. Soós, A. Telesca, P. Vande Vyvre, B. von Haller, The ALICE data acquisition system, *Nuclear Instruments and Methods in Physics Research Section A: Accelerators, Spectrometers, Detectors and Associated Equipment*. 741 (2014) 130–162. <https://doi.org/10.1016/j.nima.2013.12.015>.
 10. B. Nguyen, B. Goto, J.S. Selker, C. Udell, Hypnos board: A low-cost all-in-one solution for environment sensor power management, data storage, and task scheduling, *HardwareX*. 10 (2021) e00213. <https://doi.org/10.1016/j.ohx.2021.e00213>.
 11. G. Camprodón, Ó. González, V. Barberán, M. Pérez, V. Smári, M.Á. de Heras, A. Bizzotto, Smart Citizen Kit and Station: An open environmental monitoring system for citizen participation and scientific experimentation, *HardwareX*. 6 (2019) e00070. <https://doi.org/10.1016/j.ohx.2019.e00070>.
 12. Quigley, Morgan, Brian Gerkey, and William D. Smart. Programming Robots with ROS: a practical introduction to the Robot Operating System. " O'Reilly Media, Inc.", 2015.
 13. Arduino - Home, (n.d.). <https://www.arduino.cc/> (accessed July 12, 2021).
 14. M. Jakubowski, Open Source Ecology, in: N. Bandi, M.G. Kraft, S. Lasinger (Eds.), *Kunst, Krise, Subversion*, transcript Verlag, 2012: pp. 313–316. <https://doi.org/10.14361/transcript.9783839419625.313>.
 15. F.J. Ferrero Martín, M. Valledor Llopis, J.C. Campo Rodríguez, J.R. Blanco González, J. Menéndez Blanco, Low-cost open-source multifunction data acquisition system for accurate measurements, *Measurement*. 55 (2014) 265–271. <https://doi.org/10.1016/j.measurement.2014.05.010>.
 16. A.M. Pringle, S. Oberloier, A.L. Petsiuk, P.G. Sanders, J.M. Pearce, Open source arc analyzer: Multi-sensor monitoring of wire arc additive manufacturing, *HardwareX*. 8 (2020) e00137. <https://doi.org/10.1016/j.ohx.2020.e00137>.
 17. R. Herbst, R. Claus, M. Freytag, G. Haller, M. Huffer, S. Maldonado, K. Nishimura, C. O'Grady, J. Panetta, A. Perazzo, B. Reese, L. Ruckman, J.G. Thayer, M. Weaver, Design of the SLAC RCE Platform: A general purpose ATCA based data acquisition system, in: 2014 IEEE Nuclear Science Symposium and Medical Imaging Conference (NSS/MIC), 2014: pp. 1–4. <https://doi.org/10.1109/NSSMIC.2014.7431254>.
 18. R.A. Rohrer, S.K. Pitla, J.D. Luck, Tractor CAN bus interface tools and application development for real-time data analysis, *Computers and Electronics in Agriculture*. 163 (2019) 104847. <https://doi.org/10.1016/j.compag.2019.06.002>.

19. M. Hasler, K. Schindelwig, B. Mayr, Ch. Knoflach, S. Rohm, J. van Putten, W. Nachbauer, A Novel Ski–Snow Tribometer and its Precision, *Tribol Lett.* 63 (2016) 33. <https://doi.org/10.1007/s11249-016-0719-2>.
20. M. Meng, W.J. Zhang, P.C. Wang, D. Niedenzu, Y.Z. Tian, The Monitoring System for Stability of CNC Machining Based on cDAQ and LabVIEW, *Advanced Materials Research.* 1039 (2014) 177–182. <https://doi.org/10.4028/www.scientific.net/AMR.1039.177>.
21. R. Cipin, P. Prochazka, M. Toman, J. Martis, D. Cervinka, Automatic Li-Ion Accumulator Measuring Stand, *ECS Trans.* 74 (2016) 77. <https://doi.org/10.1149/07401.0077ecst>.
22. CompactDAQ Systems, (2021). <https://www.ni.com/en-us/shop/compactdaq.html> (accessed July 15, 2021).
23. Fisher RP, Myers BA. Free and simple GIS as appropriate for health mapping in a low resource setting: a case study in eastern Indonesia. *International journal of health geographics.* 2011 Dec;10(1):1-1.
24. Maia Chagas, A., 2018. Haves and have nots must find a better way: The case for open scientific hardware. *PLoS biology,* 16(9), p.e3000014.
25. S. Oberloier, J.M. Pearce, General Design Procedure for Free and Open-Source Hardware for Scientific Equipment, *Designs.* 2 (2018) 2. <https://doi.org/10.3390/designs2010002>.
26. Gibb, A., 2014. Building open source hardware: DIY manufacturing for hackers and makers. Pearson Education.
27. “KiCad EDA.” Accessed October 24, 2021. <https://www.kicad.org/>.
28. S. Oberloier, J.M. Pearce, Belt-Driven Open Source Circuit Mill Using Low-Cost 3-D Printer Components, *Inventions.* 3 (2018) 64. <https://doi.org/10.3390/inventions3030064>.
29. Sathyakumar, N., Kamal Prasath Balaji, Raja Ganapathi, and S. R. Pandian. “A Build-Your-Own Three Axis CNC PCB Milling Machine.” *Materials Today: Proceedings* 5, no. 11, Part 3 (January 1, 2018): 24404–13. <https://doi.org/10.1016/j.matpr.2018.10.236>.
30. S. Oberloier, N. Whisman, BREAD Slice - Template (SLC-TEMP), (2020). <https://osf.io/3xmpa/> (accessed October 24, 2021).
31. Arduino - StyleGuide, (n.d.). <https://www.arduino.cc/en/Reference/StyleGuide> (accessed October 24, 2021).
32. N. Whisman, S. Oberloier, J.M. Pearce, BREAD Slice -- Analog Reader / FFT (SLC_LVAI), (2021). <https://osf.io/742ez/> (accessed October 24, 2021).
33. N. Whisman, S. Oberloier, J.M. Pearce, BREAD Slice – Isolated Digital IO (SLC_IDIO), (2021). <https://osf.io/742ez/> (accessed October 24, 2021).
34. N. Whisman, S. Oberloier, J.M. Pearce, BREAD Slice - Audio Analysis (SLC_AAIT), (2021). <https://osf.io/a8nk5/> (accessed October 24, 2021).
35. N. Whisman, S. Oberloier, J.M. Pearce, BREAD Slice - +/- 10A Current Sensor (SLC_CR10), (2021). <https://osf.io/ajmbe/> (accessed October 24, 2021).
36. N. Whisman, S. Oberloier, J.M. Pearce, BREAD Slice - 4 Channel Relay (SLC_RLAY), (2021). <https://osf.io/5vxws/> (accessed October 24, 2021).

37. N. Whisman, S. Oberloier, J.M. Pearce, BREAD Slice - Stepper Motor Controller (SLC_STEP), (2021). <https://osf.io/q8nkc/> (accessed October 24, 2021).
38. N. Whisman, S. Oberloier, J.M. Pearce, BREAD Slice - Thermocouple Reader (SLC_THRM), (2021). <https://osf.io/sfehu/> (accessed October 24, 2021).
39. N. Whisman, S. Oberloier, J.M. Pearce, BREAD Slice - USB Port (SLC_USBP), (2021). <https://osf.io/j9rh5/> (accessed October 24, 2021).
40. MCP6004 | Microchip Technology, (n.d.). <https://www.microchip.com/en-us/product/MCP6004> (accessed October 24, 2021).
41. Comidox 4Pcs TEMT6000 Light Sensor Module Analog Light Intensity Module Visible Light Sensor for Arduino: Amazon.com: Tools & Home Improvement, (n.d.). <https://www.amazon.com/dp/B07JB5TQ93/> (accessed October 21, 2021).
42. Amazon.com: DAOKI 5PCS High Sensitivity Sound Microphone Sensor Detection Module for Arduino AVR PIC : Electronics, (n.d.). <https://www.amazon.com/dp/B00XT0PH10/> (accessed October 21, 2021).
43. G1/4" Pressure Transducer Sensor Stainless Steel 1% FS Accuracy Analog Sensor Output Signal for Water Gas Oil(0-200PSI): Amazon.com: Industrial & Scientific, (n.d.). <https://www.amazon.com/dp/B07KXXFRZP/> (accessed October 21, 2021).
44. Rizk, J, and Y Chaiko. "Solar Tracking System: More Efficient Use of Solar Panels," 2008, 3.
45. K.O. Alessio, B. Tischer, M. Voss, I.D. Teixeira, B.M. Brendler, F.A. Duarte, G.A. Helfer, A.B. Costa, J.S. Barin, Open source, low-cost device for thermometric titration with non-contact temperature measurement, *Talanta*. 216 (2020) 120975. <https://doi.org/10.1016/j.talanta.2020.120975>.
46. 12pcs AC 125V 5A 3 Pin Tact Switch Micro Limit Switches Hinge Lever for Mill CNC KW4-3Z by MUZHI: Amazon.com: Industrial & Scientific, (n.d.). <https://www.amazon.com/dp/B088QTFZQG> (accessed October 24, 2021).
47. Reyann 6x Happ Type Standard Arcade Push Button - Red - With Microswitch: Amazon.com: Tools & Home Improvement, (n.d.). <https://www.amazon.com/dp/B00V0OM7WO/> (accessed October 24, 2021).
48. Amazon.com: Chanzon 10pcs 8mm LED Pilot Diode Light 24awg (5 Colors x 2pcs Diffused Frosted Round Lens) 8mm Panel Mount + 5mm led 12V Universal Flush Dash Board Indicator Panel Socket Lights Lamp Bulb : Industrial & Scientific, (n.d.). <https://www.amazon.com/dp/B08G4X5WBT/> (accessed October 24, 2021).
49. Amazon.com: HiLetgo 2pcs SSR-60DA Solid State Relay Single Phase Semiconductor Relay Input 3-32V DC Output 24-380V AC : Industrial & Scientific, (n.d.). <https://www.amazon.com/dp/B01MSTFKIP/> (accessed October 24, 2021).
50. M. VanDam, D.K. Oller, S.E. Ambrose, S. Gray, J.A. Richards, D. Xu, J. Gilkerson, N.H. Silbert, M.P. Moeller, Automated Vocal Analysis of Children with Hearing Loss and Their Typical and Atypical Peers, *Ear Hear.* 36 (2015) e146–e152. <https://doi.org/10.1097/AUD.0000000000000138>.
51. J.Hø. Jensen, M.G. Christensen, D.P.W. Ellis, Sø.H. Jensen, Quantitative Analysis of a Common Audio Similarity Measure, *IEEE Transactions on Audio, Speech, and Language Processing*. 17 (2009) 693–703. <https://doi.org/10.1109/TASL.2008.2012314>.

52. N. Baranwal, Peak Detection based Spread Spectrum Audio Watermarking using Discrete Wavelet Transform, International Journal of Computer Applications. 24 (n.d.) 6.
53. Daniel, M23 - 23kHz Measurement Microphone, Earthworks Audio. (n.d.).
<http://earthworksaudio.com/measurement-microphones/m23/> (accessed October 24, 2021).
54. Amazon.com: TONOR Dynamic Karaoke Microphone for Singing with 16.4ft XLR Cable, Metal Handheld Mic Compatible with Karaoke Machine/Speaker/Amp/Mixer for Karaoke Singing, Speech, Wedding and Outdoor Activity : Musical Instruments, (n.d.). <https://www.amazon.com/dp/B01ISNU3X4/> (accessed October 24, 2021).
55. Vintage 1994 Fender Limited Edition 40th Anniversary American Standard Stratocaster | Billy's Guitar Shop, Jax FL | Reverb, Reverb.Com. (n.d.).
<https://reverb.com/item/37034864-vintage-1994-fender-limited-edition-40th-anniversary-american-standard-stratocaster> (accessed October 24, 2021).
56. ACS723KMATR-10AB-T Allegro MicroSystems | Sensors, Transducers | DigiKey, (n.d.). <https://www.digikey.com/en/products/detail/allegro-microsystems/ACS723KMATR-10AB-T/5225374> (accessed October 24, 2021).
57. B.-H. Nguyen, J.-H. Ryu, Direct current measurement based steer-by-wire systems for realistic driving feeling, in: 2009 IEEE International Symposium on Industrial Electronics, 2009: pp. 1023–1028. <https://doi.org/10.1109/ISIE.2009.5221999>.
58. S.-I. Jang, K.-H. Kim, An islanding detection method for distributed generations using voltage unbalance and total harmonic distortion of current, IEEE Transactions on Power Delivery. 19 (2004) 745–752.
<https://doi.org/10.1109/TPWRD.2003.822964>.
59. Pololu - A4988 Stepper Motor Driver Carrier, (n.d.).
<https://www.pololu.com/product/1182> (accessed October 24, 2021).
60. N.G. Skrzypczak, N.G. Tanikella, J.M. Pearce, Open source high-temperature RepRap for 3-D printing heat-sterilizable PPE and other applications, HardwareX. 8 (2020) e00130. <https://doi.org/10.1016/j.hsx.2020.e00130>.
61. A.L. Woern, J.R. McCaslin, A.M. Pringle, J.M. Pearce, RepRapable Recyclebot: Open source 3-D printable extruder for converting plastic to 3-D printing filament, HardwareX. 4 (2018) e00026. <https://doi.org/10.1016/j.hsx.2018.e00026>.
62. MAX31855SASA+ Maxim Integrated | Integrated Circuits (ICs) | DigiKey, (n.d.).
<https://www.digikey.com/en/products/detail/maxim-integrated/MAX31855SASA/2754400> (accessed October 24, 2021).
63. N. Bihari, I.T.S. Heikkinen, G. Marin, C. Ekstrum, P.J. Mayville, S. Oberloier, H. Savin, M. Karppinen, J.M. Pearce, Vacuum outgassing characteristics of unpigmented 3D printed polymers coated with atomic layer deposited alumina, Journal of Vacuum Science & Technology A. 38 (2020) 053204.
<https://doi.org/10.1116/6.0000178.P>.
64. Whitehurst, D. St andrew, TEMPERATURE ALARM AND CUT-OUT SYSTEM FOR USE WITH HEATED WATER HUMIDIFIERS, British Journal of Anaesthesia. 52 (1980) 557–558. <https://doi.org/10.1093/bja/52.5.557>.
65. FT232RL, FTDI. (n.d.). <https://ftdichip.com/products/ft232rl/> (accessed October 24, 2021).

66. Y. Nilsiam, Low-Cost Open-Source Gmaw-Based Metal 3-D Printing: Monitoring, Slicer, Optimization, and Applications, Ph.D., Michigan Technological University, 2017.
<https://www.proquest.com/docview/1911305832/abstract/95D6AE48408B40BAPQ/1> (accessed October 24, 2021).
67. 11 Tips to Sharpen Your MIG Welding Skills, Successful Farming. (2018).
https://www.agriculture.com/machinery/tools/welding/11-tips-to-sharpen-your-mig-welding_245-ar52169 (accessed October 24, 2021).
68. P. Scherz, D.S. Monk, Practical Electronics for Inventors, Third Edition, McGraw-Hill Education, 2013.
<https://www.accessengineeringlibrary.com/content/book/9780071771337> (accessed October 24, 2021).
69. J.M. Pearce, S. Oberloier, W. Holmes, TIGasaurus - open source TIG-based high-resolution metal 3-D printer, (2020). <https://osf.io/rd2a4/> (accessed October 24, 2021).
70. NI 9218 Datasheet - National Instruments, (n.d.) 32.
71. NI 9401 Datasheet - National Instruments, (n.d.) 10.
72. NI 9230 Datasheet - National Instruments, (n.d.) 18.
73. NI 9227 Operating Instructions and Specifications - National Instruments, (n.d.) 31.
74. NI 9482 Datasheet – National Instruments, (n.d.) 24.
75. NI 9210 Datasheet - National Instruments, (n.d.) 18.
76. G.M. Spinelli, Z.L. Gottesman, J. Deenik, A low-cost Arduino-based datalogger with cellular modem and FTP communication for irrigation water use monitoring to enable access to CropManage, HardwareX. 6 (2019) e00066.
<https://doi.org/10.1016/j.ohx.2019.e00066>.
77. K. Kurata, Open-source colorimeter assembled from laser-cut plates and plug-in circuits, HardwareX. 9 (2021) e00161. <https://doi.org/10.1016/j.ohx.2020.e00161>.
78. J.S. Botero-Valencia, J. Valencia-Aguirre, D. Durmus, A low-cost IoT multi-spectral acquisition device, HardwareX. 9 (2021) e00173.
<https://doi.org/10.1016/j.ohx.2021.e00173>.
79. J. Salazar-Vazquez, A. Mendez-Vazquez, A plug-and-play Hyperspectral Imaging Sensor using low-cost equipment, HardwareX. 7 (2020) e00087.
<https://doi.org/10.1016/j.ohx.2019.e00087>.
80. M. Cassel, O. Navratil, F. Perret, H. Piégay, The e-RFIDuino: An Arduino-based RFID environmental station to monitor mobile tags, HardwareX. 10 (2021) e00210.
<https://doi.org/10.1016/j.ohx.2021.e00210>.
81. M. Chu, A. Patton, J. Roering, C. Siebert, J. Selker, C. Walter, C. Udell, SitkaNet: A low-cost, distributed sensor network for landslide monitoring and study, HardwareX. 9 (2021) e00191. <https://doi.org/10.1016/j.ohx.2021.e00191>.
82. K.H. Hauslaib, E.W. Randall, An open source implementation of a data acquisition system for a current pulse ERT system using an industry standard interface, (n.d.) 9.
83. J. Du, W. Li, J. Guo, Design of LabVIEW based general data acquisition system, in: 2017 IEEE 2nd Information Technology, Networking, Electronic and Automation Control Conference (ITNEC), 2017: pp. 1235–1239.
<https://doi.org/10.1109/ITNEC.2017.8284973>.

84. D. Pradhan, L. Lakshminarayanan, V. Patii, A LabVIEW based power analyzer, in: 2014 International Conference on Advances in Energy Conversion Technologies (ICAECT), 2014: pp. 67–71. <https://doi.org/10.1109/ICAECT.2014.6757063>.
85. D.M. Laverty, D.J. Morrow, A. McKinley, M. Cregan, OpenPMU: Open source platform for Synchrophasor applications and research, in: 2011 IEEE Power and Energy Society General Meeting, 2011: pp. 1–6. <https://doi.org/10.1109/PES.2011.6039607>.
86. D. Newton, A Remote Area Power Supply (RAPS) Training Facility utilising SMA Sunny Island Inverter technology and National Instruments measurement package, other, Murdoch University, 2010. <https://researchrepository.murdoch.edu.au/id/eprint/4380/> (accessed July 12, 2021).
87. S. Fuhrman, D. Kitzman, S. Naegeli, Fully-Autonomous LabVIEW-Controlled Robot, (2015). <https://minds.wisconsin.edu/handle/1793/74560> (accessed July 12, 2021).
88. B. Popa, I.M. Popescu, D. Popescu, E. Bobasu, Real-time monitoring system of a closed oven, in: 2018 19th International Carpathian Control Conference (ICCC), 2018: pp. 27–32. <https://doi.org/10.1109/CarpathianCC.2018.8399597>.
89. Pearce JM. Appropedia as a tool for service learning in sustainable development. *Journal of Education for Sustainable Development.* 2009 Mar;3(1):45-53.
90. Bielefeldt, A. R., & Pearce, J. M. (2012). Service Learning in Engineering. In T. H. Colledge (Ed.), *Convergence: Philosophies and Pedagogies for Developing the Next Generation of Humanitarian Engineers and Social Entrepreneurs* (pp. 24-52): NCIIA
91. Balaji, U., 2021, July. Service Learning Through Robotics. In 2021 ASEE Virtual Annual Conference Content Access.
92. Branker, K., Corbett, J., Webster, J. and Pearce, J.M., 2010. Hybrid virtual-and field work-based service learning with green information technology and systems projects. *International Journal for Service Learning in Engineering, Humanitarian Engineering and Social Entrepreneurship*, 5(2), pp.44-59.
93. Twitchell, D.G., 2001. A rapid prototyping model for the design and development of instructional systems in theory and practice: A case study. Utah State University.

4 Low-Cost Open Source TIG-Based Metal 3-D Printer

4.1 Hardware in context

The proliferation of open-source plastic 3-D printing has had substantial impacts on the scientific and engineering community [2-7]. The technology has democratized manufacturing, allowing for individuals with no manufacturing experience to recreate componentry that would otherwise be prohibitively expensive to prototype [8]. Open source 3-D printing has fostered a substantial movement in the development of open source scientific hardware [9] ranging from instruments like automated four-point probes [10], centrifuges [11], and nutating mixers [12] to prototyping equipment including milling machines [13] and bio-printers [14]. Though 3-D printing is widely used to reduce costs [15-17] and increase accessibility [18-20], it is predominately limited to plastic components, which have limited suitability for applications at high temperatures, vacuum systems [21], clean rooms [22] or compatibility with many laboratory chemicals [23]. The aforementioned compatibility issues with use 3-D printing for a wide range of scientific tools could be remedied with the introduction of a low-cost open source metal 3-D printer, while still enjoying all of the benefits of plastic printing and the open source sharing of digital designs.

Most metal 3-D printing is relegated to high-end industry applications due to its prohibitive price point [24]. No low-cost commercial metal 3-D printers exist, and the open source selection available (i.e. [25]) have not seen the success of the self-replicating rapid prototyper (RepRap) 3-D printers [26-28]. In particular, the technical challenges associated with using welding for 3-D printing robots, cost, and limited resolution have not yet enabled the widespread hacking of metal 3-D printers observed with plastic systems [29].

The most common approach is the application of wire arc additive manufacturing (WAAM) [30-33] is the use of gas metal arc welding (GMAW)-based 3-D printing [25, 34-37]. In these cases, the end effector is the welding head of a metal inert gas (MIG) welder that functions similarly to a typical fused filament fabrication-based 3-D printer extruder. WAAM with a MIG has a lot of splatter, and a high heat input [38]. The scientific community has started building stepping stones towards a robust OS metal 3-D printing based on GMAW such as the development of slicer improvements [39], double wire systems [40], substrate removal techniques [41-42], alloys specifically for AM [43] and process [44] and weld characterizations [24,25]. Despite these efforts, however, the designs are still not widely replicated.

This manuscript proposes a new open source 3-D printer design based around a low-cost tungsten inert gas (TIG) welder coupled to a commercial open source RepRap. TIG has many advantages over MIG, such as having a low heat input, clean beads, and capable of high-resolution prints [38]. In order to make the printer more replicable, it is designed around a common and commercially available open source 3-D printer and the design could be adapted to most RepRap-class systems. TIG welding can create electromagnetic frequency (EMF) radiation, so the proper precautions are detailed. In addition, a basic yet

powerful free and open source software (FOSS) package will be introduced and used for the characterization of the 3-D printer.

4.2 Hardware description

The open source metal 3-D printer (TIG-Bot) is built based around the Lulzbot Taz 4 [45]. This is because Taz's are true commercial open source RepRaps that fabricate many of their own components and feature a standardized and flexible carriage socket, such that multiple different end effectors can be used. This ensures that the design can be used in future revisions, such as the new modular Sidekick design [46]. Additionally, choosing a commercial printer can lower the barriers to replicate the design, and potentially build up some momentum behind metal 3-D printing.

The Taz is made for plastic FFF, not metal. As such, it was adapted. The bed was replaced with a metal bed. The metal bed allows for heat dissipation, fixturing, and resilience to weld-splatter. The original FFF extruder assembly is removed, as it is not used. All unused cables can also be removed. Finally, all plastic components are coated in a reflective paint, otherwise they will lose structural integrity due to the UV exposure.

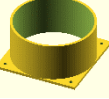
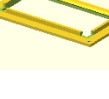
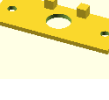
The end effector consists of a TIG torch (which came with the system), and a custom dabber assembly linked to a plastic frame. The dabber assembly is comprised of an aluminum extrusion device (normally used by Rep-RAP 3-D printers), with a stainless tube bent and threaded at both ends. The dabber is made to have an extrusion nozzle placed at the end that comes in all different sizes, allowing for accurate feed positioning. The TIG torch is mounted to a plate that allows for angle adjustment. Additionally, two constrainer pieces are used to carefully place the dabber at the right position relative to the torch electrode.

In addition, the printer must be placed in a metal box, which serves three functions. First, it acts as a Faraday cage and nullifies the EMF present in high frequency start of the arc. Secondly, it can be used to contain the high intensity light to protect user's eyes. Finally, it can contain and extract the hazardous fumes associated with welding. The box needs to be sealed in order to be effective. This makes it possible to use the device in a room not otherwise acceptable for welding. Finally, a shielded USB cable should be used to again mitigate the impact of EMF from the welder.

The system explored in this manuscript can be used for many bespoke metal scientific hardware or component fabrication as well as prototyping applications [24]. Some example use cases are:

- Near net-shape structural metal component rapid prototyping
- Adapting / depositing on existing metal structures
- A deployable system for in-field prototyping for appropriate technology applications

4.3 Design files summary

Design file name	File type	Image	Open source license	Location of the file
Mechanical / Extruder / body.stl & body.scad	STL/SC AD		OHL 2.0	https://osf.io/rd2a4/
Mechanical / Extruder / brace.stl & brace.scad	STL/SC AD		OHL 2.0	https://osf.io/rd2a4/
Mechanical / Enclosure / Plate_isolator.stl & Plate_isolator.scad	STL/SC AD		OHL 2.0	https://osf.io/rd2a4/
Mechanical / Enclosure / Plate_isolator_washer.stl & Plate_isolator_washer.scad	STL/SC AD		OHL 2.0	https://osf.io/rd2a4/
Mechanical / Enclosure / Fan_shroud.stl & Fan_shroud.scad	STL/SC AD		OHL 2.0	https://osf.io/rd2a4/
Mechanical / Enclosure / Lens_holder.stl & Lens_holder.scad	STL/SC AD		OHL 2.0	https://osf.io/rd2a4/
Mechanical / Enclosure / Lens_holder_top.stl & Lens_holder_top.scad	STL/SC AD		OHL 2.0	https://osf.io/rd2a4/
Mechanical / Enclosure / Cable_shroud.stl & Cable_shroud.scad	STL/SC AD		OHL 2.0	https://osf.io/rd2a4/
Mechanical / Extruder / Torch_plate.stl & Torch_plate.scad	STL/SC AD		OHL 2.0	https://osf.io/rd2a4/

Software / Lightning.pro	PRO	NA	OHL 2.0	https://osf.io/rd2a4/
Software / Pi.iso	ISO	NA	OHL 2.0	https://osf.io/rd2a4/

- **Body.stl** – The structural component of the carriage assembly used for connecting and positioning the extruder and torch.
- **Brace.stl** – A simple component used to constrain the torch and extruder nozzle such that they are fixed in space together.
- **Plate_isolator.stl and Plate_isolator_washer.stl** – These pieces are used to connect the build plate to the rest of the printer while providing electrical isolation.
- **Fan_shroud.stl** – A connecting piece used to fasten the ventilation hose to the enclosure.
- **Lens_holder.stl and Lens_holder_top.stl** – A bezel which holds the viewing lens and holds it in place on the enclosure door.
- **Cable_shroud.stl** – A chamfered bezel used for both the ground and torch cable / hose pass through.
- **Torch_plate.stl** – A semi-flexible plate used as an interface to connect and manipulate the pitch of the torch with regard to the carriage body.
- **Lightning.pro** – The project file for Lightning, the custom test interface for running the 3D printer
- **Pi.iso** – An image of the fully configured operating system for the Raspberry Pi

4.4 Bill of materials summary

#	Component	Qty	Cost per unit - currency	Total cost - currency	Source of materials	Material type
1	C25 Gas Cylinder	1	299.00	299.00	https://www.amazon.com/dp/B00I4Z6QCY/	Gas
2	2% Ceriated Tungsten Electrode	1	1.95	1.95	https://www.amazon.com/dp/B013KXK12S	Metal
3	Mild Steel 0.03" MIG Wire	1	35.39	35.39	https://www.amazon.com/dp/B000CFL7MI/	Metal
4	4x4" Low-Carbon Steel Substrate	1	1.79	1.79	https://www.mcmaster.com/catalog/6544k15	Metal
5	Raspberry Pi Kit	1	129.99	129.99	https://www.amazon.com/dp/B08956GVXN/	Electronics
6	LulzBot TAZ 4 3D Printer	1	2195.00	2195.00	https://www.amazon.com/dp/B00JXQZ8CC	Mechtronics

7	200A Tig Welding Machine	1	197.00	197.00	https://www.amazon.com/dp/B083HZGYCP/	Electronics
8	Flow Meter Gas Regulator & House	1	35.99	35.99	https://www.amazon.com/dp/B08P5BNHBX/	Pneumatics
9	0.25" 12" x 12" 6061 Aluminum sheet	1	54.48	54.48	https://www.mcmaster.com/89155K11/	Metal
10	200 Piece Spring Assortment	4	0.055	0.22	https://www.amazon.com/dp/B08QJ51F1J/	Hardware
11	660 Pc Nut and Bolt Assortment	120	0.038	4.54	https://www.amazon.com/dp/B098ND1GW8/	Hardware
12	4x4" Low-Carbon Steel Substrate	6	28.45	170.70	https://www.mcmaster.com/catalog/6544k15	Metal
13	L-Shaped Framing Stock	4	18.29	73.16	https://www.mcmaster.com/8968K24_8968K26/	Metal

14	Strap Hinge	2	2.10	4.20	https://www.mcmaster.com/1526A43/	Hardware
15	0310 Steel Wool	6	0.280625	1.68375	https://www.amazon.com/B001SBJFVA/	Hardware
16	24AWG Cable 100'	10	0.1219	1.219	https://www.amazon.com/dp/B00B887D80/	Cabling
17	Grounded Plug	1	2.98	2.98	https://www.amazon.com/dp/B007QVPQ96/	Cabling
18	4" Dryer Vent Hose	1	11.07	11.07	https://www.amazon.com/dp/B08FX2GFQC/	Hardware
19	Shade 11 Welding Hood Lens	1	5.75	5.75	https://www.amazon.com/dp/B07J224WJ6/	Glass
20	120mm Computer Fan	1	13.90	13.90	https://www.amazon.com/dp/B07CG2PGY6/	Electronics

21	2" Conductive Copper Tape	1	12.49	12.49	https://www.amazon.com/dp/B07C6YLNYL/	Hardware
22	25A Solid State Relay	1	9.90	9.90	https://www.amazon.com/dp/B08GNSPCND/	Electronics
23	Spade Connector	2	0.07	0.14	https://www.amazon.com/dp/B07FQB6WXP/	Cabling
24	5x5 Mild Steel Plate	1	19.96	19.96	https://www.mcmaster.com/8910K591/	Metal
25	3D Printer Nozzle Kit	1	0.35	0.35	https://www.amazon.com/dp/B07L5KJB59/	Hardware
26	1/4" Copper Tube	0.2	2.29	0.46	https://www.amazon.com/dp/B0991D3WTX/	Metal
27	Aluminum Extruder Assembly	1	16.98	16.98	https://www.amazon.com/dp/B07SY745CF/	Mechatronics

					https://www.mcmaster.com/48925K11/	Hardware
28	1/2" PVC Pipe	0.5	1.25	0.62	https://www.mcmaster.com/48925K11/	
29	Table Stand Off Component Kit	4	0.10	0.40	https://osf.io/rd2a4/	Polymer - ABS
30	Fan Shroud	1	0.50	0.50	https://osf.io/rd2a4/	Polymer - ABS
31	Cable Entry Bezel	2	0.50	1.00	https://osf.io/rd2a4/	Polymer - ABS
32	Lense Bezel	1	0.50	0.50	https://osf.io/rd2a4/	Polymer - ABS
33	Printer Carriage	1	1.00	1.00	https://osf.io/rd2a4/	Polymer - ABS
34	Feeder Constrainer	1	0.1-	0.10	https://osf.io/rd2a4/	Polymer - ABS
35	1/8" TIG Mild Steel Filler	0.01	14.19	0.14	https://www.mcmaster.com/7972A444/	Metal
36	White Latex Paint	1	11.98	11.98	https://www.amazon.com/dp/B004HZGJ72/	Paint

Line items 1 – 4 are consumables, and line 5 is an optional attachment. Because they are not part of the machine, the aforementioned line items are not included in the final cost calculation of the machine.

4.5 Build instructions

4.5.1 Printer Modifications

1. First the Taz's bed must be removed. Disconnect the four nuts bolting it to the Y-carriage at each corner. Along with the bed, the cable (including the bed power and thermistor) can be completely removed from the system.
2. Procure the 300 by 300mm by 5 mm aluminium sheet. Using the template found on the repository [47], mark all of the hole locations using a scribe. Then drill each hole using an 4mm sized drill bit. Finally tap each hole in the fixture grid (all of the holes except for the 4 corner mounting holes) using an M4 tap (Figure 4.1).

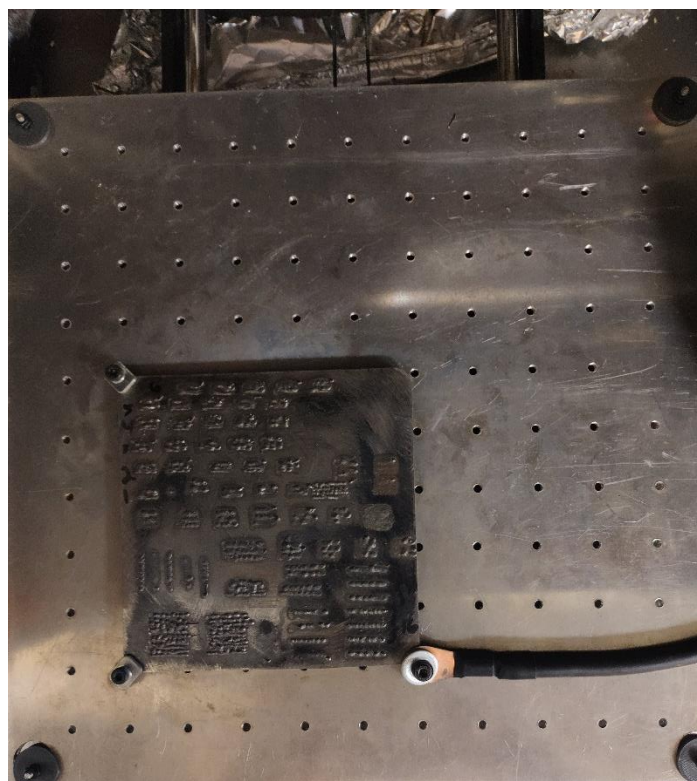


Figure 4.1: The aluminium bed with test substrate and ground attached

3. Print out the top and bottom isolation brackets for the mounting assembly in ABS, using full infill (and any layer height). At each corner of the Y carriage, place an 25mm spring, then the bottom isolation bracket, followed by the aluminium plate, the top isolation bracket, and finally two M3 Nuts (Figure 4.2).



Figure 4.2: The assembled isolation bracket

4. Remove the extruder assembly from the Taz. Additionally, remove all of it's cabling from the system with the exception of the stepper motor cable and thermistor cable. This thermistor cable must be rerouted to the external side of the printer's frame, and terminated with a 470 ohm resistor in order to provide a temperature feedback and prevent the firmware from seeing a cold extrusion (since the firmware is being left at the default, if the temperature is too low, it will not extrude).
5. Every plastic component on the printer should be painted with a reflective white outdoor paint. Critical movement parts such as belts, linear rods, and Z axis screws should be masked off using painter's tape. This paint protects the ABS part from premature wear caused by intense UV-light exposure. An example painted component can be seen in Figure 4.3.

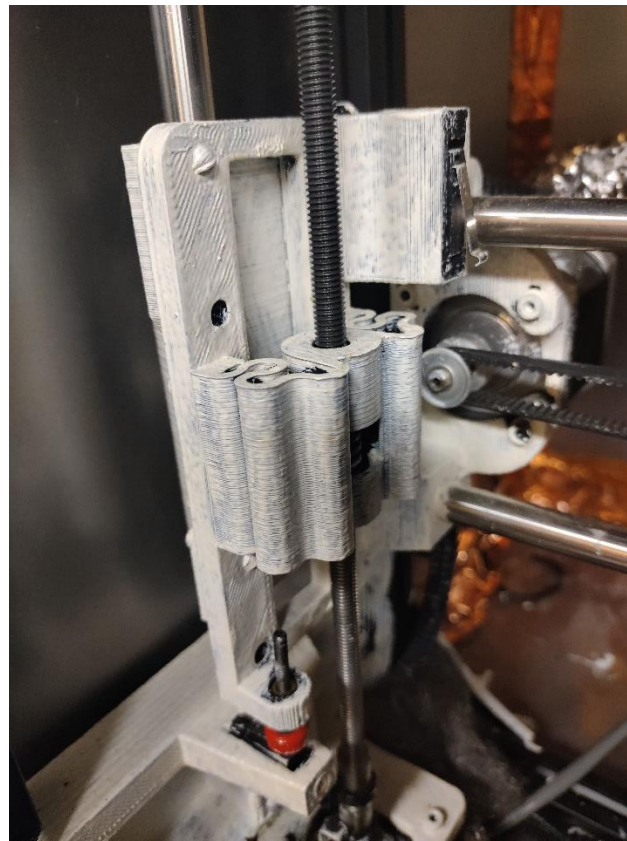


Figure 4.3: An example painted part of the Taz

6. Remove the LCD display and all associated cabling.

4.5.2 Extruder Build

1. Print off the extruder body in ABS using no less the 30% infill, and any layer height. Then, paint it with reflective paint.
2. Fasten the aluminum extruder assembly to the body. The idler bearing should be coated in 2 layers of Kapton tape to ensure consistent wire grip.
3. Cut a piece of 85 mm long stainless-steel tube, and using a small tube bender, apply a 75-degree bend at the end of the tube. Then, use an M5 tap along with tapping oil to thread both ends of the tube. A threaded tube insert can be placed in the unbent end of the tube, and an appropriately sized extruder nozzle can be connected to the bent end. Screw this assembly to the output end of the aluminum extruder assembly as seen in Figure 4.4.

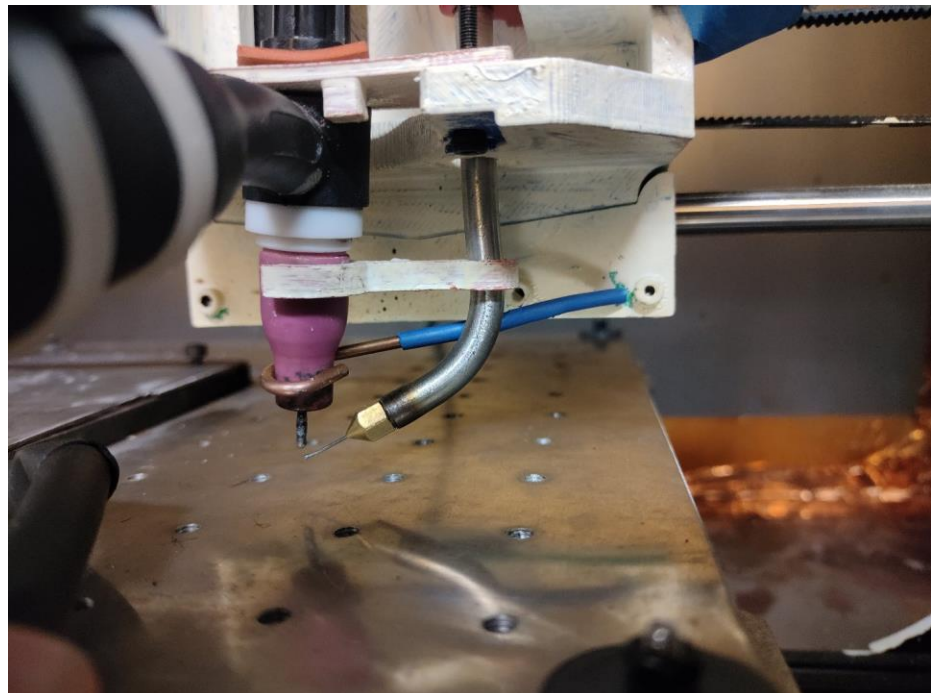


Figure 4.4: The stainless steel feeder tube

4. Print out the torch mounting plate in ABS using solid infill, any layer height. Paint it with reflective paint. Remove the back cap of the TIG torch, and place the body on the bottom side (the side with 2 constraining nubs) of the mounting plate. Then place the back cap on the opposite side of the plate tightly. If the cap is not able to tightly seat – a piece of gasket material can be cut and placed between the plate and back cap for a more secure connection. The mounting plate can then be mounted to the extruder body using M3 bolts.
5. Place the top constrainer in place, then using pliers, roughly bend the 1/8" mild steel tig filler to shape shown in Figure 4.5 using two pairs of pliers. The piece should fit snuggly around the torch nozzle and be wedged firmly between the feeder and the carriage face. Adjust the leverage of the cantilever to the point where the feeder tube's rotation is hard to adjust by hand.

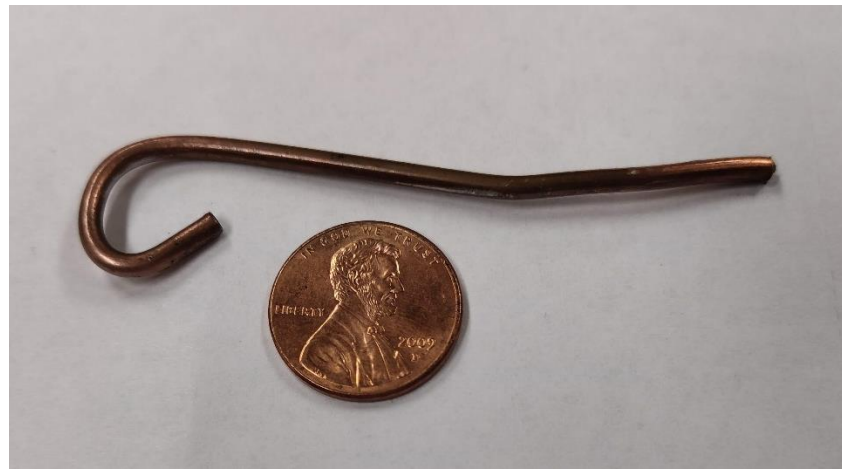


Figure 4.5: The custom cantilever

6. Mount the extruder in the X-carriage, and connect the stepper cable to the extruder motor cable from the Taz controller. The completed extruder can be viewed in Figure 4.6.



Figure 4.6: The completed and installed extruder assembly

4.5.3 Enclosure Build

1. Using a hacksaw and vice, cut a quantity of nine 610mm long pieces of steel angle extrusion. Use a file or grinder to de-burr any sharp edges.
2. Assemble the structure shown below with M5 bolts and nuts as shown in Figures 7 and 8.



Figure 4.7: The top end of the frame bolted together



Figure 4.8: A detail shot of the corner connection scheme

3. Invert the frame and place one of the 610mm by 610 mm steel sheets in the top face. Hit each corner firmly with a hammer to impress the mounting bolt's location onto the sheet. An example impression is shown in Figure 4.9.



Figure 4.9: An example of the bolt impression

Drill out the holes and mount the sheet in place (on the interior of the box). Using similar steps, construct and mount the 3 wall plates as shown in Figure 4.10.



Figure 4.10: The enclosure with 3 sides and the top plate mounted

4. Place an additional bar across the bottom of the last remaining side of the frame as shown in Figure 4.11.

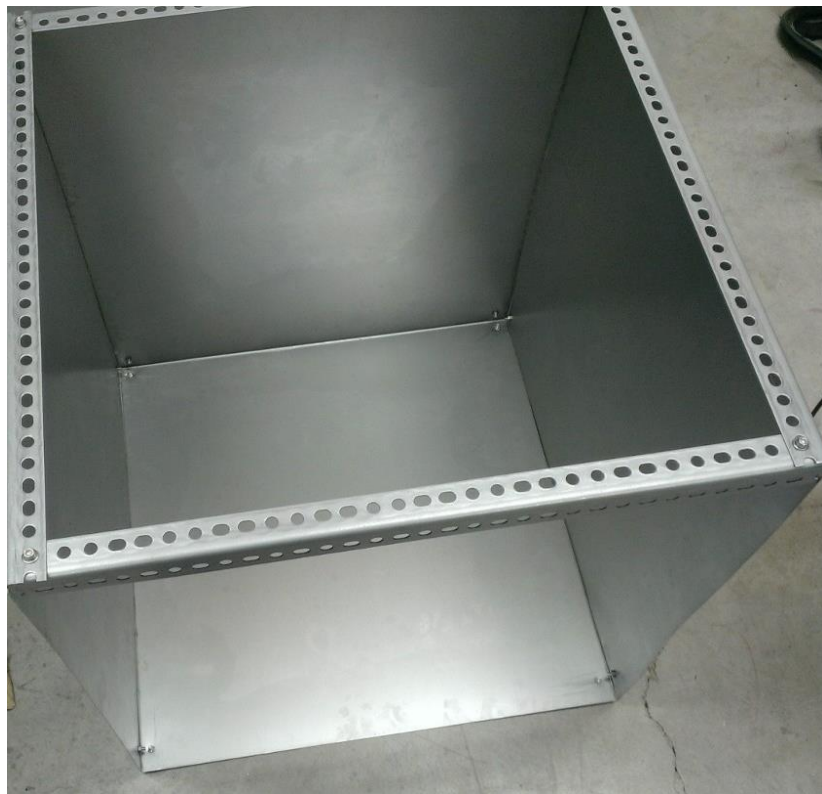


Figure 4.11: The completed frame

5. Using an angle grinder with a cut-off wheel, cut 1" (25.4mm) squares out of each corner of one of the remaining plates to create the door plate. Cut an 35mm by 35mm opening centered near the top of the door. Print out the view port bracket using solid infill and insert it into the hole with the viewing lens in place. Mount the hinges to the top part of the frame, and then attach the hinges to the door plate using M4 bolts and nuts.



Figure 4.12: The door mounted in place

6. Using an angle grinder, remove a 2" by 6" (50.8 mm 152.4 mm) by area from the bottom center of the left wall (referenced by facing the door from the exterior). This slot will be used as a cable pass through (Figure 4.13). On this same wall, place the fan on the top corner of the frame, at the corner furthest from the door. Mark out the hole positions of the fan, and then cut out an opening using the grinder. Drill the mounting holes. The mounted fan can be viewed in Figure 4.14.



Figure 4.13: The cable pass through slot



Figure 4.14: The fan mounted in place

7. Finally, place the printer on top the remaining plate. Then place the enclosure on top of the plate and printer. Pack the cable entry slot with steel wool. Seal all interior of edges of the enclosure using copper tape with conductive adhesive.

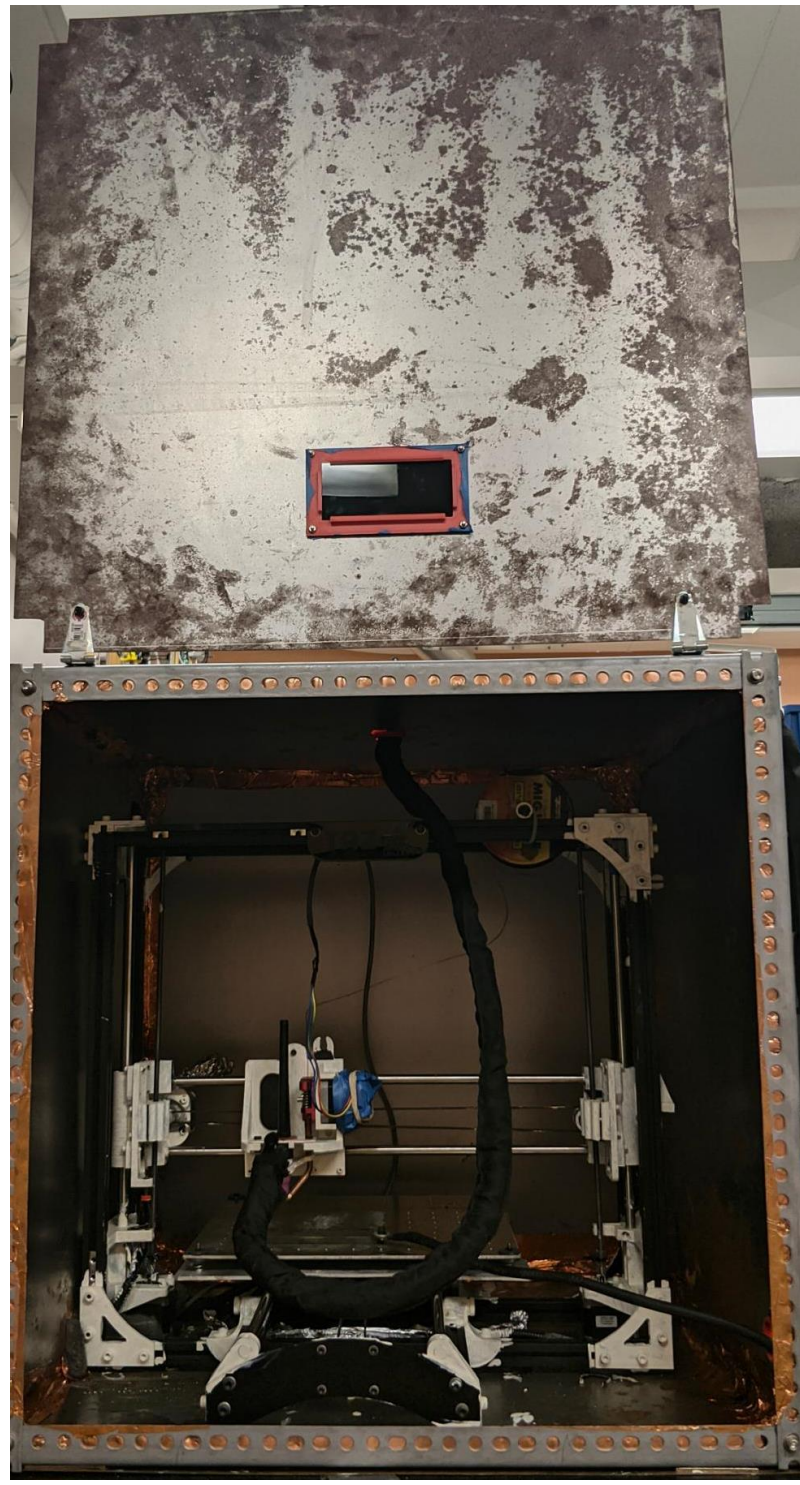


Figure 4.15: The completed enclosure with printer installed

4.5.4 Wiring

1. The fan should be wired into Jack 3 on the Taz control board
2. The coil to a solid-state relay should be wired to Jack 1 on the Taz control board. The contacts should be broken out as cables with butt splices crimped on their ends. Each butt splice can be connected to the engage switch of the welder. This connection scheme is represented schematically in Figure 4.16, and the physical connection is demonstrated in Figure 4.17.

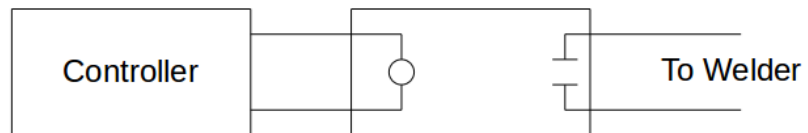


Figure 4.16: Schematic of welder engage circuit



Figure 4.17: The butt splice ends connected to the welder

4.5.5 Initial setup

Launch Lightning [48] and connect to the Taz using the standard settings. Fixture a substrate to the plate and connect the welder ground terminal. Then jog the end effector such that the Tungsten electrode is approximately 1.3 mm above the substrate. Set the welder current to 20 amps. Open the gas valve for the welder. Close the enclosure door, enable the exhaust fan, and then click the “end effect” control. This will cause the welder to begin arcing. Take careful note of where the “hot spot” of the arc is, which can be identified as a white spot among the discharge. The feeder nozzle will need to be tuned to deposit wire directly into the hot spot. If necessary the angle of the torch can be increased by packing washers under one side of the torch mounting bracket.

4.5.6 Using a Raspberry Pi as the Printer Host

It is recommended that the Raspberry Pi is used as the main interface between the operator and the printer. To utilize the Pi, provide all of the standard connections for operation (IE, keyboard, power, mouse, monitor, etc). Connect the Pi to the printer via the Taz’s standard USB cable.

Using a Linux Mint [49] or a comparable operating system, download the Pi.iso image from project repository [47]. Insert the SD card into the computer, and identify the name of the SD card within your system. Then write the image to the SD card using the following command:

```
sudo dd if=[Absolute Path of Pi.iso] of=[Name of SD card]
status=progress bs=4M
```

The SD card can be inserted into the Pi, and the system powered on.

4.6 Operation instructions

4.6.1 Safety Concerns

Welding systems can be dangerous if the proper safety precautions are not taken [38]. There are five major risks with this system:

1. Electrical Shock Hazards – The welder can deliver potentially fatal shocks if the user is touching the electrode when engaged. To mitigate this risk, ensure the welder is always turned off while the enclosure door is open.
2. Extreme Light intensity – When engaged, the TIG welding arc acts as a high intensity light source which can cause eye damage with as little as a passing glance. Ensure that the enclosure door is always closed when the welder is engaged.
3. Extreme Heat – The deposition process can cause large amounts of heat to build up in the substrate and print. Be sure to wear welding gloves when handling recently deposited prints.

4. Hazardous Gas – The welding process generates hazardous gas that should not be inhaled. Always have the exhaust fan enabled and vented appropriately.
5. High Frequency Electromagnetic Fields – The TIG welder employs a high-frequency start mechanism to initialize the arc. This high frequency pulse can effect electronics and cause malfunctions. Keeping the enclosure door shut while in operation will protect any electronic equipment. It is highly recommended, however, that all electronics are kept a minimum of 3 m away from the system. **Users should NOT operate this machine if they are relying on a pace maker or any other necessary electronic-based medical devices.**

4.6.2 Lightning Operation

Lightning is a lightweight GUI-based software developed in QtCreator [50] that employs a simple yet flexible library for reading and writing G-Code to a Marlin [51] based system. Lightning consists of a basic interface (seen in Figure 4.18), which allows for running of a G-Code script or commands, jogging axes in variable increments, enabling the end effector and fan, and homing the system. There are several other functions pictured in Figure 4.18 that are considered to be “custom functions” as they are made to be specific to the test that is being executed.

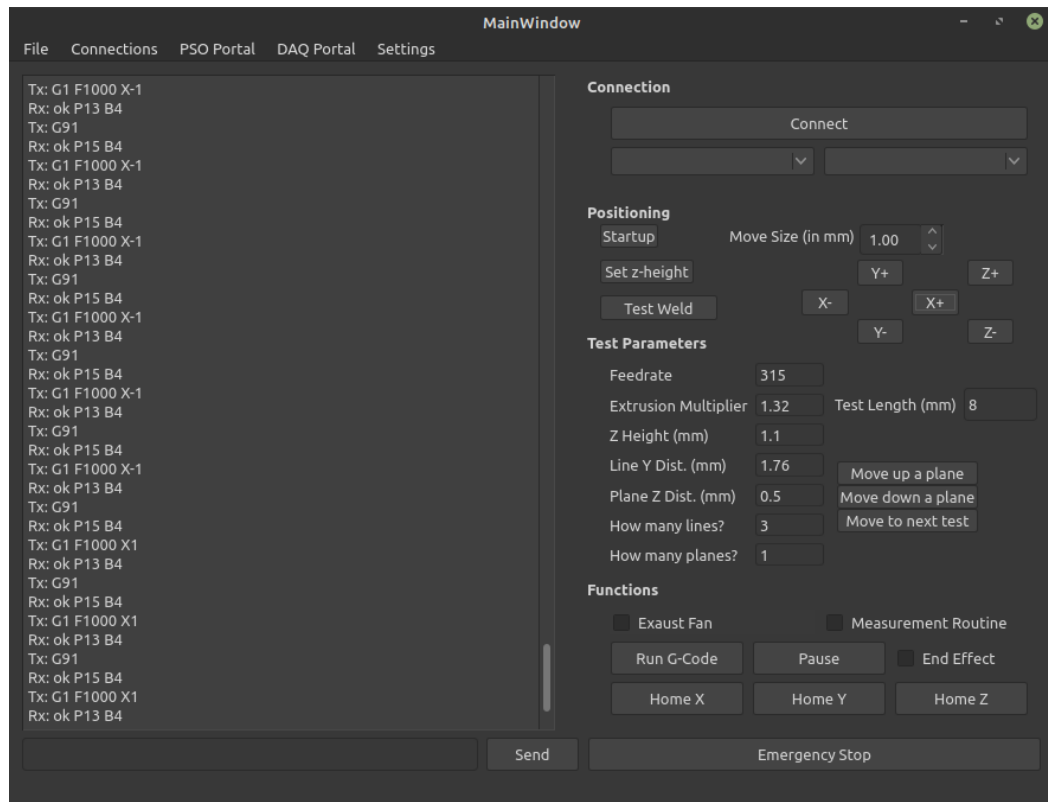


Figure 4.18: An image of Lightning’s Interface

4.6.3 Jogging Axes

The end effector can be moved in varying increments by inputting a value into the move increment GUI element and then clicking the button corresponding to the direction of desired movement. Having precise control over the movement increment is ideal for iteratively positioning test prints. In the Taz system used here the limits on step size are 0.02mm.

4.6.4 Running Commands

The command line allows for the input and transmission of a single Marlin [Marlin] G-Code command. Any command in Marlin's instruction set [51] can be executed.

4.6.5 Running Scripts

A script (a sequence of multiple G-Code commands) can be executed by loading it and then clicking "Run Script".

4.6.6 Emergency Stop

The emergency stop button issues the following actions:

- Cease all motion
- Turn off welder
- Engage the fan

4.6.7 Lightning Modification

Lightning was intentionally made to be lightweight and employ essential functions such that it can easily be modified within QT Creator, allowing for the creation of custom GUI elements which are tailored to the current test being executed. Specifically in Figure 4.18, Lightning is configured for printing planes.

4.6.8 Adding GUI Elements

Adding custom GUI elements such as text boxes or buttons can allow for altering and executing custom functions without the need to re-compile Lightning. An element can be added by openingmainwindow.ui within QT Creator, and dragging and element from the element panel to the interface. In order to tie the element to a function, right click it and select "View Slot". Buttons will likely be the only elements tied directly to functions, as text entry boxes will be parsed within the code.

4.6.9 Parametric G-Code

As the TIG-Bot is an experimental machine and Lightning is made to assist in the acquisition of ideal printing parameters. The tests involved in optimization involve running the same test script with varied parameters such as feed rate and extrusion multipliers, but unfortunately Marlin G-Code does not support parametric codes. Fortunately, Lightning allows for pseudo-parametric G-Code by implementing the script within the C++ framework.

The function “QueueGCode” allows for a QString to be added to the buffer and sent out once the machine has indicated it is ready for another command. Through use of standard string concatenation methods, loops, and reading variables from GUI elements, and other C++ functions alongside the QueueGCode command, parametric tests can be created. Below is an example function made to create a dithering pattern which can be effective in infill operations for TIG-based AM.

```
void zipperMovePosX(float x, float y, float feedrate, float extrusion, int increments)

{
    float arcLinger = 0.2;

    GCode.QueueCommand("G91",0); // Set relative movement
    GCode.QueueCommand("G1 F" + QString::number(feedrate/2) + " X4",0); // Start move

    GCode.QueueCommand("M106 P0",0); // Turn on welder
    GCode.QueueCommand("G4 P" + QString::number(arcLinger),0); // Sleep for a bit

    for (int i=0; i<increments; i++) {
        GCode.QueueCommand("G1 Y" + QString::number(y),0); // Move in +Y
        GCode.QueueCommand("G1 F" + QString::number(feedrate) + " E" +
                           QString::number((extrusion*x)/increments) + " Y-" + QString::number(y) + " X" +
                           QString::number(x/increments),0); // Move in -Y,+X, and extrude
    }

    GCode.QueueCommand("M107 P0",0); // Turn off welder

    GCode.QueueCommand("G1 F" + QString::number(feedrate/2) + " X4",0); // Finish off
    rest of the move
}
```

4.6.10 Initial Tuning

Before operation the torch angle and the filler tube rotation must be adjusted for ideal depositions. To do this, extrude the filler wire such that it is directly beneath the tungsten electrode. Then, the welder is engaged at a current of 15 amps. On observation of the arc pattern, a large light blue area is visible, with a concentrated white area (referred to as the “hot spot”). The torch mounting plate’s connecting bolts can be packed with stacked washers in order to increase the angle of the torch, which will result in an altered hot spot location on the X axis of the machine. Once the torch angle is set, the feeder rotation can then be adjusted by increasing the bend in the metal cantilever to ensure the position is rigidly kept.

4.6.11 Constraints for Operation

TIG welding to produce metal extrusion creates some unique constraints not common to plastic FFF. Specifically, there are two main factors of the welding response that must be considered: directional preference and arc response.

The directional preference of deposition is the result of the end effector design as well as standard welding constraints. The feeder tube is placed on the right side (positive X direction relative to torch) and therefore can only add material from the right side.

Attempting to exclusively print from right to left would require the feeder to force wire over already deposited weld, causing the filler to deflect, and negatively impact weld quality [38]. Therefore, when making depositions, the end effector must always be moving in a right-to-left motion. This demands G-code commands ensuring this limited travel. In this study G-code was generated that did this for all test prints. The concomitant alterations to any of the standard open source FFF-based slicing engines (e.g. Cura [52], Slic3r [53], IceSL [54]) are left for future work. Alternatively, a future generation of TigBots could have a rotating member move the weld wire to add material from any direction to compliment the standard movement of slicers.

4.7 Validation and characterization

4.7.1 Base Parameter Acquisition

There are seven main parameters that affect the quality of the prints produced by the TIG-Bot. They are:

- Torch Angle – The angle which the TIG torch is held relative to the substrate. This is adjusted only in the initial tuning phase and then left constant.
- Filler Angle – The angle which the filler material is fed relative to the substrate. This is fixed in the extruder assembly at 15° and cannot be changed without reconstructing.
- Pulse Rate – The pulse rate effects the distribution of the arc. Initial experimentation indicates that this setting should be at ~10% for optimal

depositions with 0.024" (0.6mm) mild steel wire. This setting may need to be changed with varying filler diameters.

- Gas Flow Rate – The gas flow rate is set to 20 CFH [38].
- Feed Rate – The feed rate describes how quickly the end effector moves. The ideal value for this parameter is acquired experimentally.
- Welding Current – The welding current adjusts how much energy is delivered to the weld in the form of heat. The ideal value for this parameter is acquired experimentally.
- Extrusion Multiplier – The extrusion multiplier affects how much filler is extruded per unit of end effector movement. This will affect the consistency and width of the weld. The ideal value for this parameter is acquired experimentally.

4.7.2 Optimization

Ideal printing parameters are found through the usage of a custom open source computational intelligence utility called *PSO Experimenter* [55]. PSO Experimenter utilizes the particle swarm optimization (PSO) algorithm [56], which has been found to effectively optimize for printing parameters within 6 iterations of tests [57]. PSO Experimenter takes an input of parameters and their respective ranges, and proposes experiments (referred to as particles) which must be carried out and then have the results characterized. The characterized values (fitnesses) are input into the system and the algorithm will iteratively optimize towards ideal parameters.

Three test batches are executed; printing lines, planes, and rectangular prisms. The variables, ranges, and initial guesses are listed in Table 4.1.

Table 4.1: Ideal parameters acquired via PSO Experimenter

Variable	Min	Max	Guess	Int?	Description
I	10	22	19	True	Welder current
V_P	250 mm/s	350 mm/s	245°C	True	End effector movement rate
F	100%	160%	130%	False	Extrusion flow multiplier
H	0.5mm	2mm	1.1mm	False	Z-height
S_Y	1mm	2mm	1.7mm	False	Y-line spacing
S_Z	0.5mm	1mm	0.6mm	False	Z-line spacing

4.7.3 Characterization

During the line tests, plane tests, and rectangular solid tests, the welds are characterized through a series of physical measurements for each test. Specifically, the final test for a rectangular solid is comprised of 3 stacked layers that are all 3 lines wide. The print is characterized by length, width, height, and surface roughness (the top surface). The best results are shown in Table 4.2.

Table 4.2. Recommended Printing Parameters

Variable	Description	Value
I	Welder current	20 A
V_P	End effector movement rate	295 mm/s
F	Extrusion flow multiplier	1.28 mm / mm
H	Z-height	1.5 mm
S_Y	Y-line spacing	0.5 mm
S_Z	Z-line spacing	0.36 mm

4.7.4 Microstructure Characterization

A typical printed line and loaf are analyzed for the interior microstructure. The samples are polished using the methods detailed in [58]

1. Bisect each sample to reveal its cross sectional microstructure
2. Polish at increasing grit sizes using silicon paper: 240, 360, 420, 600, 800
 - a. Wash the sample with soapy water between each step
3. Polish with 6 um silicon paper
 - a. Rinse with soapy water
 - b. Rinse with ethanol
 - c. Ultrasonic bath for 5 minutes
4. Polish with 1 um diamond paste
 - a. Rinse with soapy water
 - b. Rinse with ethanol
 - c. Ultrasonic bath for 5 minutes

Then images will be digitally acquired using a microscope at 50x zoom. Interior, and exterior structure is observed and compared to the substrate as a reference for ideal structure.

4.8 Discussion

4.8.1 Capabilities

During the optimization process, the ranges of key parameters were acquired and are listed in Table 4.3.

Table 4.3. Deposition and Movement Parameters of the TIG-based Metal 3D Printer

Parameter	Min	Max	Standard
Bead Width	1.8 mm	3.5 mm	2 mm
Bead Height	0.2 mm	0.6 mm	0.3 mm
X Dimension	-	298 mm	100 mm
Y Dimension	-	275 mm	100 mm
Z Dimension	-	250 mm	100 mm
Print Speed	30 mm/s	350 mm/s	295 mm/s

An interesting effect of the TIG welding process is that when increasing weld current while maintaining all other parameters, the metal tends towards a wider yet shallow deposition. This can allow for resolutions in the z direction as fine as 0.2 mm. The width associated with a 0.2 mm deposition is 3.2 mm. In addition, increasing current creates a smoother deposition. This suggests that high-current passes can be made as a final layer to create a more desirable surface finish, similar to the ironing feature in FFF. This resolution is mostly bound by the availability of fine filler material (for example the usage of 0.035" MIG wire can only yield a bead width of 0.889 mm or greater). Utilizing finer (~0.8mm) wire (such as that available for micro-MIG systems [59]) will yield a finer resolution with minimum machine reconfiguration.

The standard print speed of 100 mm/s paired with 1.5 mm bead width is similar to aluminum printing standard FFF metal 3D printers [41-43]. This is to be expected given the movement platform is already a fully capable FFF printer.

An unexplored advantage of TIG welding in metal 3D printing is its flexibility to deposit the following materials: steel, stainless steel, chromoly, aluminium, nickel alloys, magnesium, copper, brass, and gold [38]. This creates a uniquely flexible environment for multi-material constructions and even (with the addition of a secondary feeder) in-situ alloying. In situ alloying with such a machine is an obvious invention for all known metals [60] and should be considered for future work.

The first image (Figure 4.19) from the microstructure observation was generated from a 25 mm line deposition using the parameters detailed in Table 4.2.



Figure 4.19. A cross sectional image of a single bead deposition directly on a steel substrate

An image of the interior layer of a 3 x 3 loaf is shown in Figure 4.20, with the substrate visible near the bottom of the photo for comparison



Figure 4.20. A cross sectional image of the interface of a 3x3 loaf deposition directly on a steel substrate

The single bead deposition embodies a mostly favourable weld. There is clear and uniform penetration (dark brown band with small grain size), and no cold lapping (the two edges of the weld bead are firmly adhered to the substrate). There is slight porosity present (black dots near top of bead) which likely increases an overabundance of cover gas flow. Final, the grain size of the deposition is substantially larger than the grain size of the substrate, which will yield more ductile features.

Interior deposition, which has several opportunities to cool and reheat, has a grain structure that is slightly smaller than the substrate, indicating a hard and strong structure. This relationship ideal, as normally internal structures need to be strong, where thin external features will need increased ductility to avoid snapping under load.

4.8.2 Deposition Repeatability

To validate the repeatability of the system, five 20 mm lines were deposited using the ideal parameters listed in Table 4.3. For each sample, 3 heights and 3 widths were measured using calipers at equidistant points distributed across the line. The standard deviation of deposition widths is 11%, and the standard deviation of deposition heights is 18%. The distributions of each measurement are visualized in Figures 4.21 and 4.22

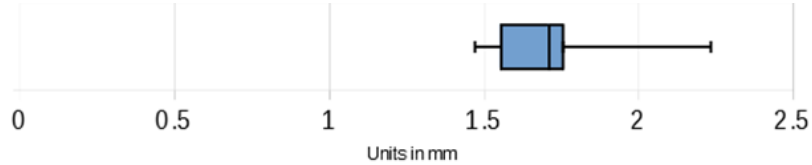


Figure 4.21. A box plot displaying the width distribution present across five 20mm line depositions

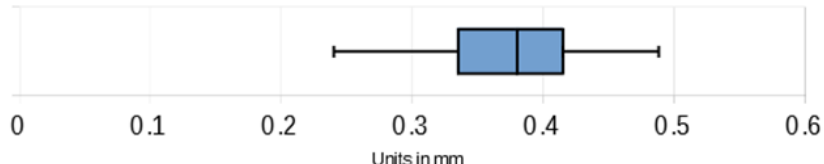


Figure 4.22. A box plot displaying the height distribution present across five 20mm line depositions

4.8.3 Constraints

The 3D printer is made to weld in the X+ direction only due to the fixed position of the filler relative to the torch. Though this constraint is simple, it is not commonly seen in other 3D printers, and therefore not supported by traditional slicers. Because of this, all G-Code has been procedurally generated, which greatly reduces the ability of the system to be used widely.

The fixed position of the filler relative to the torch creates a unique problem when printing objects. Ideal conditions occur when the filler is deposited right into the center (hot spot) of the arc. When the torch approaches an existing deposition, however, the arc will slightly deflect toward it, moving the hot spot. Since the filler is held rigidly, this causes a less-than-ideal deposition. This effect could also be countered by improving on slicer tool path generation to account for the existence of metal structures during 3D printing.

4.8.4 Cost Analyses

The majority of commercial metal 3D printers are based on laser sintering or binder jetting technologies (Table 4.4, 4.5). WAAM systems are often integrated into the manufacturing process of the production chain, where the produced parts must undergo additional post-processing. For example, high WAAM deposition rates and CNC precision are usually combined to reduce lead times and provide high flexibility in manufacturing processes. The printer explored in this paper offers a highly flexible environment at an average cost savings of 98% over commercial alternatives.

Table 4.4. Commercial metal 3D printers

Model	Technology	Volume, mm	Print System	Part Weight, kg	Resolution, µm	Material	Software	Price, USD
Desktop Metal Studio System+ [61]	Bound metal deposition	300x200x200	Dual extrusion – 1 metal, 1 ceramic interface media	6.5	50/100-220	17-4 PH, AISI 4140, H13, 316 L, Copper, Inconel 625	Fabricate	\$60,000-\$160,000
Markforged Metal X [61]	Atomic diffusion additive manufacturing (ADAM)	300x220x180	2 Nozzles – Metal Material and Support Release	10	50-200	17-4 PH Stainless Steel, Tool Steel (H13, A2, D2) Titanium Ti6Al4V, Inconel (IN) 625, Copper, Aluminum (6061, 7075)	Eiger	\$99,500
Arcam Spectra H [61]	Electron beam melting (EBM)	ø250x430	Electron Beam	—	50	Ti6Al4V, TiAl, Nickel alloy 718	—	\$100,000-\$250,000

Trumpf TruPrint 1000 [61]	Selective laser melting (SLM)	ø100x100	Fiber laser	—	10-50	Stainless steels, tool steels, and aluminum, nickel basis, cobalt-chrome, copper, titanium or precious metal alloys, amorphous metals.	TruTops Print	\$170,000-\$300,000
EOS M 100 [61]	Direct metal laser sintering (DMLS)	ø100 x 95	Yb-fiber laser	—	40	Aluminum, cobalt chrome, nickel-based, refractive metal, stainless steels, tool steels and titanium alloys.	EOSPRINT, EOS RP Tools	\$350,000
3D Systems ProX DMP 300 [61]	Direct metal laser sintering (DMLS)	250x250x330	1,070-nm fiber laser	—	20/100	Cobalt-Chrome (CoCr), Stainless Steel 17-4 PH, Maraging Steel, Aluminum Alloy AlSi12	3DXpert	\$680,000
Desktop Metal Production [61]	Binder jetting	337x337x330	SPI, 2 powder spreaders and 1 print head	—	50	17-4 PH, AISI 4140, H13, 316 L, Copper, Inconel 625	Fabricate	\$750,000

Table 4.4. Open-Source Metal 3D Printers

Model	Technology	Volume, mm	Print System	Part Weight, kg	Resolution, μm	Material	Software	Price, USD
Freemelt ONE [62]	Electron beam melting (EBM)	$\varnothing 100 \times 100$	6kW CO2 Laser	—	—	—	Freemelt ONE	—
Open-source metal 3-D printer v2 [25]	Gas-Metal Arc Welding (GMAW)	—	Low-cost MIG Welder	—	~2000 500	Aluminum alloys. Steel, Stainless steel	Cura/MOST Metal Cura/Franklin	<\$2000
FabMX (under development) [63]	Metal injection molded (MIM) pellet Fused Deposition	—	—	—	—	—	—	—
Low-Cost TIG-based Open Source Metal 3-D Printer (this paper)	Gas-Tungsten Arc Welding (GTAW)	298 x 275 x 250	Low-cost TIG Welder	5 kg	100 - 400	Mild Steel, Aluminum, Bronze, Brass, Stainless Steel	Lightning	\$2848.41

4.8.5 Future Work

The machine explored in this paper represents a minimum viable product ready to evolve into a flexible and ubiquitous platform for metal 3D printing. The following steps are recommended to further the capabilities of this machine:

- Increase the resolution by attempting depositions using finer input materials.
- Characterize the machine using additional material types, such as aluminium and bronze.
- Implement multiple extruders to allow for in-situ alloying.
- Implement a rotating extruder to allow for any direction of printing/traveling combination.
- Implement further measures to reduce probability of EMI effecting the system. This could be done by creating a new control board with better filtering capabilities. Additionally, modifying the stock firmware of the printer to use Parity bits during communication can increase the robustness of the channel.

- Create or modify a slicer to work with the unique constraints of the machine
- Create a 2 degree-of-freedom mechanism that can control the position of the filler. Linking this to sensory feedback such as light and sound can create a closed-loop control system which can actively adjust the filler position in-situ.

4.9 Conclusions

The novel TIG-based metal 3D printer offers a unique platform for prototyping metal objects. At a cost savings of 98%, the technology offers an affordable solution for researchers and makers alike to generate custom metal prototypes without knowledge of machining. With a Z resolution of 0.2mm and X resolution of 1.8mm, the machine is capable of prototyping high-resolution and strong objects.

4.10 References

1. DMP Factory 500 Solution, 3D Systems. (2021). <https://www.3dsystems.com/3d-printers/dmp-factory-500> (accessed July 20, 2021).
2. M. Attaran, The rise of 3-D printing: The advantages of additive manufacturing over traditional manufacturing, *Business Horizons*. 60 (2017) 677–688. <https://doi.org/10.1016/j.bushor.2017.05.011>.
3. Canessa, E., Fonda, C., Zennaro, M., & Deadline, N. (2013). Low-cost 3D printing for science, education and sustainable development. *Low-Cost 3D Printing*, 11(1).
4. Baden, T., Chagas, A. M., Gage, G., Marzullo, T., Prieto-Godino, L. L., & Euler, T. (2015). Open Labware: 3-D printing your own lab equipment. *PLoS biology*, 13(3), e1002086.
5. Pearce, J. M. (2012). Building research equipment with free, open-source hardware. *Science*, 337(6100), 1303-1304.
6. J. Pearce, Impacts of Open Source Hardware in Science and Engineering, *The Bridge*. (2017). <https://hal.archives-ouvertes.fr/hal-02111398> (accessed July 19, 2021).
7. J.M. Pearce, Open-Source Lab: How to Build Your Own Hardware and Reduce Research Costs, Elsevier, 2013.
8. A. Rindfleisch, M. O'Hern, V. Sachdev, The Digital Revolution, 3D Printing, and Innovation as Data, *Journal of Product Innovation Management*. 34 (2017) 681–690. <https://doi.org/10.1111/jpim.12402>.
9. J.M. Pearce, Economic savings for scientific free and open source technology: A review, *HardwareX*. 8 (2020) e00139. <https://doi.org/10.1016/j.hwx.2020.e00139>.

10. H. Chandra, S.W. Allen, S.W. Oberloier, N. Bihari, J. Gwamuri, J.M. Pearce, Open-Source Automated Mapping Four-Point Probe, Materials. 10 (2017) 110. <https://doi.org/10.3390/ma10020110>.
11. S.S. Sule, A.L. Petsiuk, J.M. Pearce, Open Source Completely 3-D Printable Centrifuge, Instruments. 3 (2019) 30. <https://doi.org/10.3390/instruments3020030>.
12. D.K. Trivedi, J.M. Pearce, Open Source 3-D Printed Nutating Mixer, Applied Sciences. 7 (2017) 942. <https://doi.org/10.3390/app7090942>.
13. S. Oberloier, J.M. Pearce, Belt-Driven Open Source Circuit Mill Using Low-Cost 3-D Printer Components, Inventions. 3 (2018) 64. <https://doi.org/10.3390/inventions3030064>.
14. A. Krige, J. Haluška, U. Rova, P. Christakopoulos, Design and implementation of a low cost bio-printer modification, allowing for switching between plastic and gel extrusion, HardwareX. 9 (2021) e00186. <https://doi.org/10.1016/j.johx.2021.e00186>.
15. E.E. Petersen, J. Pearce, Emergence of Home Manufacturing in the Developed World: Return on Investment for Open-Source 3-D Printers, Technologies. 5 (2017) 7. <https://doi.org/10.3390/technologies5010007>.
16. Coakley, M., & Hurt, D. E. (2016). 3D printing in the laboratory: Maximize time and funds with customized and open-source labware. Journal of laboratory automation, 21(4), 489-495.
17. Gwamuri, J., & Pearce, J. M. (2017, May). Open source 3-D printers: An appropriate technology for building low cost optics labs for the developing communities. In Education and training in optics and photonics (p. 104522S). Optical Society of America.[1]S. Oberloier, J.M. Pearce, General Design Procedure for Free and Open-Source Hardware for Scientific Equipment, Designs. 2 (2018) 2. <https://doi.org/10.3390/designs2010002>.
18. Maia Chagas, André. "Haves and have nots must find a better way: The case for open scientific hardware." *PLoS biology* 16, no. 9 (2018): e3000014.
19. Gwamuri, J., Poliskey, J., & Pearce, J. (2016). Open source 3-D printers: an appropriate technology for developing communities. In *Proceedings to the 7th International Conference on Appropriate Technology*.
20. S. Oberloier, J.M. Pearce, General Design Procedure for Free and Open-Source Hardware for Scientific Equipment, Designs. 2 (2018) 2. <https://doi.org/10.3390/designs2010002>.

21. N. Bihari, I.T.S. Heikkinen, G. Marin, C. Ekstrum, P.J. Mayville, S. Oberloier, H. Savin, M. Karppinen, J.M. Pearce, Vacuum outgassing characteristics of unpigmented 3D printed polymers coated with atomic layer deposited alumina, *Journal of Vacuum Science & Technology A*. 38 (2020) 053204.
<https://doi.org/10.1116/6.0000178>.
22. Pasanen, T. P., von Gastrow, G., Heikkinen, I. T., Vähänissi, V., Savin, H., & Pearce, J. M. (2019). Compatibility of 3-D printed devices in cleanroom environments for semiconductor processing. *Materials Science in Semiconductor Processing*, 89, 59-67.
23. I.T.S. Heikkinen, C. Kauppinen, Z. Liu, S.M. Asikainen, S. Spoljaric, J.V. Seppälä, H. Savin, J.M. Pearce, Chemical compatibility of fused filament fabrication-based 3-D printed components with solutions commonly used in semiconductor wet processing, *Additive Manufacturing*. 23 (2018) 99–107.
<https://doi.org/10.1016/j.addma.2018.07.015>.
24. Y. Nilsiam, P.G. Sanders, J.M. Pearce, Applications of Open Source GMAW-Based Metal 3-D Printing, *Journal of Manufacturing and Materials Processing*. 2 (2018) 18. <https://doi.org/10.3390/jmmp2010018>.
25. Anzalone, G. C., Zhang, C., Wijnen, B., Sanders, P. G., & Pearce, J. M. (2013). A low-cost open-source metal 3-D printer. *IEEE Access*, 1, 803-810.
26. Jones, R., Haufe, P., Sells, E., Iravani, P., Olliver, V., Palmer, C., & Bowyer, A. (2011). RepRap—the replicating rapid prototyper. *Robotica*, 29(1), 177-191.
27. Sells, E., Bailard, S., Smith, Z., Bowyer, A., & Olliver, V. (2010). RepRap: the replicating rapid prototyper: maximizing customizability by breeding the means of production. In *Handbook of Research in Mass Customization and Personalization: (In 2 Volumes)* (pp. 568-580).
28. Bowyer, A. (2014). 3D printing and humanity's first imperfect replicator. *3D printing and additive manufacturing*, 1(1), 4-5.
29. Rundle, G. (2014). *A Revolution in the Making*. Simon and Schuster.
30. M. Yakout, M.A. Elbestawi, S.C. Veldhuis, A Review of Metal Additive Manufacturing Technologies, *Solid State Phenomena*. 278 (2018) 1–14.
<https://doi.org/10.4028/www.scientific.net/SSP.278.1>.
31. T. Duda, L.V. Raghavan, 3D metal printing technology: the need to re-invent design practice, *AI & Soc.* 33 (2018) 241–252. <https://doi.org/10.1007/s00146-018-0809-9>.

32. Z.K. Wani, A.B. Abdullah, A Review on metal 3D printing\\$\\mathsemicolon\\$ 3D welding, IOP Conf. Ser.: Mater. Sci. Eng. 920 (2020) 012015.
<https://doi.org/10.1088/1757-899X/920/1/012015>.
33. J.Z. Li, M.R. Alkahari, N.A.B. Rosli, R. Hasan, M.N. Sudin, F.R. Ramli, Review of Wire Arc Additive Manufacturing for 3D Metal Printing, International Journal of Automation Technology. 13 (2019) 346–353.
<https://doi.org/10.20965/ijat.2019.p0346>.
34. B. Liu, H. Shen, R. Deng, Z. Zhou, J. Jin, J. Fu, Research on GMAW based non-supporting thin-wall structure manufacturing, Rapid Prototyping Journal. 27 (2020) 333–345. <https://doi.org/10.1108/RPJ-05-2020-0102>.
35. Z. Hu, X. Qin, Y. Li, J. Yuan, Q. Wu, Multi-bead overlapping model with varying cross-section profile for robotic GMAW-based additive manufacturing, J Intell Manuf. 31 (2020) 1133–1147. <https://doi.org/10.1007/s10845-019-01501-z>.
36. N.A. Rosli, M.R. Alkahari, F.R. Ramli, S. Maidin, M.N. Sudin, S. Subramoniam, T. Furumoto, [Design and development of a low-cost 3D metal printer](#) JMARD. 41 (2018) 47–54. <https://doi.org/10.26480/jmerd.03.2018.47.54>.
37. A. J. Wyman, P. G. Ikonomov. Optimization of Hybrid Metal Printing Process *International Journal of Engineering Trends and Technology*, 68(9),36-39. <https://doi.org/10.14445/22315381/IJETT-V68I9P207>.
38. Welding Resources, Guides and Calculators, (n.d.).
<https://www.millerwelds.com/resources/welding-guides> (accessed July 23, 2021).
39. Y. Nilsiam, P. Sanders, J.M. Pearce, Slicer and process improvements for open-source GMAW-based metal 3-D printing, Additive Manufacturing. 18 (2017) 110–120. <https://doi.org/10.1016/j.addma.2017.10.007>.
40. K. Wu, Z. Liang, T. Yin, Z. He, M. Zeng, Double Pulse Low-Frequency Modulation for High-Power Double-Wire Pulsed GMAW, Journal of Manufacturing Science and Engineering. 140 (2018).
<https://doi.org/10.1115/1.4040319>.
41. A.S. Haselhuhn, E.J. Gooding, A.G. Glover, G.C. Anzalone, B. Wijnen, P.G. Sanders, J.M. Pearce, Substrate Release Mechanisms for Gas Metal Arc Weld 3D Aluminum Metal Printing, 3D Printing and Additive Manufacturing. 1 (2014) 204–209. <https://doi.org/10.1089/3dp.2014.0015>.
42. A.S. Haselhuhn, B. Wijnen, G.C. Anzalone, P.G. Sanders, J.M. Pearce, In situ formation of substrate release mechanisms for gas metal arc weld metal 3-D printing, Journal of Materials Processing Technology. 226 (2015) 50–59.
<https://doi.org/10.1016/j.jmatprotec.2015.06.038>.

43. A.S. Haselhuhn, P.G. Sanders, J.M. Pearce, Hypoeutectic Aluminum–Silicon Alloy Development for GMAW-Based 3-D Printing Using Wedge Castings, *Inter Metalcast*. 11 (2017) 843–856. <https://doi.org/10.1007/s40962-017-0133-z>.
44. Pinar, A., Wijnen, B., Anzalone, G. C., Havens, T. C., Sanders, P. G., & Pearce, J. M. (2015). Low-cost open-source voltage and current monitor for gas metal arc weld 3D printing. *Journal of Sensors*, 2015.
45. LulzBot TAZ 4 3D Printer: Amazon.com: Industrial & Scientific, (n.d.). <https://www.amazon.com/dp/B00JXQZ8CC> (accessed November 14, 2021).
46. LulzBot, (n.d.). <https://shop.lulzbot.com/sidekick> (accessed November 14, 2021).
47. J.M. Pearce, S. Oberloier, W. Holmes, TIGasaurus - open source TIG-based high-resolution metal 3-D printer, (2020). <https://osf.io/rd2a4/> (accessed July 23, 2021).
48. MTU MOST / MOST_Lightning, GitLab. (n.d.). https://gitlab.com/mtu-most/most_lightning (accessed November 14, 2021).
49. Home - Linux Mint, (n.d.). <https://linuxmint.com/> (accessed November 14, 2021).
50. T.Q. Company, Embedded Software Development Tools | Cross Platform IDE | Qt Creator, (n.d.). <https://www.qt.io/product/development-tools> (accessed July 22, 2021).
51. Home | Marlin Firmware, (n.d.). <https://marlinfw.org/> (accessed July 22, 2021).
52. Ultimaker Cura: Powerful, easy-to-use 3D printing software, Ultimaker.Com. (n.d.). <https://ultimaker.com/software/ultimaker-cura> (accessed November 15, 2021).
53. 3D Slicer image computing platform, 3D Slicer. (n.d.). <https://slicer.org/> (accessed November 15, 2021).
54. IceSL, (n.d.). <https://icesl.loria.fr/> (accessed July 27, 2021).
55. S. Oberloier, PSO Experimenter, (2021). <https://osf.io/muevs/> (accessed July 22, 2021).
56. D. Wang, D. Tan, L. Liu, Particle swarm optimization algorithm: an overview, *Soft Comput*. 22 (2018) 387–408. <https://doi.org/10.1007/s00500-016-2474-6>.
57. S. Oberloier, N.G. Whisman, J.M. Pearce, Finding Ideal Parameters for 3-D Printing Using Particle Swarm Optimization, to be published (2021)

58. A.M. Pringle, S. Oberloier, A.L. Petsiuk, P.G. Sanders, J.M. Pearce, Open source arc analyzer: Multi-sensor monitoring of wire arc additive manufacturing, *HardwareX*. 8 (2020) e00137. <https://doi.org/10.1016/j.hx.2020.e00137>.
59. SKS: microMIG / microMIG-cc, (n.d.). <https://www.sks-welding.com/en/torch-systems/single-wire/frontpull-7/micromig-micromig-cc.html> (accessed November 15, 2021).
60. Pearce, J. M. (2015). A novel approach to obviousness: An algorithm for identifying prior art concerning 3-D printing materials. *World Patent Information*, 42, 13-18.
61. Best Metal 3D Printers of 2021 – Buyer’s Guide, All3DP Pro. (2021). <https://all3dp.com/1/3d-metal-3d-printer-metal-3d-printing/> (accessed November 15, 2021).
62. Freemelt ONE: The 3D printer for materials R&D, Freemelt. (n.d.). <https://freemelt.com/freemelt-one/> (accessed November 15, 2021).
63. Project FabMX - FabMX - FabLab München, (n.d.). <https://wiki.fablab-muenchen.de/display/FABMX/Project+FabMX> (accessed November 15, 2021).

5 Particle Swarm Optimization of Printing Parameters for Open Source TIG-Based Metal 3-D Printing

5.1 Introduction

Rapid prototyping of metal objects is normally contracted to a manufacturing service [1,2] due to the prohibitively high cost of owning a metal 3-D printer of the commercialized varieties, which include: bound metal deposition (BMD), atomic diffusion additive manufacturing (ADAM), laser metal fusion (LMF), electron beam melting (EBM), direct metal laser sintering (DMLS), binder jetting, single pass jetting, selective laser sintering (SLS) or selective laser melting (SLM) machines [3]. Costs range from >\$60,000 USD for bound metal deposition to \$750,000 USD for single pass jetting [3]. High component costs such as a 1000W laser source [4], hazardous materials and the concomitant safety equipment [5] render SLS and the other high-resolution powder metal-based 3-D printing methods unsuitable to be implemented as low-cost open source solution for distributed metal additive manufacturing (AM). The scientific community has pursued alternative metal-based additive methods. These methods include a version of BMD using fused filament fabrication (FFF)-based 3-D printing polymer filament with a high metal powder density, which behaves more like plastic [6]. Then this polymer-metal composite is treated at high temperatures and sintered [7- 9]. This process makes metal products, but suffers from challenges related to porosity, dimensional accuracy and strength of the final parts [7,8]. Thus, most of the efforts in low-cost metal AM have centered around the utilization of metal inert gas (MIG) or gas metal arc welding (GMAW)-based wire arc additive manufacturing (WAAM). MIG-based 3-D printing [10] was developed on open source self-replicating rapid prototyper (RepRap)-class 3-D printers [11-13] and has been predominately used since the deposition mechanism for WAAM because it is analogous to plastic filament extruders and can be made compatible with existing open source FFF slicers [10,14,15]. After considerable progress related to WAAM-specific alloy development [16], monitoring [18-20], substrate release mechanisms [21,22], and process improvements and slicing [14] GMAW-based 3-D printers are capable of near-net-shape depositions [14, 23-28], but print at resolutions much worse than SLS [23-28]. Although GMAW-based 3-D printing can make high quality metal parts, there is a fundamental limitation of the technique because the current is passing through the metal filament. As the filament diameter decreases first the weld bead and horizontal resolution improve, but as it continues to decrease the filament becomes mechanically unstable and ‘wags’ during welding actually increasing the size of 3-D printed line.

Another promising approach to obtain high-resolution high-quality metal components is based around tungsten inert gas (TIG) welding, as it is theoretically capable of low-splatter, low energy, and high resolution [29,30]. Though despite the advantages of TIG welding, print performance of existing systems have resolutions from 6.8 mm [31] to 7.7 mm [32], which is not nearly high enough for most desired applications such as printing structural fixturing [33-36], for replacing other high temperature AM materials [37-41], and robotics systems [42-45]. The open source TIG-based 3-D printing system (TIG-Bot) used in this study is made to be low-cost by adapting an existing commercial open-source

Rep-Rap 3-D printer by adding an end effector made for varying filler diameters allowing for increasingly finer resolutions with a standard TIG welder.

One reason for the slow approach towards better resolution for WAAM in general is the vast number of parameters involved in the manufacturing process. For TIG AM this includes: type of material and diameter of feedstock, feed rate, extrusion rate, gas flow rate, type of cover gas, standoff distance, tungsten distance, tungsten tip geometry, torch angle, feed angle, welding current, and arc frequency [46-48].

Even when isolating a single feedstock (material and diameter), the permutations involved in TIG-based 3-D printing create a vast and complex processing space, which has historically required substantial time investments to identify optimal 3-D printing parameters [49-51]. Fortunately, optimization problems like this can be simplified by leveraging computational intelligence methods, which have matured substantially in the last several years and will result in a substantial savings in time and material [49].

In this article, free and open source software called *PSO Experimenter* is utilized to find optimal printing parameters for the open source TIG-Bot [49]. The software is a GUI implementation of the particle swarm optimization (PSO) method [52], designed specifically for hardware-in-loop testing (typically PSOs are used in numerical analysis problems, but this software is designed to optimize physical systems). PSO Experimenter allows for the input of experimental variables and their respective ranges, and then will propose iterations of experiments. A custom fitness function is defined to characterize the experimental result and provide feedback to the algorithm. Three separate trials are carried out to find optimal parameters. First, an experiment is designed to deposit and optimize parameters for a single line. Second, an experiment is carried out to optimize parameters for a single layer plane. Then, an experiment will be performed to find optimal printing parameters for a cube. Finally, to demonstrate the robustness of this open hardware and software, the identified optimized printing parameters are used to fabricate a useful product. The results are presented and discussed in the context of expanding WAAM to more systems and material class for distributed digital manufacturing.

5.2 Materials and Methods

5.2.1 Open Source TIG-Bot

The TIG-Bot is an open source Lulzbot Taz 4 [53] outfitted with a custom TIG welding end effector. In addition, a specialized bed is added to allow ease of fixturing, as well as to electrically isolate the welding system and dissipate excess heat. Since the TIG welder employs a high-frequency start mechanism, which generates large amounts of electromagnetic frequencies (EMFs) [54], the TIG-Bot must be housed in a full-metal Faraday cage [55]. Detailed specifications can be found from [56].



Figure 5.1: The open source TIG-Bot inside of a Faraday cage.

The TIG-Bot can work with any open source Marlin [57] compatible control software, but for this study a lightweight C++ based software called *Lightning* v1.0 is used to control the tests. Lightning is free and open source software available at the Open Science Framework [58]. The tool employs a basic library for sending and receiving G-Code commands, and can be quickly modified to execute parametric G-Code. This allows for rapid testing and substantial flexibility in machine control.

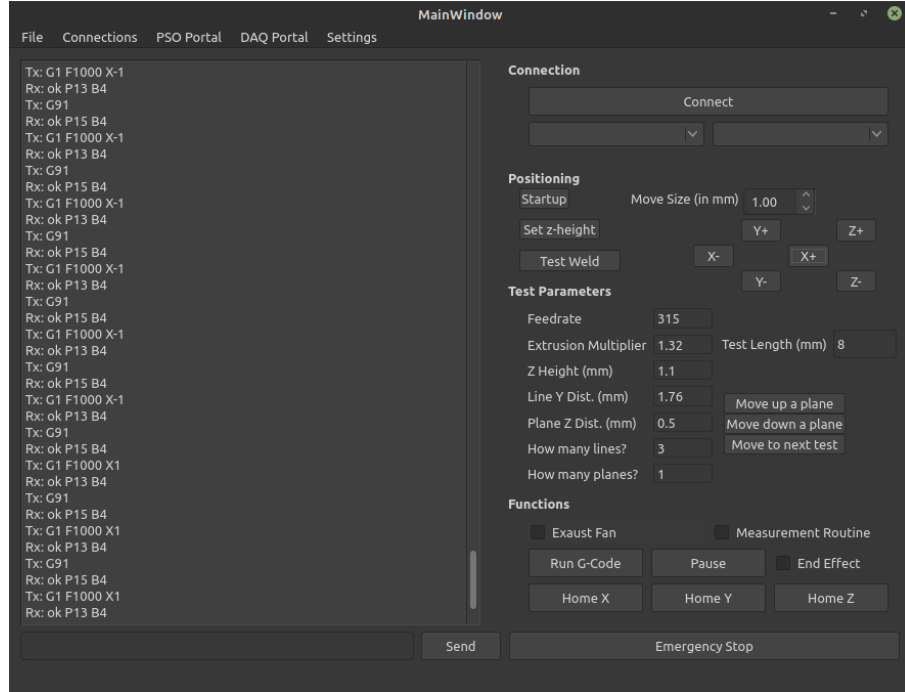


Figure 5.2: A screenshot of the Lightning control interface.

The welder being used is an TIG-165S [59], chosen for its low cost (<\$200USD), low power settings, and high-frequency start mechanism. Though the high-frequency start causes problematic noise, it prolongs the lifespan of the tungsten electrode since it does not have to scratch start [60].

2% Ceriated (with Cerium) 1/16" (1.6mm) Tungsten electrodes [61] are used, along with 0.024" (0.6mm) mild steel MIG wire [62] as filler material. The tests will be carried out on 0.25" (0.64mm) mild steel substrates.

5.2.2 PSO Experimenter

PSO Experimenter [63] is a free and open source GUI interface software developed in QtCreator [64] that allows for the generic application of the PSO algorithm. The software has three main pages:

- 1) Particles – Particles allows for the viewing of different iterations of particles. Each particle represents a set of test parameters to be executed, and iterations occur as the particles “move” during their optimization process. Additionally, the fitness value (a measurement of success for the test) for each particle is entered in this screen. In this case the test parameters are related to the process parameters of the OS TIG-Bot
- 2) Experimental Variables – This screen is used in the initial configuration of the experiment. It allows for new variables to be created with names and minimum and maximum value. These variables can be integer only or constrained to a single value. Additionally, an initial guess can be input to help narrow down the initialization pattern

to cut down on optimization time. The minimum, maximum, and constraint value can be changed at any time during the testing process, allowing the user to alter conditions as needed.

3) PSO Variables – This screen contains all of the pertinent parameters for PSO operation, as detailed in Table 5.1.

Table 5.1: Main parameters for tuning PSO behavior.

Variable	Description
N_P	Number of particles to optimize with
P_I	Proximity particle positions are initialized from the initial guess
k_v	The emphasis given to the velocity of the particle
k_p	The emphasis given to a particle's personal best position
k_g	The emphasis given to the swarm's group best position

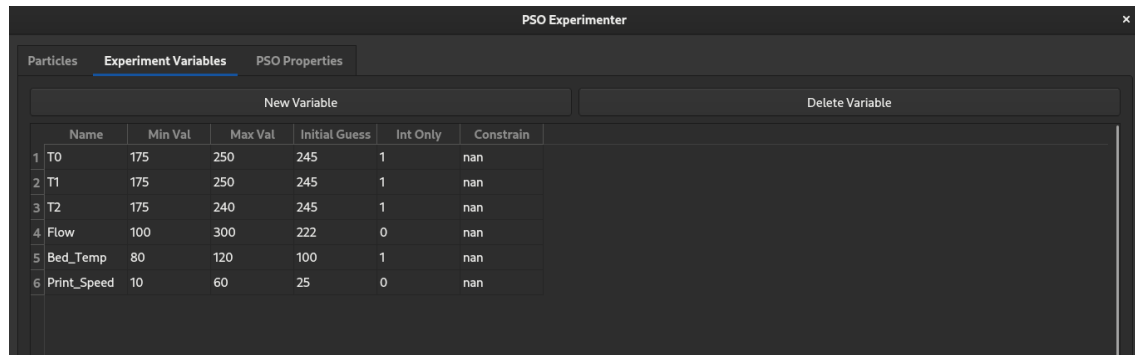


Figure 5.3: A screenshot of the variable entry screen of PSO Experimenter.

5.2.3 Process Variables

There are two types of variables that will be discussed in this section: fully constrained values and experiment parameters. The fully constrained values are variables that are known to effect weld quality, but for this set of experiments will be held constant. Their values are either found from the literature or initial experimentation and are summarized in Table 5.2.

Table 5.2: List of fully constrained values.

Variable	Description	Value
Torch Angle	The angle which the TIG torch is held relative to the substrate	93°
Filler Angle	The angle which the filler material is fed relative to the substrate	15°
Pulse Rate	The pulse rate effects the distribution of the arc	~10%
Gas Flow Rate	The cover gas flow rate	40 CFH

The experimental parameters are found from a combination of literature review and initial experimentation and are shown in Table 5.3.

Table 5.3: List of experiment parameters values and ranges.

Variable	Min	Max	Guess	Int?	Description
I	10	22	19	True	Welder current
V_P	250 mm/s	350 mm/s	245°C	True	End effector movement rate
F	100%	160%	130%	False	Extrusion flow multiplier
H	0.5mm	2mm	1.1mm	False	Z-height
S_Y	1mm	2mm	1.7mm	False	Y-line spacing
S_Z	0.5mm	1mm	0.6mm	False	Z-line spacing

5.2.4 Test structures

The three test structures are a line, plane and cube and are shown in a G-code rendering and image of a non-optimized metal 3-D print in Figure 5.4.

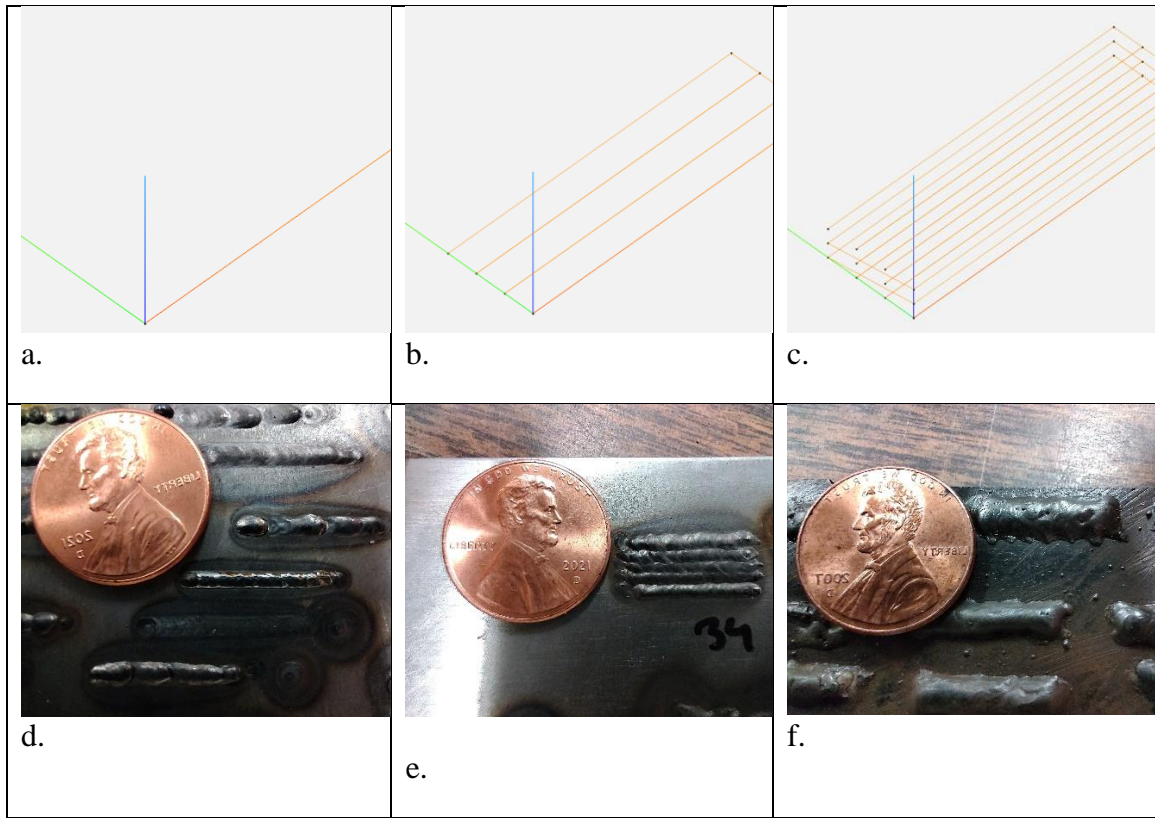


Figure 5.4. G-code rendering of a) a line, b) plane and c) rectangular prism and image of an optimized metal 3-D print for the d) line, e) plane and f) rectangular prism.

5.2.5 Line Optimization Test

The line optimization test entails attempting to deposit a singular 16 mm bead of weld along the X-axis. Given this test consists of a sole line, the parameters I , V_p , F , H will be optimized. The quality of the weld is characterized by the physical dimensions of length (l) accuracy, width (w) accuracy, width consistency and height (h) accuracy. where accuracy is defined in equation 1, and consistency is defined in equation 2. Additionally, a failed weld will be penalized with a non-zero I (incomplete) score (assigned an integer value of 1 for 80 completion, 2 for 60% completion, and so on) The fitness of the extrusion is characterized by a weighted sum of the physical measurements in equation 3. The weight values are set according to expert opinion, and the comparison values are set from initial testing to understand reasonable expectations.

$$A(X_m, X_d) = \frac{|X_m - X_d|}{X_d} \dots (1)$$

Where X_m is the measured value (or in some cases the averaged measured value), and X_d is the desired value.

$$C(X_{m1}, X_{m2} \dots X_{mn}) = \text{avgdev}(X_{m1}, X_{m2}, \dots, X_{mn}) \dots (2)$$

$$f_{line} = 0.4C(w_{m1}, \dots, w_{m5}) + 0.3A(w_{avg}, 1.5mm) + 0.15A(l_m, 16mm) + 0.15A(h_m, 0.5mm) + I \dots (3)$$

5.2.6 Plane Optimization Test

The plane optimization test entails attempting to deposit three 8 mm parallel lines with varying spacing. For this test, the initial guess for values will be the best fitness value from the line optimization test. All the parameters from the line test can still be altered / optimized, with the addition of S_Y . The quality of the weld is characterized by the physical dimensions of length (l) accuracy, width (w) accuracy, height consistency and height (h) accuracy. The fitness of the extrusion is characterized by a weighted sum of the physical measurements in equation 4.

$$f_{plane} = 0.4C(h_{m1}, \dots, h_{m5}) + 0.3A(w_{avg}, 4mm) + 0.15A(l_m, 8mm) + 0.15A(h_m, 0.25mm) + I \dots (4)$$

5.2.7 Rectangular Prism Optimization Test

The final test involves depositing three consecutive 3-line wide layers stacked along the Z-axis. This test optimizes all parameters in Table 5.3. The optimization function for the prism test will be defined as the same function for the plane optimization, equation 4.

5.3 Theory/Calculation

5.3.1 Particle Swarm Optimization Summary

Banks, Vincent & Anyakoha [52] summarize how PSOs operate by accepting a description of the sample space, variables and their ranges, and iteratively proposing candidate solutions (particle positions) for the optimum position in the space. First, each particle in the swarm is initialized according to a uniform distribution in the sample space. The variables in the space represent experimental configurations that must be tested and characterized. Characterization depends (within the context of hardware-in-loop testing) on the desired outcome of the experiment, and user's expert on their priority. Each feature of the outcome must be quantified and plugged into a defined fitness function to generate a score for the fitness of the particle. After each particle has been tested, the particle will adjust its position based on 4 factors -it's velocity (it will tend towards the direction it was previously heading), personal best fitness, group best fitness, and random variables multiplying each previously stated component. The algorithm can be run until a desired fitness threshold is met, or for a fixed number of iterations. The PSO operation summarized in Figure 5.5.

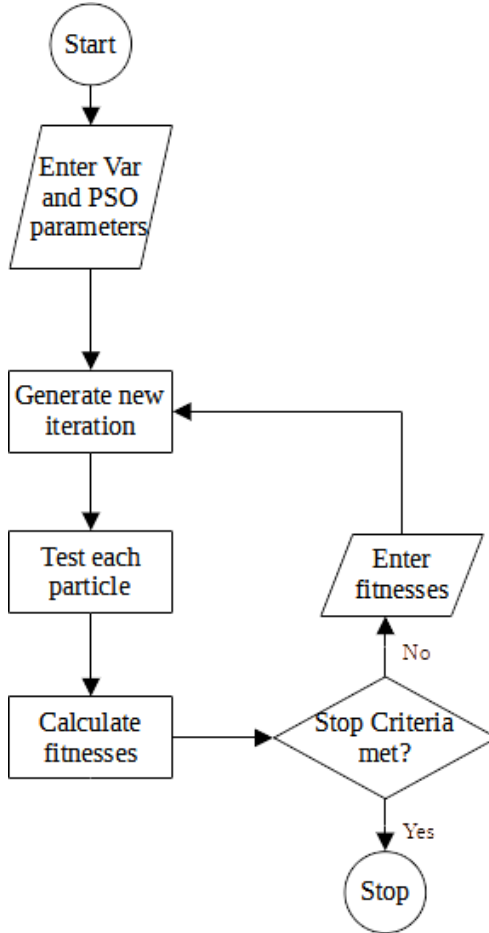


Figure 5.5. The general workflow for PSO.

5.3.2 TIG Welding Theory and Variables

The TIG-165S is used as the welder for the TIG-Bot and employs a high frequency start [59]. Such welders with a high frequency start will first ionize the air by charging the tungsten with a high frequency pulse, causing the air-path between the tungsten and substrate to ionize, reducing resistance and allowing for the high current arc to start [60]. Additionally, during the arc process a solenoid valve is opened, allowing for cover gas to flow.

The arc generated by the torch holds a conic pattern defined by the tungsten geometry, cover gas flow rate, and Z-height. Within the arc distribution is a higher intensity zone referred to as “the hot spot”, where filler should be applied. The location of this hot spot can be altered on the TIG-Bot by adjusting the torch angle. Additionally, the feeder tube can be rotated about the Z axis to better position the filler into the hot spot. Adjusting the Z-height upwards causes the arc to become more sporadic and the heat input to increase, which decreases weld quality. Decreasing the Z-height, however, increases the probability of touching the tungsten to the weld pool, leaving it contaminated. The Z-height used is 1mm.

Since the optimization is being performed on mild steel, C-25 (75% argon, 25% carbon dioxide) is used as the cover gas. The cover gas is an inert gas that prevents the freshly deposited metal from corroding, creating a more difficult surface to weld to [65]. The flow rate should be set at a value that yields low corrosion and then kept constant. The flow rate used was 130%.

Finally, movement rates and extrusion rates are closely coupled in that they work together to effect weld consistency, height, and width.

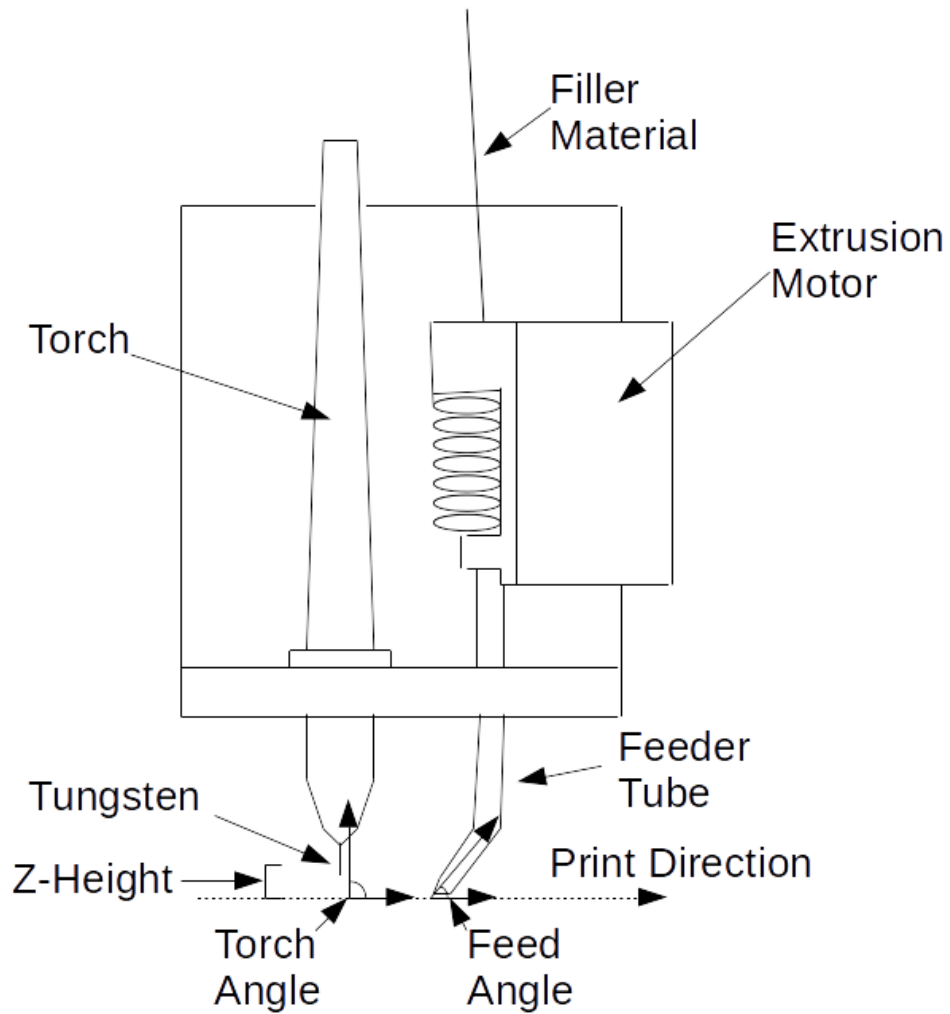


Figure 5.6. A schematic labeled representation of the extrusion mechanism of the TIG-Bot

5.4 Results

5.4.1 Line Optimization

The line trial was able to optimize from a fitness of 0.43 to 0.22 after 6 iterations. The optimization performance can be viewed in Figure 5.7. The ideal parameters for printing lines are listed in Table 5.4 column 3.

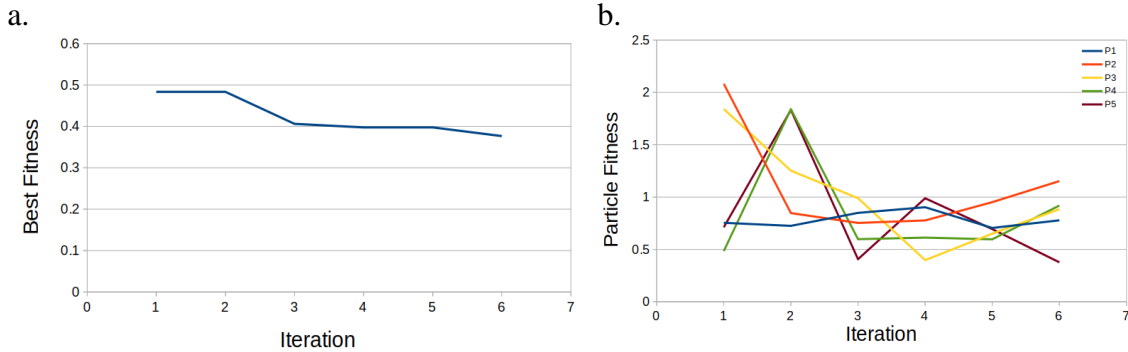


Figure 5.7: Performance of PSO on line tests a. Total best fitness b. Particle fitness over time

Table 5.4: List of experiment parameters values and ranges.

Variable	Description	Line Value	Plane Value	Cube Value
I	Welder current	15 A	20 A	20A
V_P	End effector movement rate	259 mm/s	311 mm/s	295 mm/s
F	Extrusion flow multiplier	159%	100%	128%
H	Z-height	1.21 mm	1.2 mm	1.5mm
S_Y	Y-line spacing	NA	1.68 mm	0.5mm
S_Z	Z-line spacing	NA	NA	0.36mm

5.4.2 Plane Optimization

The plane trial was able to optimize from a fitness of 0.26 to 0.18 after 6 iterations. The optimization performance can be viewed in Figure 5.8. The ideal parameters for printing lines are listed in Table 5.4 column 4.

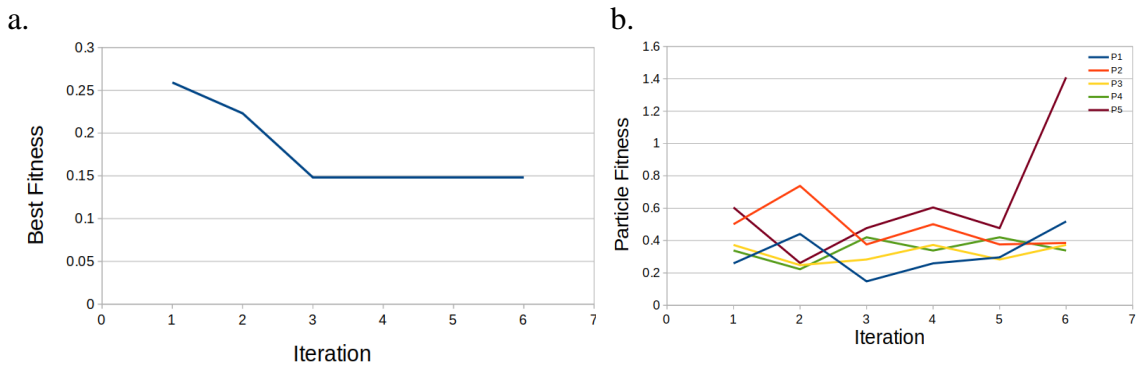


Figure 5.8: Performance of PSO on plane tests a. Total best fitness b. Particle fitness over time

5.4.3 Prism Optimization

The plane trial was able to optimize from a fitness of 0.32 to 0.16 after 5 iterations. The optimization performance can be viewed in Figure 5.9. The ideal parameters for printing lines are listed in Table 5.4 column 5.

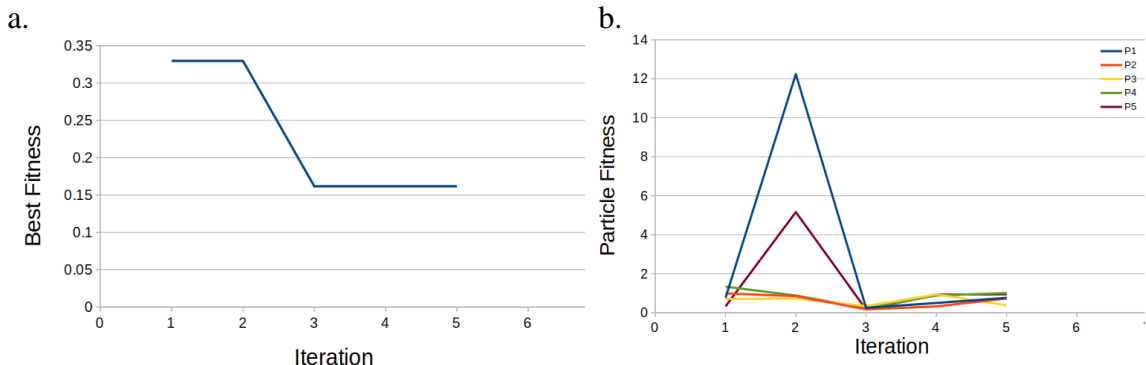


Figure 5.9: Performance of PSO on prism tests a. Total best fitness b. Particle fitness over time

5.5 Discussion

5.5.1 Particle Swarm Optimization Effectiveness

The particle swarm optimization was able to produce parameters that yielded a minimum Z resolution of 0.3mm and line resolution of 1.7mm in 6 iterations of 5 particles. A total of 30 tests at ~5 minutes per test yields a total optimization time of 2.5 hours. This rate is substantially faster than guided-guessing or matrix tests. For instance, if the line test were carried out as a matrix parameter sweep, with 4 variables divided into 5 increments, would create 625 tests and take 52 hours. Even if the proposed matrix test was ran, the granularity of the search may prohibit from finding true optiums.

5.5.2 Limitations and Future Work

The largest constraint of the TIG-Bot machine that it is bound to depositing in one direction only (along the positive X axis). There is potential that optimizations could be ran along the Y axis to find ideal parameters for each direction. However different per-direction parameters will greatly increase the difficulty of implementing a custom slicer.

An additional constraint is that the filler of the machine is not capable of moving relative to arc deflections. Creating a system which monitors arc quality and actively adjusts the filler angle cold be use to increase surface uniformity [66].

The only material explored in this manuscript is mild steel, however TIG is capable of depositing with a wide range of materials including aluminum and bronze [66]. Additional experiments can be devised using the method detailed in this manuscript to optimize and expand the capabilities of the TIG-Bot.

Additionally, new experiments can be devised using increased particle counts, iterations, and variables to potentially optimize further. A key variable that may prove impactful is allowing for minor adjustments on the gas flow, which will affect porosity [66]

5.5.3 Implications for Distributed Metal Additive Manufacturing

Distributed AM is already maturing in plastic 3-D printing [67-68] and a high resolution low-cost metal 3-D printing has a wide range of applications from repairing complex products [69], making high-value scientific equipment [15, 70-71], high temperature, chemically resistant, high strength, dishwasher safe, sterilizable medical equipment, etc.

5.6 Conclusions

PSO Experimenter was used to identify sets of ideal printing parameters for a TIG-Based Metal 3D Printer. After 3 test sets, parameters were acquired that can be used to print at resolutions of 0.36mm (in the Z axis). Though the resolution of the printer theoretically high-detailed depositions, the machine is severely hindered by a lack of slicing software which can accommodate the unique constraints of the machine.

5.7 References

1. Metal 3D Printing & CNC Machining Services | Stratasys Direct, Stratasys. (2021). <https://www.stratasysdirect.com/materials/metals> (accessed July 22, 2021).
2. Metal 3D Printing Service for Custom Parts | Online Quoting, (2021). <https://www.protolabs.com/services/3d-printing/direct-metal-laser-sintering/> (accessed July 22, 2021).
3. How Much Does a Metal 3D Printer Cost?, All3DP. (2020). <https://all3dp.com/2/how-much-does-a-metal-3d-printer-cost/> (accessed July 22, 2021).
4. 1000W HandHeld Fiber Laser Welding Machine Laser Welder - - Amazon.com, (2021). <https://www.amazon.com/1000W-HandHeld-Welding-Machine-Welder/dp/B08DTHGYBF> (accessed July 22, 2021).
5. M. Piscator, Health hazards from inhalation of metal fumes, Environ. Res.; (United States). 11:2 (1976). [https://doi.org/10.1016/0013-9351\(76\)90085-2](https://doi.org/10.1016/0013-9351(76)90085-2).
6. John Laureto, Julie Tomasi, Julia A. King, Joshua M. Pearce Thermal Properties of 3-D
7. Printed Polylactic Acid - Metal Composites. Progress in Additive Manufacturing 2(1), 57-71 (2017). doi: <http://dx.doi.org/10.1007/s40964-017-0019-x>
8. C. Tosto, J. Tirillò, F. Sarasini, G. Cicala, Hybrid Metal/Polymer Filaments for Fused Filament Fabrication (FFF) to Print Metal Parts, Applied Sciences. 11 (2021) 1444. <https://doi.org/10.3390/app11041444>.
9. I. Ait-Mansour, N. Kretzschmar, S. Chekurov, M. Salmi, J. Rech, Design-dependent shrinkage compensation modeling and mechanical property targeting of metal FFF, Prog Addit Manuf. 5 (2020) 51–57. <https://doi.org/10.1007/s40964-020-00124-8>.
10. Industrial Additive Manufacturing Platform, Markforged. (2021). <https://markforged.com/> (accessed July 22, 2021).
11. Gerald C. Anzalone, Chenlong Zhang, Bas Wijnen, Paul G. Sanders, and Joshua M. Pearce, Low-Cost Open-Source 3-D Metal Printing. *IEEE Access* 1, 803-810, (2013). DOI: <http://dx.doi.org/10.1109/ACCESS.2013.2293018>
12. R. Jones, P. Haufe, E. Sells, P. Iravani, V. Olliver, C. Palmer, A. Bowyer, RepRap – the replicating rapid prototyper, Robotica. 29 (2011) 177–191. <https://doi.org/10.1017/S026357471000069X>.

13. E. Sells, S. Bailard, Z. Smith, A. Bowyer, V. Olliver, RepRap: The Replicating Rapid Prototyper: Maximizing Customizability by Breeding the Means of Production, in: *Handbook of Research in Mass Customization and Personalization*, World Scientific Publishing Company, 2009: pp. 568–580.
https://doi.org/10.1142/9789814280280_0028.
14. A. Bowyer, 3D Printing and Humanity's First Imperfect Replicator, *3D Printing and Additive Manufacturing*. 1 (2014) 4–5.
<https://doi.org/10.1089/3dp.2013.0003>.
15. Y. Nilsiam, P. Sanders, J.M. Pearce, Slicer and process improvements for open-source GMAW-based metal 3-D printing, *Additive Manufacturing*. 18 (2017) 110–120. <https://doi.org/10.1016/j.addma.2017.10.007>.
16. Nilsiam, Y., Sanders, P., Pearce, J.M. (2018). Applications of Open Source GMAW-based Metal 3-D Printing. *Journal of Manufacturing and Materials Processing*. 2(1): 18.
17. Amberlee S. Haselhuhn, Paul G. Sanders, Joshua M. Pearce. Hypoeutectic Aluminum-Silicon Alloy Development for GMAW-Based 3-D Printing Using Wedge Castings. *International Journal of Metalcasting* 11(4) 843-856 (2017). doi: <https://doi.org/10.1007/s40962-017-0133-z>
18. A. Pinar, B. Wijnen, G. C. Anzalone, T. C. Havens, P. G. Sanders, J. M. Pearce. Low-cost
19. Open-Source Voltage and Current Monitor for Gas Metal Arc Weld 3-D Printing. *Journal of Sensors*. Vol. 2015, Article ID 876714, 8 pages, 2015. DOI: <http://dx.doi.org/10.1155/2015/876714>
20. Yuenyong Nilsiam, Amberlee Haselhuhn, Bas Wijnen, Paul Sanders, & Joshua M. Pearce. Integrated Voltage - Current Monitoring and Control of Gas Metal Arc Weld Magnetic Ball-Jointed Open Source 3-D Printer. *Machines* 3(4), 339-351 (2015). DOI: <http://dx.doi.org/10.3390/machines3040339>
21. Pringle, A.M., Oberloier, S., Petsiuk, A.L., Sanders, P.G., Pearce, J.M. (2020). Open Source Arc Analyzer: Multi-Sensor Monitoring of Wire Arc Additive Manufacturing. *HardwareX*. 8
22. Amberlee S. Haselhuhn, Bas Wijnen, Gerald C. Anzalone, Paul G. Sanders, Joshua M. Pearce. In situ Formation of Substrate Release Mechanisms for Gas Metal Arc Weld Metal 3-D Printing. *Journal of Materials Processing Technology* 226, 50–59 (2015). DOI: <http://dx.doi.org/10.1016/j.jmatprotec.2015.06.038>
23. Amberlee S. Haselhuhn, Eli J. Gooding, Alexandra G. Glover, Gerald C. Anzalone, Bas Wijnen, Paul G. Sanders, Joshua M. Pearce. Substrate Release

- Mechanisms for Gas Metal Arc 3-D Aluminum Metal Printing. *3D Printing and Additive Manufacturing* 1(4): 204-209 (2014). 181.
24. O. Yilmaz, A.A. Uglu, Microstructure characterization of SS308LSi components manufactured by GTAW-based additive manufacturing: shaped metal deposition using pulsed current arc, *Int J Adv Manuf Technol.* 89 (2017) 13–25.
<https://doi.org/10.1007/s00170-016-9053-y>
25. J.L. Prado-Cerdeira, J.L. Diéguez, A.M. Camacho, Preliminary development of a Wire and Arc Additive Manufacturing system (WAAM), *Procedia Manufacturing.* 13 (2017) 895–902.
[https://doi.org/10.1016/j.promfg.2017.09.154.](https://doi.org/10.1016/j.promfg.2017.09.154)
26. N.A. Rosli, M.R. Alkahari, F.R. Ramli, S. Maidin, M.N. Sudin, S. Subramoniam, T. Furumoto, DESIGN AND DEVELOPMENT OF A LOW-COST 3D METAL PRINTER, *JMERD.* 41 (2018) 47–54.
[https://doi.org/10.26480/jmerd.03.2018.47.54.](https://doi.org/10.26480/jmerd.03.2018.47.54)
27. B. Liu, H. Shen, R. Deng, Z. Zhou, J. Jin, J. Fu, Research on GMAW based non-supporting thin-wall structure manufacturing, *Rapid Prototyping Journal.* 27 (2020) 333–345. [https://doi.org/10.1108/RPJ-05-2020-0102.](https://doi.org/10.1108/RPJ-05-2020-0102)
28. Z. Hu, X. Qin, Y. Li, J. Yuan, Q. Wu, Multi-bead overlapping model with varying cross-section profile for robotic GMAW-based additive manufacturing, *J Intell Manuf.* 31 (2020) 1133–1147. [https://doi.org/10.1007/s10845-019-01501-z.](https://doi.org/10.1007/s10845-019-01501-z)
29. K. Wu, Z. Liang, T. Yin, Z. He, M. Zeng, Double Pulse Low-Frequency Modulation for High-Power Double-Wire Pulsed GMAW, *Journal of Manufacturing Science and Engineering.* 140 (2018).
[https://doi.org/10.1115/1.4040319.](https://doi.org/10.1115/1.4040319)
30. T.J. Donegá, T.F. Costa, R.V. Arencibia, L.O. Vilarinho, Comparison of thermal efficiency between A-TIG and conventional TIG welding, *Welding International.* 30 (2016) 255–267. [https://doi.org/10.1080/09507116.2015.1096472.](https://doi.org/10.1080/09507116.2015.1096472)
31. R.W. Niles, Weld Thermal Efficiency of the GTAW Process, (2021) 8.
32. Geng, Haibin, Jinglong Li, Jiangtao Xiong, Xin Lin, and Fusheng Zhang. “Optimization of Wire Feed for GTAW Based Additive Manufacturing.” *Journal of Materials Processing Technology* 243 (May 1, 2017): 40–47.
[https://doi.org/10.1016/j.jmatprotec.2016.11.027.](https://doi.org/10.1016/j.jmatprotec.2016.11.027)
33. Liu, Shuang, and Yaoyu Ding. “Wire-Based Direct Metal Deposition with Ti6Al4V.” In *Laser 3D Manufacturing VI*, 10909:109090J. International Society for Optics and Photonics, 2019. [https://doi.org/10.1117/12.2510521.](https://doi.org/10.1117/12.2510521)

34. J.O. Milewski, Additive Manufacturing Metal, the Art of the Possible, in: J.O. Milewski (Ed.), *Additive Manufacturing of Metals: From Fundamental Technology to Rocket Nozzles, Medical Implants, and Custom Jewelry*, Springer International Publishing, Cham, 2017: pp. 7–33. https://doi.org/10.1007/978-3-319-58205-4_2.
35. Patalas-Maliszewska, Justyna, Marcin Topczak, and Sławomir Kłos. “The Level of the Additive Manufacturing Technology Use in Polish Metal and Automotive Manufacturing Enterprises.” *Applied Sciences* 10, no. 3 (January 2020): 735. <https://doi.org/10.3390/app10030735>.
36. Sarvankar, Shruti Ganesh, and Sanket Nandaram Yewale. “Additive Manufacturing in Automobile Industry,” no. 4 (2019): 11.
37. Wittbrodt, Ben, and Joshua M. Pearce. “3-D Printing Solar Photovoltaic Racking in Developing World.” *Energy for Sustainable Development* 36 (February 1, 2017): 1–5. <https://doi.org/10.1016/j.esd.2016.08.001>.
38. Woern, Aubrey L., Joseph R. McCaslin, Adam M. Pringle, and Joshua M. Pearce. “RepRapable Recyclebot: Open Source 3-D Printable Extruder for Converting Plastic to 3-D Printing Filament.” *HardwareX* 4 (October 1, 2018): e00026. <https://doi.org/10.1016/j.ohx.2018.e00026>.
39. Zhang, Chenlong, Nicholas C. Anzalone, Rodrigo P. Faria, and Joshua M. Pearce. “Open-Source 3D-Printable Optics Equipment.” *PLOS ONE* 8, no. 3 (March 27, 2013): e59840. <https://doi.org/10.1371/journal.pone.0059840>.
40. Gardner, John, Christopher J. Stelter, Edward A. Yashin, and Emilie J. Siochi. “High Temperature Thermoplastic Additive Manufacturing Using Low-Cost, Open-Source Hardware,” 2016. <https://doi.org/10.13140/RG.2.2.20690.15049>.
41. Skrzypczak, Noah G., Nagendra G. Tanikella, and Joshua M. Pearce. “Open Source High-Temperature RepRap for 3-D Printing Heat-Sterilizable PPE and Other Applications.” *HardwareX* 8 (October 1, 2020): e00130. <https://doi.org/10.1016/j.ohx.2020.e00130>.
42. Marchelli, Grant, Renuka Prabhakar, Duane Storti, and Mark Ganter. “The Guide to Glass 3D Printing: Developments, Methods, Diagnostics and Results.” Edited by Dave Bourell and Brent Stucker. *Rapid Prototyping Journal* 17, no. 3 (January 1, 2011): 187–94. <https://doi.org/10.1108/1355254111124761>.
43. Tian, Li, Nadia Magnenat Thalmann, Daniel Thalmann, and Jianmin Zheng. “The Making of a 3D-Printed, Cable-Driven, Single-Model, Lightweight Humanoid Robotic Hand.” *Frontiers in Robotics and AI* 0 (2017). <https://doi.org/10.3389/frobt.2017.00065>.

44. Saeedvand, Saeed, Hadi S. Aghdasi, and Jacky Baltes. "Mechatronic Design of ARC Humanoid Robot Open Platform: First Fully 3D Printed Kid-Sized Robot." *International Journal of Humanoid Robotics* 17, no. 03 (June 1, 2020): 2050010. <https://doi.org/10.1142/S0219843620500103>.
45. Kim, Joonyoung, Taewoong Kang, Dongwoon Song, and Seung-Joon Yi. "Design and Control of a Open-Source, Low Cost, 3D Printed Dynamic Quadruped Robot." *Applied Sciences* 11, no. 9 (January 2021): 3762. <https://doi.org/10.3390/app11093762>.
46. Kentzer, Jakob, Bjarke Koch, Michael Thiem, Richard W. Jones, and Egon Villumsen. "An Open Source Hardware-Based Mechatronics Project: The Replicating Rapid 3-D Printer." In *2011 4th International Conference on Mechatronics (ICOM)*, 1–8, 2011. <https://doi.org/10.1109/ICOM.2011.5937174>.
47. N. Chandrasekhar, M. Vasudevan, Intelligent Modeling for Optimization of A-TIG Welding Process, Materials and Manufacturing Processes. 25 (2010) 1341–1350. <https://doi.org/10.1080/10426914.2010.529584>.
48. Nagesh, D. S., and G. L. Datta. "Genetic Algorithm for Optimization of Welding Variables for Height to Width Ratio and Application of ANN for Prediction of Bead Geometry for TIG Welding Process." *Applied Soft Computing* 10, no. 3 (June 1, 2010): 897–907. <https://doi.org/10.1016/j.asoc.2009.10.007>.
49. Vijayan, D., and V. Seshagiri Rao. "Process Parameter Optimization in TIG Welding of AISI 4340 Low Alloy Steel Welds by Genetic Algorithm." *IOP Conference Series: Materials Science and Engineering* 390 (July 30, 2018): 012066. <https://doi.org/10.1088/1757-899X/390/1/012066>.
50. Oberloier, S., Whisman, N. G., Pearce, J. M. PSO Experimenter / to be published
51. Wibawa, Tri, Hasan Mastrisiswadi, and Ismianti Ismianti. "3D Print Parameter Optimization: A Literature Review." *Proceeding of LPPM UPN "Veteran" Yogyakarta Conference Series 2020 – Engineering and Science Series* 1, no. 1 (October 27, 2020): 146–51. <https://doi.org/10.31098/ess.v1i1.105>.
52. Woern, Aubrey L., Dennis J. Byard, Robert B. Oakley, Matthew J. Fiedler, Samantha L. Snabes, and Joshua M. Pearce. "Fused Particle Fabrication 3-D Printing: Recycled Materials' Optimization and Mechanical Properties." *Materials* 11, no. 8 (August 2018): 1413. <https://doi.org/10.3390/ma11081413>.
53. Banks, Alec, Jonathan Vincent, and Chukwudi Anyakoha. "A Review of Particle Swarm Optimization. Part I: Background and Development." *Natural Computing* 6, no. 4 (October 18, 2007): 467–84. <https://doi.org/10.1007/s11047-007-9049-5>.

54. LulzBot. “Introducing the LulzBot TAZ 4 3D Printer,” May 7, 2014. <https://www.lulzbot.com/learn/announcements/introducing-lulzbot-taz-4-3d-printer>.
55. Paul, Arun Kumar. “Optimizing the Transition Process from Sparking for Non-Contact TIG Welding Inverters.” In *2006 IEEE International Conference on Industrial Technology*, 1413–18, 2006. <https://doi.org/10.1109/ICIT.2006.372439>.
56. Paul, Clayton R. *Electromagnetics for Engineers: With Applications to Digital Systems and Electromagnetic Interference*. Wiley, 2004.
57. Oberloier, S., Holmes, W. J., Pearce, J. M. Low-Cost TIG-based Open Source Metal 3-D Printer / to be published
58. MarlinFirmware. “Home.” Marlin Firmware. Accessed July 22, 2021. <https://marlinfw.org/>.
59. Oberloier, Shane. “Lightning Metal 3DP Control Software,” July 23, 2021. <https://osf.io/hzmue/>.
60. “Tig Welder, HF TIG/Stick/Arc TIG Welder, 200 Amp 110 & 220V Dual Voltage TIG Welding Machine -- Amazon.Com.” Accessed July 22, 2021. <https://www.amazon.com/Portable-Welding-Inverter-Manufacturers-Warranty/dp/B083HZGYCP/>.
61. “TIG Welding: What Is Scratch-Start, Lift-Arc and HF Ignition?” Accessed July 22, 2021. <https://www.weldclass.com.au/blog/40-tig-welding-what-is-scratch-start-lift-arc-and-hf-ignition->.
62. “TIG Welding Tungsten Electrodes 2% Ceriated (Grey, WC20) 10-Pack (1/16") -- Amazon.Com.” Accessed July 22, 2021. <https://www.amazon.com/Welding-Tungsten-Electrodes-Ceriated-10-Pack/dp/B013KWPFR2/>.
63. “Forney Mig Wire Mild Steel 0.024 Dia 2 Lbs. Spool Bulk -- Amazon.Com.” Accessed July 22, 2021. <https://www.amazon.com/Forney-Wire-Steel-0-024-Spool/dp/B00QZ2TLUW>.
64. Oberloier, Shane. “PSO Experimenter,” July 23, 2021. <https://osf.io/muevs/>.
65. Company, The Qt. “Embedded Software Development Tools | Cross Platform IDE | Qt Creator.” Accessed July 22, 2021. <https://www.qt.io/product/development-tools>.
66. Sandvik Materials Technology. “Shielding Gas Recommendations for MIG and TIG Welding.” Accessed July 23, 2021. <https://www.materials.sandvik/en/materials-center/shielding-the-weld/>. Electronics Cooling. “Estimating Parallel Plate-Fin Heat Sink Thermal Resistance,” February

- 9, 2003. <https://www.electronics-cooling.com/2003/02/estimating-parallel-plate-fin-heat-sink-thermal-resistance/> .
67. Welding Resources, Guides and Calculators [WWW Document], n.d. URL <https://www.millerwelds.com/resources/welding-guides> (accessed 7.23.21).
68. Petersen, E.E., Kidd, R.W., Pearce, J.M., 2017. Impact of DIY Home Manufacturing with 3D Printing on the Toy and Game Market. *Technologies* 5, 45. <https://doi.org/10.3390/technologies5030045>
69. Laplume, A.O., Petersen, B., Pearce, J.M., 2016. Global value chains from a 3D printing perspective. *J Int Bus Stud* 47, 595–609.
<https://doi.org/10.1057/jibs.2015.47>
70. Park, M., 2017. Print to repair: 3D printing and product repair, in: Routledge Handbook of Sustainable Product Design. Routledge.
71. Oberloier, S., Pearce, J.M., 2018. General Design Procedure for Free and Open-Source Hardware for Scientific Equipment. *Designs* 2, 2.
<https://doi.org/10.3390/designs2010002>
72. Pearce, J.M., 2013. Open-Source Lab: How to Build Your Own Hardware and Reduce Research Costs. Newnes.

6 Conclusions

6.1 General Conclusions

Many of the component parts of this dissertation can act as useful tools for researchers to optimize, automate, and understand a wide range of processes. The TIG-based metal 3D-printer has demonstrated potential to create solid and ductile depositions, however it is severely hindered by a lack of a compatible model slicer.

6.2 Conclusions on Finding Ideal Parameters for 3-D Printing Using Particle Swarm Optimization

Despite the GigaBotX's complexity and inconsistency paired with the difficult thermal properties of LDPE, PSO Experimenter was definitively able to optimize the process settings. PSO Experimenter can be used for substantial time savings in optimizing any process (compared to parameter sweeps)

6.3 Conclusions on Open Source Framework for a Broadly Expandable and Reconfigurable Data Acquisition and Automation Device (BREAD)

BREAD as a framework and system have been proven as a flexible system for data acquisition and process automation. When compared to commercial systems, BREAD is substantially less expensive, and for many cases available in literature, just as well suited.

6.4 Conclusions on Low-Cost Open Source TIG-Based Metal 3-D Printer

The TIG-Based Metal 3D printer is an easy-to-adapt and low-cost system to commercial componentry. Utilizing TIG welding as the deposition methods provides capabilities of depositing a wide range of materials. Though Lightning supplied a flexible and efficient tool for characterization, the system requires a customized slicer for creating complex models.

6.5 Conclusions Particle Swarm Optimization of Printing Parameters for Open Source TIG-Based Metal 3-D Printing

PSO Experimenter was used to identify sets of ideal printing parameters for a TIG-Based Metal 3D Printer. The printer can practically deposit at resolutions of 0.36mm (in the Z axis).